Predictions of visible and occluded motion in the primary visual cortex

Thesis

for the degree of

doctor rerum naturalium (Dr. rer. nat.)

approved by the Faculty of Natural Sciences of Otto von Guericke University Magdeburg

by M. Sc. Camila Silveira Agostino

born on 08th of April of 1991 in São Bernardo do Campo, São Paulo, Brazil.

Examiner: Prof. Dr. rer. nat. Toemme Noesselt

Prof. Dr. rer. nat. Mark W. Greenlee

submitted on: 30.08.2022

defended on: 01.02.2023

Summary

Processing dynamically occluded objects, also known as motion extrapolation, is a most complex cognitive process and fundamental for the survival of human and non-human animals. Understanding how humans extrapolate occluded objects has been the focus of psychologists and cognitive scientists since the 40s, when there was a growing interest in comprehending how gunners can better track targets even if they are occluded by clouds. Early behavioural studies showed that motion extrapolation works through a tracking mechanism, rather than a simple internal countdown clocking, as once hypothesized. Later, other researchers concluded that extrapolating objects rely on spatially-specific mental representation. However, most fMRI studies so far only reported the engagement of higher-level visual areas during dynamic occlusion which lack a fine-grained spatial specificity. Here, I investigate the engagement of the primary visual cortex during the processing of motion extrapolation, by addressing three central questions: what is the role of the primary visual cortex in the processing of dynamic occluded objects? Can the manipulation of the predictability of temporal information of occluded target differently enhance activity of the primary visual cortex, as posited by the predictive coding theory? What is the causal relation between processing of temporal information of a moving stimulus and activity in the primary visual area?

The first question was addressed by using a prediction motion paradigm and a combination of techniques, such as fMRI, retinotopic maps and multivariate pattern analysis (MVPA) at the single-subject level, to account for subject-specific anatomical variability and other methodological issues. Results indicated that extrapolating occluded motion trajectories enhanced activity in low-level visual regions, including the primary visual area. Additionally, occluded motion direction could be predicted from activity patterns in low-level visual areas during visible period of motion, supporting the idea of a mental representation of motion trajectory in a visually-specific format.

The second question was addressed by using the interception paradigm and the same combination of techniques. Results demonstrated that higher and lower predictability levels equally increased responses in the primary visual cortex; and here I discuss that if motion extrapolation is processed according to the predictive coding model, predictive error may have been silenced by additional attentional mechanisms, as proposed by an interactive prediction-attention model. In addition, it was observed that fast motion consistently enhanced activity pattern in the primary visual cortex, compared to slow velocity. Moreover, findings from the first study were replicated, by showing that response during visible and occlusion periods follow a similar pattern of activity.

The third question was addressed by using transcranial magnetic stimulation (TMS) over the primary visual cortex and by observing the effect on stimulus temporal information. However, results did not provide robust evidence to draw conclusions about the causal involvement of V1 with temporal information processing.

In sum, these studies provided evidence that temporal information can be found along the stimulus trajectory potentially pointing at a conjoined spatio-temporal representation in low-level visual areas during visible and dynamically occluded stimulations, thereby significantly extending previous research.

Zusammenfassung

Die Verarbeitung dynamisch verdeckter Objekte, auch bekannt als Bewegungsextrapolation, ist ein äußerst komplexer kognitiver Prozess und grundlegend für das Überleben von Menschen und nichtmenschlichen Tieren. Das Verständnis, wie Menschen verdeckte Objekte extrapolieren, war seit den 40er Jahren das Hauptaugenmerk von Psychologen und Kognitionswissenschaftlern, angesichts eines wachsenden Interesses daran, zu verstehen, wie Kanoniere Ziele besser verfolgen können, selbst wenn diese von Wolken verdeckt sind. Frühe Verhaltensstudien zeigten, dass die Bewegungsextrapolation über einen Verfolgungsmechanismus funktioniert und nicht über einen einfachen internen Countdown, wie früher angenommen wurde. Später kamen andere Forscher zu dem Schluss, dass die Extrapolation von Objekten auf einer räumlich spezifischen mentalen Repräsentation beruht. Die meisten fMRT-Studien berichteten bisher nur über eine Modulation der Aktivität in höheren visuellen Arealen während der dynamischen Okklusion, denen allerdings eine feinkörnige räumliche Spezifität fehlt. In der vorliegenden Arbeit untersuchte ich die Beteiligung des primären visuellen Kortex an der Verarbeitung von Bewegungsextrapolation, indem ich drei zentrale Fragen stellte: Welche Rolle spielt der primäre visuelle Kortex bei der Verarbeitung dynamischer verdeckter Objekte? Kann eine Manipulation der Vorhersagbarkeit zeitlicher Informationen von verdeckten Zielen die Aktivität des primären visuellen Kortex modulieren, wie dies von der prädiktiven Codierungstheorie postuliert wird? Welcher kausale Zusammenhang besteht zwischen der Verarbeitung zeitlicher Informationen eines Bewegungsreizes und der Aktivität im primären visuellen Cortex?

Die erste Frage wurde durch die Verwendung eines Vorhersagebewegungsparadigmas und einer Kombination von Techniken wie fMRI, retinotoper Kartierung und multivariater Musteranalyse (MVPA) auf Einzelsubjektebene angegangen, um subjektspezifische anatomische Variabilität und andere methodische Probleme zu berücksichtigen. Die Ergebnisse weisen darauf hin, dass die Extrapolation einer verdeckten Bewegungsbahn die Aktivität in niederen visuellen Arealen, einschließlich des primären Sehbereichs, verstärkt. Darüber hinaus kann die verdeckte Bewegungsrichtung aus Aktivitätsmustern in niederen visuellen Arealen während sichtbarer Bewegungsperioden vorhergesagt werden, was die Idee einer mentalen Repräsentation der Bewegungsbahn in einem visuell spezifischen Format unterstützt.

Die zweite Frage wurde unter Verwendung des Interception-Paradigmas und der gleichen Kombination von Techniken untersucht. Die Ergebnisse zeigen, dass höhere und niedrigere Vorhersagbarkeitsniveaus die Aktivität in primären visuellen Kortex gleichermaßen modifizieren; möglicherweise wird der Vorhersagefehler durch zusätzliche Aufmerksamkeitsmechanismen ausgeglichen - wie von einem interaktiven Prädiktions-Aufmerksamkeitsmodell vorgeschlagen. Darüber hinaus werden die Ergebnisse der ersten Studie repliziert, indem gezeigt wird, dass die neuronalen Antworten während sichtbarer und verdeckter Perioden einem ähnlichen Aktivitätsmuster folgen. Des Weiteren wird beobachtet, dass schnelle Bewegungen - im Kontrast zu langsamen - konsistent das Aktivitätsmuster in primären visuellen Kortex erhöhen.

Die dritte Frage wurde durch die Verwendung transkranieller Magnetstimulation (TMS) über dem primären visuellen Kortex und durch Beobachtung der Wirkung auf die zeitliche Information des Stimulus beatwortet. Die hier angewandte TMS-Doppelpuls-Methode über dem primären visuellen

Kortex lieferte jedoch keine robusten Belege, um Schlussfolgerungen über die Beteiligung von primärem visuellem Kortex an der zeitlichen Informationsverarbeitung zu ziehen.

Zusammenfassend liefern diese Studien Beweise dafür, dass der zeitlichen Informationsverarbeitung entlang der Stimulus-Trajektorie gefunden werden kann, was möglicherweise auf eine verbundene räumlich-zeitliche Repräsentation in niederen visuellen Arealen während sichtbarer und dynamisch verdeckter Stimulationen hinweist, wodurch bisherige Forschungsergebnisse erheblich erweitert werden.

Inhalt

List of Abbreviation

A1 – primary auditory cortex

BOLD – Blood-oxygenation level-dependent

fMRI – Functional magnetic resonance imaging

HP – High predictability

IP – Interception paradigm

IPC – Inferior parietal cortex

LDA – Linear discriminant analysis

LIP – Lateral intraparietal sulcus

LOC – Lateral occipital cortex

LP – Low predictability

M1 – Primary motor cortex

MD – Mean difference

MEG – Magnetoencephalography

MFC – Medial frontal cortex

MM – Markov model

MOT – Multiple object tracking

MT or hMT/V5+ or V5 – medial temporal cortex

MTS – medial superior sulcus

MVPA – Multivariate pattern analysis

PM – Prediction motion

ROI – Region of interest

SFG – Superior frontal gyrus

STG – Superior temporal gyrus

TMS – Transcranial magnetic stimulation

TTC – Time-to-contact

V1 – Primary visual cortex

VQ – Visual quadrant

Chapter 1 - General Introduction

While driving or walking by a busy street, there are intrinsic rules that drivers and pedestrians commonly follow. For instance, in Germany, at a non-signalized crossing, drivers have the preference coming from the right side. Knowing that, the driver from the left stops and waits until the other driver passes by. Another situation in which drivers tend to give preference is when pedestrians cross a street with no traffic lights. In Brazil, this is not a common practice, but we always imagine that drivers in many countries in Europe always do that, as shown in movies or TV shows. When I came to Germany for the first time, I expected that it would happen when I crossed a non-signalized street. However, in many situations, this was not the case, while in others it did happen. When my expectation to have a car stopping so I could cross the street was first violated, my predictions about what would happen in the same situation in the future were updated. After experiencing both situations, I was uncertain: is it safe to cross or should I wait until the car passes by? In situations like this one, our brain systematically evaluates and potentially update its predictions.

Prediction is of utmost importance in survival situations, as they help us planning next actions and making decisions. But what does is mean in a scientific context? In the next paragraphs, I will present the definition of this term as it highlights essential theoretical concepts underlying this thesis. In addition, the situation presented above will also follow us in the upcoming chapters, as it is a good example to illustrate the main questions of this work which are related to the investigation of the brain mechanisms involved in predicting and extrapolating missing information in motion. For instance, if a car gets occluded by a bus, its reappearance must be predicted in order to cross the street safely. Before defining prediction, it is important to explain how regularities, i.e. events presented in the environment, are learned by the brain.

How does the brain learn regularities?

The flow of events in the natural environment often follows a spatially and temporally organized structure, of which the patterns can be learned by humans. These patterns are also known as regularities or statistics, and usually they can be highly predictable (Turk-Browne, 2012; Schapiro & Turk-Browne, 2015). For instance, when walking around known surroundings, there is a high chance for the bus stop, traffic lights and other immobile elements to be at locations, predictable by our prior specific knowledge. Further, we do not expect to see a light pole on the top of a house based on our general knowledge about the world. Because many parts of the world are dynamic, regularities are characterized not only by *where* they appear, but also *when* they happen; thus,

structured and sequenced information extraction is fundamental for learning and predicting future events. In a recent review, Conway (2020) explains statistical learning in three dimensions: amount of structure in the input, amount of exposure to the input and amount of instruction/feedback related to the input. For the learning of regularities available in the environment to happen, it is necessary to have highly structured input and multiple exposures. For instance, learning a new language involves comprehending heavily structured patterns and being able to subsequently apply this knowledge. In early stage of ontogenetic development, it is already possible to observe learning through simple observation or through listening (Saffran et al., 1996; Sengupta et al., 2018). Also, through simple observation, studies reported that infants at around 4-5 months of age were able to represent moving objects which became temporarily occluded (Rosander & von Hofsten, 2004; von Hofsten, Kochukhova & Rosander, 2007). Von Hofsten and Rosander (2007) investigated how 4-month-old infants extrapolated - i.e. estimate future position of - occluded moving objects. The authors measured the infants' gaze shift when the occluder and the object velocity changed. After numerous exposures, the authors observed, in two experiments, that infants were able to follow the target before and after the occlusion in 89% and 77% of the time that the target moved. In addition, infants shifted the gaze to the final location before the reappearance, suggesting that they were able to track the occluded object and anticipate its final location. These findings corroborate Conway's dimensions, as infants were able to learn due to the highly structured experimental environment, vast exposure and non-instructed learning.

In the visual domain, extraction of temporal regularities from a continuous stream is rapidly achieved, often occurs in an unsupervised manner and can modify performance (Fiser and Aslin, 2002), based on valid predictions of the future event. At the neural level, sequence of regularities presented in different predictive levels enhance response in different brain regions, suggesting that different processes are required, depending on the level of predictability. For instance, Wang and colleagues (2017) investigated differences between events presented in random and context-based levels (i.e. more or less regularity structure). In particular, participants observed sequences of four symbols which were generated probabilistically through a simple or a complex temporal Markov Model (MM). The simple MM was composed by random events, meaning that the following event was not related to the previous one, while in the complex MM, one stimulus was sequence-dependent on each other. Participants were instructed to indicate what the upcoming stimulus would be. Functional magnetic resonance imaging results pointed to several brain areas with enhanced BOLD signal as a function of the level of randomness. The fully random level increased responses in bilateral frontal regions (Superior Frontal Gyrus, Precentral Gyrus and Inferior Frontal Gyrus), while the predictable level enhanced responses in dorsal frontal (SFG), limbic (Anterior

Cingulate Cortex) and subcortical (putamen) regions, suggesting that several regions are engaged in the learning and predicting new statistics, and may form flexible networks during this process.

The level of predictability in the environment is intrinsically related to the level of volatility in it, and a volatile environment here can be understood as unstable, fast-changing (Behrens et al., 2007). Studies presented evidence that the higher the volatility, the higher the learning rate (Zylberberg et al., 2016; Behrens et al., 2007). Behrens and colleagues (2007) investigated whether observers could keep track of statistics presented in a reward environment and adjust their learning rate according to the presented changes. The authors presented green and blue rectangles to the participants, which were modified at the trial-by-trial level, according to their expectations and outcome reward. Their responses were categorized in two stages: stable and volatile environment, and at each category a reinforcement-learning model was adjusted to the participant's decision. Results indicated that humans are able to optimally estimate and use volatility, judging the value of each new learned statistics. In accord, Zylberberg and colleagues (2017) hypothesized that greater volatility would lead to a quick diffusion of decision variable, i.e. decision reached after enough evidence has been accumulated. To test this hypothesis, the study was conducted on humans and non-human primates. By presenting random-dot motion paradigm, the authors observed that, for both monkey and humans, higher introduced noise resulted in faster reaction time and more accurate choices, meaning that the higher the noise, the more rapid decisions were made and the more confident the individuals were over the presented stimuli.

Overall, learning new regularities in the volatile environment can only happen when spatial and/or temporal information follow an extractable structure, meaning that the higher the amount of structure, the more effective is the learning and the more predictable an event will be.

After all, what is prediction? How does it work?

The term *prediction* can be defined as the process that generates or integrates information about the past to extrapolate likely future events of the natural environment (Bubic et al., 2010). Prediction rarely comes alone in the context of dealing with upcoming events. For instance, *expectation* frequently appears as a synonym, and etymologically they, indeed, have comparable meanings (prediction, from Latin *praedicere*, means foretell; expectation, from Latin *expectare/exspectare* means anticipation, await. https://www.etymonline.com/). In scientific context, Summerfield and Egner (2009) defined expectation as the brain state related to prior knowledge about possible future events from the environment. Most importantly, the employment of this prior knowledge may be used to decrease computational load in a way that expectations (or predictions) can aid visual information acquisition and facilitate the interpretation of the visual

input (Summerfield & Egner, 2009), thereby optimizing the processing of the incoming information (Zuanazzi & Noppeney, 2019). For this reason, many models tried to explain how prediction happens, such as predictive coding and its numerous variations (e.g. Mumford, 1992; Rao and Ballard, 1999; Friston, 2003; Spratling, 2017).

Predictive Coding

Models of predictive coding attempt to explain how different levels of a hierarchical model network propagate predictions to each other. Rao and Ballard (1999) suggested that higher levels of the visual system form a prediction and send it to the adjacent lower level through feedback connections. The higher levels receive the information about the difference between the prediction and the actual response via feedforward projections, and consequently this error is used by the system to make corrections on the estimation of the input signal. The authors illustrated these ideas through models as presented in Figure 1. Figure 1A depicts lower-level regions sending forward error about incoming discrepant information to a predictive estimator (PE), while PE sends backward predictions about the correct estimates from higher-level regions, i.e. generating new predictions. Figure 1B zooms into the predictive estimator unit which represents different types of neurons, such as feedforward neurons, which encode synaptic weights ($\mathbf{U^T}$); predictor estimator neurons, which maintain the current estimate $\mathbf{r}$ of the incoming stimulus; feedback neurons, which encode $\mathbf{U}$ and carry the prediction $\mathbf{f(Ur)}$ to lower stages; and finally, error detecting neurons, which compute the differences ($\mathbf{r}$ - $\mathbf{r^{td}}$) between the current prediction $\mathbf{r}$ and the top-down prediction $\mathbf{r^{td}}$ from an adjacent higher level. In sum, this course of receiving feedback predictions and sending feedforward errors assumes that top-down input affects projections from low-level areas and bottom-up input influences projections from high-level areas (Rao & Ballard, 1999).

Friston (2003) extended this idea suggesting that the brain's hierarchical system, routed in its anatomical organization, could be explained by a Free-energy principle model. Free-energy is a term borrowed from statistical physics, as its meaning is related to converting complex integration problems, innate to inference, into easier optimisation problems (Friston & Stephan, 2007; Friston, 2003; Friston et al., 2006; Friston & Kiebel, 2009). The model differs from the previous one in the sense that it attempts to consider the relation between action and perception and to explain how these processes are used to decrease energy consumption by using prior information (Friston & Stephan, 2007). For instance, the model is designed to account for attention and perceptual salience, the latter based on stimulus features. Even though Free-energy principle models expands the predictive coding approach, both attempts to explain how the brain predicts information which constantly overflows the systems streams (for mathematical formulations, see Spratling, 2017).

Additionally, predictive coding was further related to Bayesian inference (Aitchison & Lengyel, 2017). The authors suggested that, while predictive coding explains responses at the neural level and Bayesian inference explains behaviour, both are complementary. Their relation is given by the fact that the second grants an optimized calculation for the computation of predictions which occurs in the neural circuits and will be handled by the first.
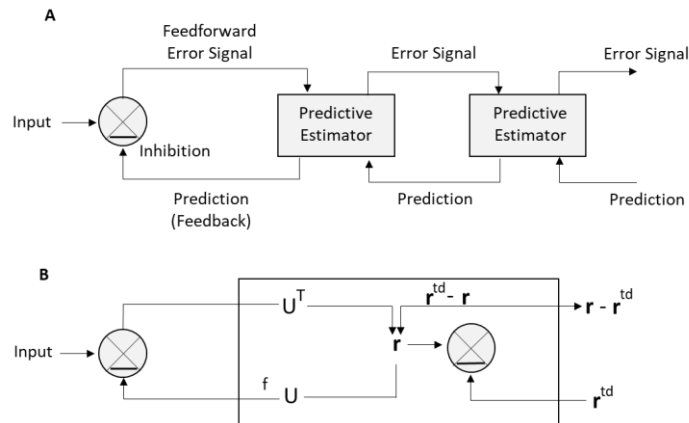
Figure 1- Figure adapted from Rao and Ballard (1999). Rao and Ballard's Hierarchical Network of Predictive Coding. (A) Overall scheme of predictive coding model. The model depicts that lower levels send feedforward errors, obtained from discrepancies between top-down input and the actual input, and receive back predictions from predictive estimators. Predictive estimators are different types of neurons with different roles in the system. (B) Composition of a PE. A PE unit is formed by the synaptic weight U^T which is encoded by feedforward neurons. Information is carried on to neurons which produces responses (r), used to maintain the ongoing estimation of the incoming signal. f(U) represents feedback neurons which encode and deliver predictions f(Ur) to lower levels. The differences obtained from the estimations is represented by r (the current prediction) – r^{td} (top-down prediction).

Predictive coding models have been used to explain predictions in the different systems, such as auditory, multisensory, and even in the motor system (Adams et al., 2013). In the auditory domain, Todorovic and Auksztulewicz (2019) tested whether the primary auditory cortex would present low increase of activity once temporal predictability was high. While brain activity was monitored using MEG, participants listened to two pure tones of 5ms long: a standard (1000 Hz), followed by the same tone or a deviant (1200 Hz), and were instructed to press a button as soon as they heard the deviant tone. The interval between the tones could vary so temporal expectation could be built. Results indicated that networks involving the primary auditory cortex (A1), superior temporal gyrus (STG) and inferior parietal cortex (IPC) were differently modulated depending on the temporal expectation. In particular, activity in higher-level areas were enhanced by low predictable stimulation, but these regions were not affected by signals coming from the primary auditory cortex. The authors also suggested that prediction errors were not supressed by elapsed-time prediction, they rather affect the connectivity pattern.

A recent fMRI multisensory integration study reported the enhancement of bottom-up stimuli and suppression of top-down information along the integration pathway (Krala et al., 2019). In this study, participants were asked to estimate their own motion speed in a visual, auditory or bimodal context. Results indicated an enhancement of fMRI-signals in areas related to the sensory stimulation, but a suppression in higher-level cortical regions, suggesting that predictions related to these modalities played a role in shaping information processing, in accord with other previous studies (Kok et al., 2012, van Kemenade et al., 2017). Additionally, the authors also stated that the availability of the sensory information, and thus bottom-up processing, may have been enhanced to boost the predictions in higher-level visual areas, and this enhancement was suggested to have occurred due to the interaction between task relevance and prediction. Finally, while the increase of sensory signals can promote perceptual inference improvement and prediction facilitation for future events, the decrease of signals in higher-level areas can be interpreted as a coherence between prediction and bottom-up information, regardless the sensorial system.

How does the brain complete missing information?

Hermann von Helmholtz revolutionized the way that researchers understand perception when he proposed that sensory images are not represented by the brain, but, instead, these images are extrapolated from sensory impressions, as the cause for their existence cannot be directly perceived (Helmholtz 1860/1962). Helmholtz added that, as we cannot perceive the cause of sensory images, the brain has to perform unconscious inferences, so that the image that is on the retina corresponds to the image of the real world. Having this in mind, the processing of complex images starts on the retina. The eye has evolved to primarily deal with complex types of information and one of them is motion. It is not rare that the visual system is confronted with missing information, such as simple eye blinks and other visually disruptive changes, which may also fragment part of the coming information. Through evolution, the eye adapted to track other living beings not only during visible periods, but also occlusion moments in a predator or, eventually in a prey role. Consequently, the human brain should be well equipped to process not only the completion of these missing information (Bosco et al., 2018), but also to perform complex computation to estimate the reappearance of a dynamically occluded objects (phenomenon also known as "Tunnel Effect" - Burke, 1952). In the modern times, we have to deal with similar situation as our ancestors in a completely different, yet dynamic, environment. We do not need to predict and estimate the reappearance of a prey, for instance, but the reappearance of a car occluded behind a bus, when driving or crossing a street to make our next action safely. Our survival goals changed, but the computation carried out by our brain may still be the same.

This fundamental ability is essential for survival and has been observed in humans starting from early age of development (Rosander & von Hofsten, 2004, Hosften, Kochukova & Rosander, 2007), as well as other other animals (Assad & Maunsell, 1995). From now on I will refer to this ability as *motion extrapolation* (following Battaglini & Ghiani, 2021). Besides the extensive research on motion extrapolation, mostly at the behavioural level, the neural mechanisms underlying this process are still to be established. In particular, how do early stages of visual processing deal with dynamically occluded objects? How is the inherent temporal information of occluded moving objects processed in low-level visual areas? This work was developed to answer questions like these.

Motion extrapolation

Motion extrapolation is part of a phenomenon called amodal completion, which is comprehended as the process of completing an object which lacks direct visual input due to occlusion (see van Lier & Gerbino, 2015, for review), meaning that, although the physical visual input is missing (amodal), the occluded parts are still represented (completion). This term should not be confused with modal completion, which describe the illusion of vivid perception image features, as contours and surfaces, such as in the famous Kanizsa triangle (Kanizsa, 1976, 1985).

In a recent overview, Battaglini & Ghiani (2021) pointed out the common confusion between "*amodal phase*" and *motion extrapolation* observed in some psychological and psychophysical studies which investigated the cognitive processes related to extrapolating motion behind an occluder. In general, amodal phase is the *period* that the physical stimulus is temporarily occluded and participants, during tasks, are instructed to make inferences about the feature of that stimulus or to detect something in the surroundings of the target. For instance, in a study using multiple object tracking (MOT) and occlusion, participants were instructed to tracked up to three targets which became occluded by two vertical occluders. At the same time, they had to detect a probe stimulus, which would appear on the centre of a target, when it appeared between the occluders or behind one occluder (Flombaum et al., 2008). In contrast, motion extrapolation is the *estimation* of the reappearance of an occluded object in movement, based on the past information (space, time and speed) acquired during the visible phase (Battaglini & Ghiani, 2021). Such term, also present in mathematics is defined as the estimation of values beyond the original and observed data range. Both definitions share the fact that extrapolation means estimating ahead of the known information, and for this reason, motion extrapolation is used here to define the cognitive process related to estimating the time-to-contact (time) and point-of-contact (space) of a dynamically occluded object.

The interest in understanding the processing of motion extrapolation dates from decades ago and the motivation for researching this topic varied. Gottsdanker (1952) pointed out that the interest in supporting such research, post-World War II, originated from scenarios, in which aerial gunners still needed to track the target even when it is occluded by clouds. The idea was to find means to test and select the best soldiers during recruitment and train them afterwards, in order to improve this ability. In seminal studies, Gottsdanker (1952, 1956) explore the ability of tracking occluded trajectories, focusing on the continuation after positive acceleration.

In the same decade, Burke (1952) investigated the ability to perceive continuation based on the "Tunnel Effect" phenomenon (Burke, 1952; Michotte, 1946, 1950). If we imagine again the example of a moving car becoming occluded by a bus and reappearing, we have no doubts that the car was continuously in movement. Having this in mind, Burke (1952) posited the questions *"Is this merely a matter of belief, or of knowledge based on past experience, or is the continuity of the movement actually "seen" by the observer?"*. In his series of experiments, participants reported "seeing" the object moving during the occlusion period, which was supported by participants drawing. The findings of these experiments opened new questions about estimation and prediction of dynamic occluded objects which were tried to be answered and explained by different hypotheses.

Motion extrapolation hypotheses

Decades ago, Gibson (1968) ran a series of experiments to study the perception of motion and suggested a hypothesis that gave way to studies involving partially occluded stimulation and its time-to-contact (TTC). In general, he hypothesized that the visual information necessary for processing motion was dependent on the changes in the optic array of an individual's eyes. He suggested that motion can be perceived when the retina registers continuous information of an object's features, such as form and texture. Gibson's assumption gave foundation to the *tau (*time quantity) hypothesis, which was vastly used as basis of subsequent studies. Lee (1974) mathematically described the *tau* hypothesis as the ration between the angular separation of two image points of an obstacle and the rate of separation of two image points. In his study, he developed a whole new theory to explain how drivers control their braking. His theory postulated that simple visual variables were necessary to provide drivers with enough information for controlling their brakes. Lee found out that the most relevant variable that a driver needs to consider is the TTC. Therefore, he proposed safety measurements for drivers to avoid accidents, such as an "imperative" brake light signal indicating that the driver from the back should start decelerating as soon as possible in case of abrupt brake.

The t*au* hypothesis was revisited by Tresilian (1995), who suggested a broader approach to be considered in different contexts. His extended *tau* hypothesis accounted not only for a simple event foresight, as Lee's study suggested, but also the relative arrival judgement of two targets, in which one had to indicate which target would arrive first, before both disappeared. In other words, TTC would require a timing count down strategy and no visual imagery would be necessary (DeLucia & Liddel, 1998). In the late 90's, the *tau* hypothesis was revised and falsified by Tresilian (1999). He acknowledged that TTC estimation is related to *tau*, but presented a series of limitations, such as, the acceleration is ignored, the TTC information is obtained by the eyes, objects should be spherically symmetric and object's image size should be suprathreshold. Despite the fact that this hypothesis was used to stimulate many studies, TTC appears to be a much more complex process to be explained and other mechanisms should be considered.

Another hypothesis suggested by Tresilian (1995) also proposed that people are able to estimate an occluded object's TTC due to an internal clocking mechanism, in which they would use the visible information to accumulate time and count it down until the final position. This hypothesis was tested by DeLucia and Liddel (1998) and results indicated that individuals not only used a *clocking* mechanism, but also motion extrapolation through visual imagery. In this study, the authors used a prediction motion paradigm (PM - Box 1) in which they estimated the time-to-contact of the target; and an interception paradigm (IP - Box 1) in which participants judged whether the reappearance location of the target was either correct or incorrect. The rationale to use both tasks was to compare the extrapolation and the clocking mechanisms, respectively; and investigate whether the outcome of both tasks was similar. The authors observed some level of

---

Box 1 – Motion extrapolation Paradigms

On a general level, motion extrapolation can be accessed through two main different paradigms:

Prediction Motion (PM) – in this paradigm, the participant's time-to-contact (TTC) of an occluded target is measured (DeLucia & Liddell, 1998; Makin & Poliakoff, 2011; Battaglini & Ghiani, 2021). The target moves during a visible period and becomes occluded by a visible or invisible occluder. Participants are instructed to judge when the target reaches the end of the occluder or a certain mark. The important feature of this paradigm is that the target never reappears after the occlusion.

Interception Paradigm (IP) – in this paradigm, opposing to PM, the target reappears. Participants are instructed to judge whether the reappearance of a target was earlier or later than a baseline, or whether the reappearance position was correct or wrong (DeLucia & Liddell, 1998; Makin & Poliakoff, 2011; Battaglini & Ghiani, 2021).

The paradigm for testing motion extrapolation should be carefully picked up, as they can engage different neural processes and stimulation protocols, such as the lack or presence of the stimulus reappearance.

consistency between both tasks, suggesting that in both, extrapolation, rather than only countdown clocking mechanism, was necessary for performing the task accurately.

Also, in contrast to the clocking hypothesis, Lyon & Waag (1995) investigated the extrapolation accuracy of time, hypothesizing that target tracking before and after the occlusion were essential to perform extrapolation. The rationale behind it was that: if individuals were accurate in tracking the visible trajectory, keeping tracking after the occlusion should reduce estimation error. Participants observed a target moving clockwise or counter clockwise in a circle marked with a perpendicular line, at one of three different velocities. At a certain period, the target disappeared, as well as the line. While the line was still present on the screen, participants were instructed to consider that the target was still moving and to indicate whether the it crossed the line or not. Results showed a significant decrease in the proportion of correct responses with extrapolation time, suggesting that accuracy time error increases after tracking the target during occlusion for a longer period. They additionally tested the same paradigm but with the inclusion of a distractor during the target occlusion and observed a decrease in accuracy, i.e. an impairment in the extrapolation performance. The author interpreted these results as evidence that participants use a tracking mechanism during occlusion and this mechanism requires visual attentional resources.

In support to this tracking hypothesis, Makin and Poliakoff (2011) reported that the extrapolation of occluded objects is guided by reallocation of visuospatial attention, and manipulated free eye movements vs. fixed eye position. Participants performed two different tasks, one PM paradigm and the other, a modified version of the IP, but without the occluder. All in all, results indicated that better accuracy when participants could move their eyes to track the occluded stimulus. Additionally, the authors also observed small eye movements (<2°) during occlusion period even when participants were instructed to keep their gaze on a fixation point, and interpreted the results as possible visuospatial attention related to motor planning (premotor theory of attention – Rizzolatti et al., 1987); or a certain level of mental imagery (Huber & Krist, 2004), in line with the postulation of DeLucia and Liddel (1998).

In a series of experiments, Kerzel (2003) investigated whether attention would be related to disrupting or maintaining mental extrapolation, by asking participants to judge the final position of a moving target, with or without the present of a distractor. In all experiments, he observed that participants accurately estimated the final position of a target, even with the absence of a systematic eye movement or with the presence of distractors, suggesting that attention is associated with the maintenance of *spatially-specific* mental extrapolation. One possible

interpretation given by Kerzel is that attention maintains extrapolation due to a "spreading" of activation in different visual regions (Hubbard, 1995; Müsseler et al., 2002), meaning that visible motion stimulation would enhance activity in part of the visual regions and activation would be carried on during implied motion, engaging higher-visual areas. In contrast, Baurès and colleagues (2018) investigate the effect of attention in TTC estimation and found opposite results. The authors compared the participants' TTC estimation in two contexts: (1) when they were required to simply estimate the time when a target would reach a vertical bar (single-task), and (2) when they had to do the same judgement but keeping the information of a previous unrelated stimuli in the working memory (dual-task). TTC estimations during dual-task performance were highly accurate, indicating that TCC can be performed without much attention. One possible interpretation for these results suggested by the authors is that the attention during the TCC dual-task may change higher cognitive mechanisms, as suggested by the common rate controller hypothesis (Makin, 2018). During the occlusion of a target, individuals can still keep its features in their mind, such as position, colour, speed. The common rate control hypothesis, postulated by Makin (2018), suggests that observers are able to do that, as they perform a mental simulation "at a chosen speed" in an amodal fashion. For that, it is proposed that the brain accounts for a rate control network, which is temporarily paired with the sensory maps during stimulus occlusion. This network would engage areas such as DLPFC, Basal ganglia, SMA and sensory regions (Makin, 2018; Makin & Chauhan, 2014; Lencer et al., 2004).

The literature about motion extrapolation is rich with hypotheses that attempt to explain the mechanisms underlying the processing of dynamically occluded targets, as described above. Some of them indeed agree that there is some kind of visual representation of the stimulus (DeLucia & Liddell, 1998; Makin, 2018), and consequently an engagement of visual areas (Gilden et al., 1995; de'Sperati & Deubel, 2006). Gilden and colleagues (1995) tested whether there is an interaction between imagined time-to-contact and adaptation of the visible moving stimulus. They investigated changes in real motion adaptation by manipulating the occluder region and adapting a group of moving dots. Their findings indicated that when observers adapt to motion, a specific bias pattern, which does not depend on the direction orientation of the adaptation, emerges in the context of judgment of the mentally represented TTC. In line with this study, de'Sperati & Deubel (2006) tested whether there is a facilitation in detecting a probe stimulus during motion extrapolation of a main target. They compared the appearance of the probe in a location where the target was being imagined after occlusion with another location where it was not being imagined. Participants were instructed to keep their gaze in a fixation mark and make saccades to the imagined locations when the probe appeared. Results indicated that saccades happened faster

when the probe appeared in the vicinities of the imagined target location than when it was presented far from the imagined position, suggesting again that observers held some level of *spatially-specific* mental representation during target occlusion. Although studies showed evidence for the involvement of mental imagery as a mechanism of motion extrapolation, few fMRI studies investigated the involvement of low-level visual areas, especially the primary visual cortex, with motion extrapolation.

What are the neural correlates of occluded information in motion?

The neural underpinnings of dynamically occluded objects were found to be much more present in higher-level areas than in low-level visual regions (Olson et al., 2004; Shuwairi et al., 2007). Accordingly, electrophysiological studies in non-human primates revealed an important role of posterior parietal cortex, specifically lateral intraparietal sulcus (LIP), which was found to be involved with the sustainability of activity during the absence of visual stimulus (Assad & Maunsell, 1995), plus medial superior temporal sulcus (MTS) and medial intraparietal area (MIP), which was best related to inferred visual and hand motion (Eskandar and Assad, 1999). In humans, the homologue area, intraparietal sulcus (IPS), was also robustly seen to play an important role when visual extrapolation tasks involved oculomotor control or manual interception (Olson et al., 2004; Shuwairi et al., 2007), as well as lateral occipital cortex (LOC, Hulme and Zeki, 2007) and MT (Olson et al., 2003).

Box 2 – Functional Magnetic Resonance Imaging (fMRI)

Since the beginning of 1990s, fMRI technique has become one of the most used methods in Neuroscience research (Poldrack, Mumford & Nichols, 2011). FMRI provides a high spatial resolution compared to other methods, such as electroencephalogram, which enable the researchers to make inferences about regions and its functionality, in a safe and non-invasive fashion. This functionality is accessed by measuring the signal changes which are related to the change in ratio of oxy- and deoxyhaemoglobin when neuronal activity increases, thus the signal obtained from fMRI is called blood oxygenation level dependent, or BOLD signal.
The increase of BOLD response, followed by a short period of neural activity is called *hemodynamic response.* There are some characteristics of this response, which are essential to know before planning any experiment. For instance, hemodynamic response is slow, as the blood flow takes around 5-6 seconds to reach its peak. This peak is followed by decrease which does not go completely back to the baseline for approximately 15-20 seconds. The other characteristic is that the hemodynamic response can be handled as a linear time invariant system (Cohen, 1997; Dale, 1999), i.e. the response obtained from a longer-period activity can be computed by summing up shorter-period of activity (Poldrack, Mumford & Nichols, 2011). This linearity allows the computation of a statistical model which compares the estimated hemodynamic time course with the measured signal.

For instance, Hulme and Zeki (2007) presented faces and houses, which could become visible, occluded by a moving screen, while fMRI data were acquired. Participants were instructed to attend to the main stimulus, while keeping their eyes at a central fixation cross, and to monitor changes in this cross by pressing a button. The authors observed that during visible and occlusion phases, faces and houses equally enhanced fMRI-signals in fusiform area and in the LOC, respectively. These findings were attributed to the visual "awareness of the object's presence", as visible and occluded objects may share this brain state, which could be related to the active maintenance of the invisible object (Battaglini et al, 2013; Pasternak & Greenlee, 2005). Using a similar approach, Olson and colleagues (2003) compared occlusion and disappearance, and observed fMRI-response when participants watched a ball travelling behind an occluder. Results revealed greater engagement of IPS and MT during occlusion compared to disappearance, and a decrease in low-level visual areas, suggesting that dynamically occluded stimulation may mainly be processed in these areas. Similar findings were also observed by Schuwairi and colleagues (2007), who also reported that low-level visual regions showed enhanced responses during the presentation of unoccluded compared to occluded targets. In contrast, only few studies found dynamically occluded objects to be represented also in low-level visual cortex. However, these studies are mainly related to the representation of certain moving object features (Erlikhman & Caplovitz, 2017), active mental imagery (Emmerling et al., 2016), apparent motion (Ekman et al., 2017), bistable stimulation (van Kemenade et al., 2021). A common approach of all these above mention studies is the combination of fMRI (Box 2) with retinotopic mapping (Box 3) and the use of multivariate pattern analysis (MVPA – Box 4). In particular, the differences between the studies which showed effect in low-level visual cortex and the other which did not could be due to the lack of the anatomical and function specificity provided by retinotopic mapping. The studies with retinotopic mapping usually define subject-specific ROIs in visual areas (Erlikhman & Caplovitz, 2017), which provide a level of spatial accuracy much higher than the traditional voxel-based group approach with normalized brains. For instance, Emmerling and colleagues (2016) not only defined each ROI individually, but also presented results at the single-subject level. Their findings demonstrated robust evidence that individuals do engage low-level visual areas during mentally imagery of visual motion. Accordingly, in this project, we use the combination of all three methods – fMRI (Box 2), retinotopic maps (Box 3) and MVPA (Box 4) – to address the central questions of this thesis.

Box 3 – Retinotopic Mapping

The visual cortex is organised in a complex manner, with many functional separations, each area containing different neural properties (Zeki and Shipp, 1988). In addition, there is a high level of between-subject anatomical variability (Amunts et al., 2000) and accounting for this variability is fundamental to for prudent visual imaging research. For this reason, the method of mapping retinotopic fields is commonly used together with the conventional fMRI analysis. Retinotopic fields are areas organized in a such a way that a continuous mapping is formed between the visual field and the cortical surface (Warnking, 2002), and the visual field boundaries, lower and upper, can by identified by the change in orientation of the local visual representation (Sereno, et al., 1994). This delineation is the key factor for establishing subject-specific maps of low-level visual cortex.

The method of retinotopy is based on connecting the position of each retinotopic neuron to the position in the visual field related to the centre of its receptive field, thus the spatial location of the neurons can be better depicted in two-dimensional coordinates: eccentricity and polarity, on the cortical sheet (Warnking, 2002). To obtain these two measures, specific stimuli are used. For eccentricity maps, a ring periodically and slowly contracts and expands while the participant fixates in a central point, whereas, for polarity maps, one (or two wedges, opposite to each other) rotates clock- and counterclockwise (Engel, et al., 1994; DeYoe et al., 1994). Both stimuli establish a connection between positions in the visual field and to an exclusive periodic stimulation delay, which is described as phase in the frequency domain. The opposite moving stimulation is used to correct a response phase shift created by the hemodynamic delay.

The data acquired from retinotopic mapping also requires special analysis (for details, see Warnking, 2002). In general, it requires the construction of a surface model, i.e. a selection of the brain regions of interest (occipital cortex), which will be inflated and flattened. The first makes it possible to have the representation of the whole hemisphere without gyri and sulci, while the second requires surface cutting, in order to have a complete view of the whole occipital cortex. Therefore, results of retinotopic maps are commonly displayed over flattened brains, as the visualization of distant areas of the visual cortex can be readily displayed in one image.

What is the role of the primary visual cortex in motion processing?

Previously, I have introduced the Predictive Coding model, which proposes that the brain is hierarchically organized. In the visual domain, higher-level visual regions may send backward predictions about incoming information to lower-level regions and receive back errors from low-level regions based on bottom-up information (Rao & Ballard, 1999; Mumford, 1992; Friston, 2003). In this section, I review the current knowledge on motion processing and the interaction between low-level visual regions, as V1, and high-level visual regions, as V5.

One of the core brain regions involved in motion processing is MT/V5. Many studies have observed the engagement of this area during motion processing in primates (Born & Tootell, 1992; Fellemann & Van Essen, 1991; Born & Bradley, 2005, for review) and in humans (Goebel et al., 1998;

Kolster et al., 2010; Muckli et al., 2002; Hampson et al., 2004). For instance, Born and Tootell (1992) reported that motion processing in monkeys happens in segregated columnar neurons in V5 and two different kinds of motion information are processed: local and global. Later on, Goebel and colleagues (1998) demonstrated that, in humans, not only visual motion stimulation, but also motion imagery, increased fMRI-responses in hMT/V5, when using apparent motion. Further, the study also showed that motion imagery enhanced activity in the primary visual area, although here we cannot discard the possibility that short-term memory could have influenced the imagery process (Kaas et al., 2010). Nonetheless, many other studies investigated the relation between V1 and V5 during motion processing (Railo & Hurme, 2021, for review), and linked it to the awareness of the visual input.

Box 4 – Multivariate Pattern Analysis (MVPA)

Machine Learning is an umbrella term to describe the use different kinds of tools to classify datasets. Using Machine Learning to investigate brain imaging data has helped lots of researchers from all kinds of fields to answer questions that traditional univariate analysis would not allow to answer (Haxby, 2012). For this reason, Multivariate Pattern Analysis (MVPA) became essential in neuroscience research, as it is formed by a collection of tools serving specific purposes. For instance, it allowed researchers to change the questions from "what is the function of this area?" to "which pattern of information can this area encode?". Having said that, the main focus of MVPA is to detect pattern of activities which are informative regarding to participants' perceptual or cognitive state. This approach can be divided in four steps (Norman et al., 2006): (1) selection of voxels which will be part of the analysis. This selection can be made including a subset of voxels (ROI-analysis, Cox and Savoy, 2003) or all brain voxels at once (whole-brain analysis, Mourao-Miranda et al., 2005). (2) Experimental conditions will be categorized in numerical targets, chunks and labels. (3) An algorithm, as known as classifier, will be applied in part of this data, in which a separation boundary will define the difference between the targets. This part is commonly called training phase. Different classifiers can be chosen, such as Support Vector Machine (SVM, Cox and Savoy, 2003), Linear Discriminant Analysis (LDA, Kriegeskorte et al., 2006), Neural Networks (Hanson et al., 2004) and Gaussian Naïve Bayes (GNB, Mitchell et al., 2004). Finally, (4) the trained classifier will be applied to the remaining dataset to characterize if the learned pattern of activity can be used to accurately discriminate patterns of activity of different experimental conditions during the so-called test phase. In sum, MVPA is an effective approach to decode neural representational patterns, as it is takes as input activation patterns related to different tasks and stimuli (Mumford, et al., 2012). Therefore, this technique has superior sensitivity compared to the traditional univariate GLM analysis (Haxby, Connolly & Guntupalli, 2014).

Studies showed that, during motion processing, V1 sends feedforward projections to V5, which in turn sends back projections to V1 (Koivisto et al., 2010; Vetter et al., 2013). In a TMS (Box 5) study, Koivisto and colleagues (2010) asked participants to discriminate the direction of moving dots, using a random-dot motion (RDM) paradigm, while a single-pulse TMS was applied over

V1/V2 and V5 on different intervals (20, 40, 60, 80 or 100 ms) after motion offset. The authors reported that when TMS pulse delivered at earlier (20 ms) and at later (60 ms) intervals over V1/V2, the conscious- and unconsciousness of visual perception were compromised, respectively. Note that, "conscious vision" was defined as the perception of visual stimulation which is capable of promoting any change in behaviour, such as accuracy or reaction time, and can also be reported as perceived by the observer, while "unconscious" vision follows the same definition, but perception cannot be reported by the observer (Railo & Hurme, 2021). Nonetheless, they suggested that on one hand, the observed impairment during the earlier interval might be related to the sending information to higher levels, such as V5 ("feedforward sweep" - Lamme, 2001). On the other hand, the later interval might be associated with the feedback projections from V5 to V1. This critical stimulation interval was different for V5, though. When stimulation was delivered at 40 ms, an impairment on conscious visual perception was observed, supporting the idea that this region is receiving and sending information to V1.

Box 5 – Transcranial Magnetic Stimulation (TMS)

Transcranial magnetic stimulation (TMS) is a non-invasive neurostimulation and neuromodulation method, based on the principle of electromagnetic induction of an electric field in the brain (Rossi, et al. 2009). The magnetic field generated and delivered by a specific coil is high enough to depolarize neurons, modulating their activity in an excitatory or inhibitory manner, depending on the established parameters: intensity, frequency and combination of pulses.

What makes TMS such a potent tool is the possibility to draw causal inferences between behavioral phenomenon and brain activity, as the application of TMS pulse can temporarily disrupt activity in a cortical region. This intense manipulation of neural activity allows investigation of some brain lesion conditions, such as cortical blindness, in healthy patients. Additionally, TMS has been used as a therapeutic interventional to treat disorders such as depression, panic, hallucinations, bipolar disorders, post-traumatic stress disorder, drug craving, among others (George et al., 2007; Aleman et al., 2007; Fregni and Pascual-Leone,2007).

In contrast, other studies suggested that motion information might not necessarily pass V1 to reach V5. Studies with primates demonstrated that V5 also receives direct input from sub-cortical regions, as superior colliculus (Berman & Wurtz, 2010, 2011; Lyon et al., 2010) and pulvinar (Baldwin et al., 2017). In line with these findings, early studies (Ffytche, Guy and Zeki, 1995; 1996) demonstrated that patients with cortical blindness in V1 are still able to react to fast motion (>15°/sec), compared to participants with lesion in V5, who could detect only very slow motion (<6°/sec). Based on these reports, Ffytche, Guy and Zeki (1995) postulated that motion might take two different pathways to reach V5 and introduced the Dynamic Parallelism theory. This theory

was later on tested by Grasso and colleagues (2018) which used a double-pulse TMS on healthy participants, using random-dot motion paradigm. The authors used similar stimulation time window and also found that TMS over V5 delivered at an early (~30 ms) time window was related to impairment in the processing of fast motion, and a later (~80 ms), related to an impairment in slow motion processing. In contrast, TMS over V1 provoked an overall deterioration in motion discrimination unrelated to the TMS interval. Although, the results did not fully support the dynamic parallelism theory, results from V5 suggested that different motion may be to some extent processed by different pathways. For this reason, in this project, we further investigated the relation of V1 and V5 with one of the most important features of visual motion: speed. The rationale behind it is that, to our knowledge, the studies did not test speed per se, but usually direction discrimination, or apparent motion. Here, we extended the investigation of the dynamic parallelism theory, by directly accessing the role of V1 on speed discrimination.

Overview of the thesis

This work was divided in three main parts which address questions such as: what is the role of the primary visual cortex in the processing of dynamically occluded objects? Can the manipulation of temporal predictability of occluded target alter activity of the primary visual cortex, as posited by predictive coding theory? What is the causal relation between processing of temporal information of a moving stimulus and activity in the primary visual area?

Chapter 2 introduces the first fMRI study of this thesis. Here, we investigated how the trajectory of an occluded moving stimulus is represented in low-level visual areas, specifically in the primary visual cortex. We rationalized that if stimulus occlusion enhances activity in low-level visual cortex in a spatially selective manner, this would indicate the existence of a mental representation in a visual-spatial format. To this end, we used a modified PM design, in which it was presented a visual stimulus moved horizontally and changed direction at a certain point (upward/downward). The upward and downward movement were associated with a particular velocity. Participants first learned velocity-direction associations with visible stimuli and secondly made temporal and spatial estimations of occluded stimuli without additional feedback (i.e. no reappearance of the stimulus). Participants' brain activity during visible and partially occluded stimulation was measured using fMRI (Box 2), retinotopic mapping (Box 3) and data were analysed with univariate analysis and MVPA (Box 4). Functional MRI was here chosen, as it is the technique which offers the best spatial resolution among the available non-invasive imaging techniques. Besides the importance of having maximized spatial resolution to characterize the modulation of activity in the brain, MRI also enables to map the spatial layout of low-level visual cortex individually for each participant, and for that, we used retinotopic mapping (Warnking, et al., 2002; Amunts et al., 2000). In addition, for the

analysis of neural-activity, we used MVPA. MVPA is commonly used to measure the encoded informational pattern of activity in different brain areas, presenting advantages over the traditional univariate analyses (for review see, Anzellotti & Coutanche, 2018). This ensemble of techniques was applied at single-subject level, making it possible to obtain unprecedented results in the realm of motion extrapolation. Further, the results indicated that occluded motion direction could be predicted from activity patterns in low-level visual areas during visible period of motion, supporting the idea of a mental representation of motion trajectory in a visually-specific format.

Chapter 3 presents the second fMRI experiment of this thesis, which replicates and extends the findings of the first study. In this second study, we manipulated the predictability of the velocity-direction association and investigated the effect of this manipulation on the informational content in the primary visual cortex. We hypothesized that during the estimation of temporal information of an occluded moving stimulus, different predictability levels should modulate different response enhancement in V1. To test this hypothesis, we used an adapted version of the Interception Paradigm, using the reappearance of the stimulus as feedback for the participant to learn and make correct spatial and temporal estimations. The tasks had two levels of predictability: high (100%), in which the reappearance time and position of the dot were constant; and lower (70%), in which the reappearance position was certain, but the movement velocity changed in 30% of the trials, i.e. the reappearance occurred earlier or later than predicted. The same techniques used in the previous study was used here. Results demonstrated that higher and lower predictability levels equally increase responses in V1, and we discuss a possible prediction-attention interaction. We, further, replicated the finding from the first study, showing that activity during visible and occlusion periods are similar. Additionally, a remarkable result of this study was the difference between the movement velocities. Fast motion consistently enhanced activity pattern in V1, compared to slow velocity. These findings suggested that V1 may be more promptly receiving feedback projections from V5 during fast motion, which could increase the response signal, whereas processing of slow motion would be taking longer to reach V5 and reach V1 back. This relationship of V1 and V5 as a function of velocity was investigated in third study.

Chapter 4 reports a TMS (Box 5) experiment, which investigated the role of V1 in velocity discrimination under the dynamic parallelism hypothesis, which postulates that V1 may be engaged in the processing of slow, but not necessarily fast velocity. If this theory proves correct, we would expect that disruption of V1 impairs the discrimination of slow velocity compared to a baseline velocity, while no impairment would be observed during discrimination of fast and baseline velocities. Here we used a simplified velocity discrimination paradigm with a robust within-subject stimulation approach. A double-pulse TMS was delivered to V1 as real and SHAM stimulation. In

addition, we stimulated V5 using the same paradigm – due to its engagement in the processing of motion – in order to directly compare the influence of both areas in the processing of velocity discrimination. Results indicated that stimulation applied to V1 and V5 did not yield difference in velocity discrimination, thus, lacking evidence to support the hypothesis of the dynamic parallelism. Reasons for this outcome is extensively discussed in this chapter.

Chapter 5 compiles the findings from the three studies and discuss them, relating to the past studies and future perspectives of the prediction and motion extrapolation domains. In sum, the results of our studies shed light to the field of motion extrapolation, proposing that spatial information during visible and partially occluded stimulations is represented similarly in low-level visual areas, as well as temporal information.

Chapter 2 - Seeing and Extrapolating motion trajectories share common informative activation patterns in the primary visual cortex

Abstract

The natural environment is dynamic and moving objects become constantly occluded, engaging the brain in a challenging completion process to estimate where and when the object might reappear. Although motion extrapolation is critical in daily life – imagine crossing the street while an approaching car is occluded by a larger standing vehicle – its neural underpinnings are still not well understood. While the engagement of low-level visual cortex during dynamic occlusion has been postulated, most of the previous group-level fMRI-studies failed to find evidence for an involvement of low-level visual areas during occlusion. In this fMRI-study, we therefore used individually-defined retinotopic maps and multivariate pattern analysis to characterize the neural basis of visible and occluded motion in humans. To this end, participants learned velocity-direction pairings (slow motion-upwards; fast motion-downwards or vice versa) during a training phase without occlusion and judged the stimulus direction, based on its velocity, during a following test phase with occlusion. We find that occluded motion direction can be predicted from the activity patterns during visible motion within low-level visual areas, supporting the notion of a mental representation of motion trajectory in these regions during occlusion.

Introduction

 In our daily life, we often miss critical input from our visual environment: simple eye blinks, occlusion of moving objects and other internal and external disruptive changes may fragment part of the incoming information. The human brain has evolved to make adequate inferences about these missing inputs (for review, see e.g. Thielen et al., 2019). For instance, when driving or crossing a street, we are able to estimate the time when a vehicle will reappear, after being occluded by a bus, to plan our next action accordingly, which indicates that we can successfully infer the reappearance of a dynamically occluded object (e.g. Coull et al., 2008, Dittrich & Noesselt, 2018). Although such inference mechanisms underpin many actions of our daily life, little is known about their exact neural representations and their informational content. In this study, we used brain imaging to identify the low-level visual regions instrumental in the processing of dynamically occluded objects. In particular, we use fMRI (Box 3) and MVPA (Box 4) to compare the encoding of occluded and visible information in individually-defined low-level visual regions.

Engagement of low-level visual areas in processes related to motion prediction remain ambiguous. For instance, a recent fMRI study (Ekman, Kok & de Lange, 2017) on *apparent* motion reported that enhanced fMRI-responses in V1 could be triggered by the sole presentation of the first stimulus of a series of spatially-distinct flashes. Remarkably, V1 activity resembled the entire stimulus sequence even though the subsequent visual input was not present. In addition, the activity pattern during prediction was temporally compressed, suggesting that V1 anticipates the presence of the expected targets. In the realm of *continuous* motion extrapolation, behavioural studies also suggest the engagement of V1 during dynamic occlusion of a moving object; and several hypotheses have been proposed to account for the mechanisms underlying motion prediction. One of the most common hypotheses postulates that time-to-contact (TTC, DeLucia & Liddell, 1998) estimation of the occluded object would engage early stages of visual processing by using a mental representation of the visual trajectory (de'Sperati & Deubel, 2006; Battaglini et al., 2014) and memory of temporal information acquired during watching the visible trajectory (Pasternak & Greenlee, 2005; Khoei et al., 2013; Makin et al., 2008; Makin & Bertamini, 2014; Makin & Poliakoff, 2011; Battaglini et al., 2013). Additionally, enhanced attentional resource allocation was already observed at locations that contain temporarily occluded moving targets in behavioural studies (Scholl & Pylyshyn, 1999; Flombaum et al., 2008). In accord, an anisotropic distribution of representational enhancement was found in the direction of predicted motion (Verghese & McKee, 2002; Atsma, Koning & van Lier, 2012; Frielink-Loing, Koning, van Lier, 2017). Importantly, such attentional extrapolation can usually only be observed with a very low number of simultaneously

relevant trajectories (Keane & Pylyshyn, 2006; Zhong, et al., 2014; Vul, et al., 2009). These behavioural studies all show modulations along a spatial gradient relative to the location of the extrapolated object, thus pointing at an involvement of retinotopically organized areas, i.e. low-level visual regions, in motion extrapolation.

In contrast, previous fMRI-studies focusing on the neural underpinnings of occluded moving objects often failed to observe evidence for the involvement of low-level visual areas and rather observed a recruitment of parietal regions especially intraparietal sulcus (IPS), (Shuwairi et al., 2007; O'Reilly, Mesulam, & Nobre, 2008); or reported decreased fMRI-signals in these regions instead (Olson et al., 2003). An alternative hypothesis, in accord with this reduction of fMRI-signal in low-level visual areas, would be that inference of predictable trajectories reduce neural activity, similar to signal decrease in other highly predictable environment in a variety of tasks (Alink et al., 2010, Krala, et al., 2019, van Heusden et al., 2019). This hypothesis is in line with Rao and Ballard's (1999) hierarchical predictive coding model, which postulates that feedback and feedforward connections convey predictions to lower levels and error estimates to higher levels, respectively, and that deviations from a predicted outcome would lead to enhanced signalling in low-level areas. Another reason why many of previous fMRI-studies on the neural basis of motion extrapolation may have failed to observe the involvement of low-level visual areas may be grounded in conceptual and methodological issues. The exact anatomical location of functionally distinct visual areas is highly variable across humans (Greenlee, 2000; Amunts, 2000), hence, any effects may be diminished when using standard voxel-based group mean analyses, as it was done by most previous investigations (Olson et al., 2003; Shuwairi et al., 2007; O'Reilly et al., 2008). So far, there are few studies which investigated dynamic occlusion used retinotopic maps to identify subject-specific regions of interest and observed modulations of fMRI-signal in low-level visual areas. Recently, Erlikhman and Caplovitz (2017) used subject-specific retinotopic mapping to identify subject-specific the primary visual cortex together with multivariate pattern analysis (MVPA) to test whether differences in the shape of dynamically occluded objects moving along a single trajectory are already decodable in low-level visual areas. The authors reported enhanced activation in V1 during occlusion, but failed to observe evidence for the objects' shape in the activity patterns in this region.

To our knowledge, no study so far investigated whether the neural representation of different extrapolated trajectories can already be decoded in low-level visual areas. Therefore, the main aim of this study was to differentiate patterns of activity in individually defined low-level visual cortex for different visible and occluded trajectories during the presentation of dynamically occluded stimulus. To this end, we employed a prediction motion paradigm (Box 1; Hecht &

Savelsbergh, 2004, Battaglini & Ghiani, 2021), where participants learned specific motion velocity-trajectory associations during an initial familiarisation phase based on visible motion and had to judge time- and point-of-contact during a test phase in which the motion was dynamically occluded. We further employed a subject-specific ROI-based multivariate pattern analysis investigating systematic BOLD modulations within low-level visual cortex associated with the spatial trajectory of occluded and visible targets. Focusing on V1, we tested whether changes in the V1-activity pattern are predictive of the stimulus trajectory during occlusion. In addition, we tested for similarities in informational content during visible and dynamically occluded stimulation, not only in V1, but also in neighbouring regions V2 and V3, plus within regions which have been related to motion processing (V5) and object identity (LO1, LO2) using probability maps of these regions. We hypothesised that a spatially-specific mental representation of different trajectories should result in an engagement of low-level visual areas, especially V1, during the occlusion phase. We also hypothesised that the activation pattern during the visible and dynamically occluded stimulus motion periods should be similar in low-level visual areas. Finally, we tested for the spatial layout in the modulated subregions of low-level visual areas using receptive field mapping. To anticipate, classification analyses yielded above chance accuracies already in the primary visual cortex when the classifier was trained on the visible data and tested on occluded data. The patterns of predictive informational content were highly similar to the pattern observed for visible trajectories and this result was further corroborated by visual field mapping.

Material & Methods

Participants

Twenty-two right-handed participants (mean age=24.45, ±4.47, 14 women), with normal or corrected-to-normal vision, no history of psychiatric or neurological disorders and no regular intake of medications known to interact with central nervous system functions were recruited from the student community of Otto-von-Guericke Universität Magdeburg and gave informed consent to participate in the study, which was approved by the ethics committee of the Otto-von-Guericke-University. Participants could take part in the fMRI study only after successfully performing a velocity threshold determination task in a behavioural lab outside the scanner (see below for details). Six participants were excluded either due to poor performance during the main task (three with accuracy below 60%), absence on the last day of experiment (two participants) or poor quality of retinotopic mapping (one participant). The data of 16 participants (mean age=23.25, ±3.61, 12 women) were included in the final analysis.

General overview of the study design

The volunteers of this experiment performed a total of 8 tasks: a threshold determination task outside the scanner, one inside the scanner, twice familiarisation task with visible stimulation, twice prediction motion task with dynamically occluded stimulation, one independent functional localizer of the visual stimulation and a retinotopic mapping task. Here, we first present the chronological sequence of each task and below we describe the details of each paradigm. The first task was a behavioural threshold determination performed on a day prior to the scanning sessions, in which we ensured that participants could reliably perceive two different motion velocities. On day 1 of the scanning session, participants performed the same threshold determination task inside the scanner, to confirm the threshold of the previous session. This second threshold verification was followed by the functional localizer, and the first part of the main experiment (one session of familiarisation task followed by a session of the prediction motion task). On day 2, participants performed the second part of the main experiment (again one session of familiarisation followed by prediction motion task), and the retinotopic and receptive field mapping.

Behavioural threshold determination: pre-scan session

Participants were placed in a dark room, 70 cm from the monitor (a 22-in., 120 Hz, LCD Screen, Samsung 2233RZ, recommended for vision research; Wang & Nikolić, 2011). All tasks were programmed using Psychophysics Toolbox (Version 3; Brainard, 1997) and run in Matlab 2012b (Mathworks Inc., Natick, MA, USA). On each trial, a white dot (1.24° visual angle) moved from the left to the centre (-6° to 0°) of a black screen. First, we presented a standard velocity of 16°/s (duration=300ms) which was randomly followed by one of the 11 possible velocities (t=t+t*0.05)[1] including the standard velocity. The two moving stimuli were separated by an interstimulus interval (ISI) of 500 ms. Participants were instructed to keep their eyes fixed on the fixation cross (0.2°), attend to the movements and, after the disappearance of the second moving stimulus, to indicate whether the velocity of the second stimulus differed from the standard one. A total of 330 trials were presented divided in 6 blocks. The experiment lasted approximately 18 minutes. After the completion of the threshold experiment the data were fitted with a sigmoidal psychometric function (Curve Fitting Toolbox, Matlab, Mathworks Inc., Natick, MA, USA), and the time interval corresponding to 75% accuracy was estimated. This first task served to confirm that subjects were able to successfully discriminate velocities used in the main experiment. The same task was again

---

[1] The intervals used for slow stimulation were taken from the set of milliseconds: in degrees/second: {16, 15.23, 14.51, 13.8, 13.16, 12.53, 11.93, 11.37, 10.82, 10.31, 9.822}.

performed inside the scanner in order to verify the participant's threshold, which was used for all following prediction motion tasks inside the scanner.

Functional Localizer: Delineating low-level visual ROIs

The functional localizer was collected to identify areas in the visual cortex which responded to the visual stimulation used in our experimental runs and to later compare them with the location of the MVPA-spheres instrumental in motion extrapolation. We presented a high contrast checkerboard stimulus (1.6°) at seven different positions along the trajectories used in the main experiment (~6.2°, ~3.1°, ~0°, horizontally and ~6.2° and ~3.1° vertically up- and downwards, while participants were asked to maintain fixation. The fixation cross (0.26°) was placed 14.2° to the right side of the stimulus central position. The stimulus flashed for 160ms, with an ISI that could vary from 2 to 6 seconds (Poisson-distributed) for 25 s at each position. Participants were asked to covertly attend the stimulation while keeping their eyes on the fixation cross. Fourteen blocks were separated in two runs, lasting in total approximately 7min20sec to complete the session.

Visible Phase: Association Learning during Visible Stimulation

During this initial association-learning phase, participants performed a PM task (Box 1) and got familiarised with the main task by passively observing a stimulus moving first horizontally and then vertically on the screen (see Fig.1A). To this end, we used two velocities (fast = 300 ms, 20°/s or slow = individual participant's threshold, on average 443.82 ms, ±24.20 ms or 14°/s) which were paired with two trajectories (upward or downward), leading to a 2 x 2 design with 4 possible combinations (order 1: up-fast, down-slow; order 2: down-fast, up-slow). The moving object consisted of a white dot (1.6°) moving from the left side of the screen to the centre (horizontal: 6.2° to 0°), then from the centre to the bottom (vertical: 0° to -6.2°) or top (vertical: 0° to +6.2°) of the screen. The stimulus was visible during the whole motion (in contrast to the occluded phase, see below). Participants completed a total of 100 trials divided into five runs, which in total lasted around 10 minutes. The ISI varied from 2 to 6 seconds (Poisson-distributed). No information about the velocity-direction association was provided to participants. The order of velocity-direction association was reversed on day 2 and the starting order was counterbalanced across subjects.

Participants were instructed to just observe the moving stimulus on the screen, with no further instruction for not priming them in any way. After the second run, we asked them, first, whether they had observed any regularities and, second, if they observed differences related to the direction-velocity information. We expected them to report the correct association (e.g. "when the dot moves fast it goes upward and when it moves slowly it goes downward", or vice versa). If

the participants didn't report this relationship after the second run, they would be asked again[2] after the next run. All participants completed a total of 5 runs of familiarisation.

Occluded Phase: Prediction of Dynamically Occluded Stimulation

Experimental set-up during testing was identical to the visible with the following exceptions: the moving stimulus was visible only during the horizontal movement and a grey rectangle (28.4° in width and 35.6° in height) was displayed during the whole run occluding the vertical trajectories. The respective end positions of the occluded vertical movements were marked by an "X" (1.6°) and the dot did not reappear. Participants performed a time and point of contact, i.e. prediction motion task. For this they were asked to respond when the moving stimulus would reach the top or bottom "X" mark (see Fig. 1B) and to indicate which of the two positions would be reached by pressing one of two buttons with their right index and middle finger. A total of 240 trials were presented divided in six runs. This experiment lasted approximately 33 minutes.
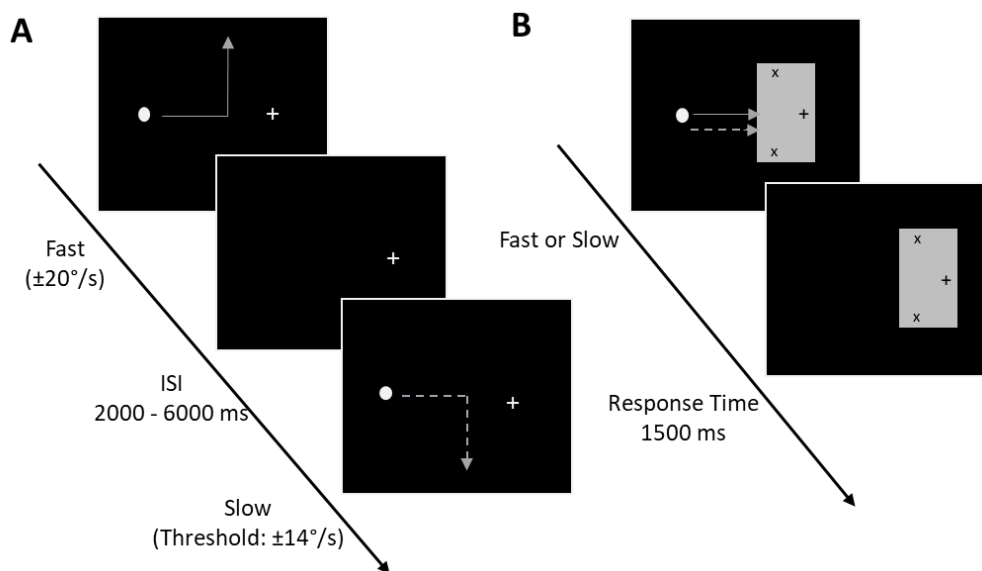
Figure 2 - Display of the visual stimulation of the main experiment. (A) Visible Phase: Sequence of two trials observed by the participants. A white dot moved from the left side of the screen to the centre, then upwards or downwards as indicated by the arrows. The direction of the trajectory depended on the velocity of the dot here indicated by different types of line (solid and dashed). The full line represents fast movement and dashed line, slow movement. The lines are put here for illustrative purposes only, but were not displayed during the task. (B) Occluded Phase: The horizontal trajectories remained visible while vertical trajectories were occluded by a grey rectangle present during the whole trial. The "X" marks represented the stimulus final positions presented in the visible phase. Participants judged the time-to contact and the point-of-contact that the stimulus would reach using the velocity information acquired during the visible horizontal movement.

---

[2] All participants were able to report the association after the third run. Some didn't understand exactly what they had to report after the second run. However, after observing the third run, they all reported the correct association.

Retinotopic Mapping Phase

Seventeen participants were scanned in two sessions (nine participants performed the session on separate days due to maximal scanning time restrictions). The procedure used for measuring the retinotopic maps was adapted from Warnking et al. (2002) and Bordier et al. (2015). Stimuli were presented on a grey background. Visual eccentricity was mapped using a checkerboard ring which slowly contracted or expanded from the fixation dot. The speed of the expansion and the contraction varied linearly with the eccentricity (Bordier et al., 2015) and the ring reached a maximum diameter eccentricity of 6.6° and a minimum of 0.2°. When the maximum (expansion) or the minimum (contraction) was reached, a new ring would start from the original position. Polarity was mapped using one checkerboard wedge (10°) slowly rotating at a constant speed. Specific stimulation parameters were similar as the ones described by Warnking and colleagues (2002): the checkerboard stimulation flickered at a frequency of 8 Hz, in 10 cycles of 36 s each. The aspect ratio of the checkboards was kept constant (1.09) by scaling the height linearly with the eccentricity. In order to account for the effects of the hemodynamic signal, the wedges were presented clock- and counter-clockwise, and the rings were presented expanding annuli and contracting annuli (Warnking et al., 2002). In total, eight functional runs were acquired, two for each modality and direction, in two days, which in total lasted around 24 minutes per day.

fMRI Experiment

The scanning sessions were conducted in a 3 Tesla Siemens PRISMA MR-system (Siemens, Erlangen, Germany), using a 64-channel head coil. The data of participants were acquired in 26 functional runs divided into two sessions, i.e. 210 volumes for the localization phase, 550 volumes for the visible phase and 1920 volumes for the occluded phase. Blood oxygenation level-dependent (BOLD) signals were acquired using a multi-band accelerated T2*-weighted echo-planar imaging (EPI) sequence (multi-band acceleration factor 2, repetition time (TR)=2000 ms, echo time (TE)=30 ms, flip angle=80°, field of view (FoV)=100 mm, voxel size=2.2 × 2.2 × 2.2 mm, no gap). Volumes were acquired in interleaved order. Identical slice selection on both days was achieved using the Head Scout Localizer which calculation is based on Autoalign (Siemens, Erlangen). Participants were placed inside the scanner and performed all tasks described above. Note that for threshold determination no fMRI data were collected. All visual stimuli were displayed on a rear-projection screen (302x170), approximately 350 mm from their eyes (± 10 mm depending on participant's head size). Participants were asked to fixate on a cross (1.6°) and covertly attend to the stimuli. Fixation was controlled online during the whole fMRI-experiment using a fibre-optic camera (Kanowski et al., 2007).

In addition to the functional data a high-resolution three-dimensional T1-weighted anatomical map (TR = 2500 ms, TE = 2.82 ms, FoV = 256 mm, flip angle = 7°, voxel size = 1 × 1 × 1 mm, 192 slices, parallel imaging with a GRAPPA factor of 2, and 8 min scan duration) covering the whole brain was obtained using a magnetization-prepared rapid acquisition gradient echo (MPRAGE) sequence. This scan was used as a reference image to the EPI data during coregistration procedure and used as an overlay for the retinotopic and functional maps after inflation.

Retinotopy

Blood oxygenation level-dependent (BOLD) signals were acquired using a multi-band accelerated T2*-weighted EPI sequence (multi-band acceleration factor 2, TR=2000 ms, TE=30 ms, flip angle=90°, FoV=128 mm, voxel size=2.2 × 2.2 × 2.2 mm, no gap). For each run, 180 volumes were acquired in interleaved order.

A high-resolution three-dimensional T1-weighted anatomical map was obtained only for the occipital lobe (TR=2500 ms, TE=2.82 ms, FoV=256 mm, flip angle=7°, voxel size=1 × 1 × 1 mm, 192 slices, parallel imaging with a GRAPPA factor of 2, and 8 min scan duration) using a magnetization-prepared rapid acquisition gradient echo (MPRAGE) sequence. This scan was used as anatomical reference to the EPI data during the registration procedure.

Statistical Analysis

Behaviour

Subjects' temporal and spatial estimates of target stimulation were measured by subjects' response time after stimulus occlusion and correct prediction of vertical direction (accuracy), respectively. Missed trials, trials with RT smaller than 0.1 s and greater than the mean + 3 std were excluded from the analysis. In addition, we calculated the temporal estimation error by taking the difference between the amount of time the stimulus travels behind the occluder and participants' response time. We used a 2x2 repeated measures ANOVA (direction x velocity) for investigating differences in accuracy, response time and temporal estimation error. All analyses were calculated using JASP (v. 0.15.0, https://jasp-stats.org/). JASP was also used to compute post hoc tests (simple main effects function) and effect size (partial η2).

Retinotopy

A three-dimensional reconstruction of the cortical sheet based on the structural image of each of the 16 subjects was performed using the recon-all function of Freesurfer

(https://surfer.nmr.mgh.harvard.edu/). Retinotopic maps along the polar and eccentricity dimensions were calculated for each of the cortical surfaces using the "selxavg3-sess" function of Freesurfer. The right-hemispheric low-level visual areas V1, V2, V3 were delineated manually on the flattened cortical sheets based on the boundaries of phase reversals within the polar angle maps (Abdollahi et al. 2014). Delineation of borders were created based on of Georgieva et al. (2009) and Kolster et al. (2010). Based on these delineations, we created six masks of V1, V2 and V3 for upper and lower visual areas, which later was used to identify region-specific local maxima during the visible and occluded phase. Probabilistic maps of MT and LOs as provided by Freesurfer parcellation for each subject were included in the analyses. Freesurfer labels were converted to volume ROIs based on Freesurfer mri_vol2roi function. LO masks were separated in LO1 and LO2 using Georgieva et al. (2009) and Kolster et al. (2010) delimitations. Results of the LO and MT ROIs can be found in the appendix A.

fMRI preprocessing

Participants' data from both days were analysed using SPM12 (www.fil.ion.ucl.ac.uk/spm, Wellcome Trust Centre for Neuroimaging, London, UK). The first five volumes of each run were discarded to allow for steady state magnetization. Functional images were slice-timing corrected and spatially realigned (registered to the mean image). Head motion parameters were later used as nuisance regressors in the general linear model (GLM). Finally, the structural image was coregistered (estimate and reslice) to first functional image of the first run. Resliced images were smoothed with a gaussian kernel of 6 mm.

fMRI data Modelling

The participants' functional data of day 1 and day 2 for each task were modelled with a single general linear model (GLM, Friston et al., 1995), which included the run-wise condition parameters, derivatives, and six motion regressors as nuisance covariates. In particular, regressors of each condition (up-fast, down-slow, up-slow, down-fast or up-slow, down-fast, up-fast, down-slow) were specified by using canonical hemodynamic response function (HRF). Temporal and dispersion derivatives of each regressor were added to the model in order to account for variability in the onset response (Friston et al., 1998). From the condition-specific maps of beta weights averaged across runs of each participant, we extracted beta weights from subject-specific V1, V2, V3 (see below for details of retinotopic analysis) for the univariate group analysis using MarsBar 0.44 (Brett, et al., 2002). A 2x2x2x3 repeated measures ANOVA was calculated with the factors: direction (upward, downward), velocity (fast/slow), visual region quadrants (VQ; upper/lower) and visual

regions (V1, V2, V3) for both visible and occluded phases, followed by post-hoc analyses, when necessary.

Multivariate Pattern Analysis

In order to complement the univariate analysis, we executed a series of multivariate pattern analyses, using CoSMoMVPA (Oosterhof et al., 2016), designed to identify whether patterns of activity during visible stimulation can be used to accurately classify the patterns of activity during occlusion. To this end, we performed volume-based searchlight analyses with a 4.4 mm radius using run-wise beta weights (proportional to percent signal change), in native space for each condition, as datasets (two beta-values per run: one for each condition). Searchlight analyses were chosen to retain a high spatial specificity. In particular, a linear discriminant analysis (LDA) classifier was trained in the 10 runs of the visible phase (20 beta values), using a leave-one-run-out approach, and tested in the 12 runs of the occluded phase (24 beta values). As sanity checks, the classifier was also trained and tested on the runs of visible only and occluded only, using n fold partitions. As a further manipulation check, the classifier was also trained and tested on motion velocity (see Appendix A for this last sanity check).

We carried out one searchlight analysis per region of interest (upper and lower V1-V3 etc.), to increase the spatial specificity to the classification and to be able to draw conclusions per functional region. For each searchlight within a given region one accuracy value was obtained. We focused the analysis on the specific spheres inside the ROIs which contained informative voxels and, for that, we adopted a thresholding procedure. We applied a cut-off allowing only values above 0.5 to be in the analysis, excluding chance level spheres, as we predicted that only a restricted number of searchlight spheres would contain meaningful information, and computed the average of the 5% highest accuracy values of the distribution. Hence, by using an information-based rather than a visual-localizer based criterion, we ensured to have a spatially unbiased selection criterion (see below next section 4.6. for an independent assessment of this novel thresholding approach introduced here).

To evaluate the statistical significance for each ROIs, permutation tests was carried out for each subject. The permutation included 1,000 iterations which contained randomised data labels per run, keeping the same original dataset. For a spatially accurate comparison, we obtained the accuracy value from the same searchlight spheres included in the 5% highest accuracy sample, for all 1000 samples for each individual person. The 5% maximum values were averaged across spheres for the original and permuted dataset permutation. For group level analysis, we followed the Etzel (2017) approach. The null distribution contained the average across participants for each of the

1000 permutations with the addition of the true-labelled group-level average, resulting in 1001 group-level accuracies. The permutation p value was computed by taking the sum of the permuted accuracies higher or equal to the true-labelled accuracy and dividing by the number of iterations plus 1.

Projecting the spatial layout of MVPA-results on visual field maps

By utilizing the well-established knowledge that low-level visual cortex is spatially organised, we tested whether the searchlight spheres with the highest decoding accuracy were overlapping across the independent statistical tests (decoding of visual motion, occluded motion and occluded motion by visual motion). The rationale behind that was to confirm whether the regions inside each visual area, which encoded trajectory information, were common across visible and occluded phases. To this end, statistical maps were first projected onto the flattened cortical sheets. Based on the specific polar and eccentricity maps, each vertex of the univariate and multivariate result maps could be associated with a specific location within the visual field and later be overlaid for comparison. Hence, in addition to showing flattened anatomical maps, visual field maps were used as well for a standardized projection of the results independent on individual cortical sheets. We restricted this analysis to lower and upper V1, as these regions contain neurons with the smallest receptive field size (Barbot et al., 2021). An overlap of significantly modulated spheres would suggest at least spatial proximity during the processing of the visible stimuli and during visual extrapolation. To further corroborate these findings, the univariate results of the functional localizer phase (contrast: up vs down condition) were also overlaid, to confirm independently that the regions containing patterns of significant MVPA-results were in close proximity to the areas responding to visual stimulation in the independent functional localizer.

Results

Behavioural results

Spatial Estimation (Where): After the visible phase, we expected the participants to accurately indicate the motion direction according to the velocity-direction association. Results corroborate our expectations, indicating that participants had very high-performance accuracy (Figure 3.A). Group averages for all occluded conditions were above .92 accuracy (up-fast: mean (M)=.951, ±.035; up-slow: M=.969, ±.025; down-fast: M=.923, ± .070; down-slow: M=.952, ±.039). Main effects of direction and velocity were not significant ($F_{(1,15)}$=3.734, p=0.072, η^2 =.199; $F_{(1,15)}$=3.851, p=0.069, η^2=.204, respectively). No interaction between factors ($F_{(1,15)}$=.318, p=.581, η^2= .021) was observed. These non-significant differences across conditions observed here

may suggest that the association learning had the same level of difficulty independently of direction and velocity.

Temporal Estimation (When): Participants showed a high consistency in their time estimation (Figure 3.B): Average response times (RT) were consistent with physical stimulus velocity, i.e. the time-to-contact in the slow condition was estimated to be later than the fast condition (up-fast: M=.528, ±.154; up-slow: M=.694, ±.244; down-fast: M=.566, ±.114; down-slow: M=.654, ±.247). Accordingly, a main effect of velocity ($F_{(1,15)}$=8.704, p=.010, η^2=.367) was observed. No significant main effect was found for direction ($F_{(1,15)}$=.003, p=.957, η^2=.000), as well as no interaction between factors ($F_{(1,15)}$=1.059, p=.320, η^2=.066).

Temporal Estimation Error: Figure 3.C shows similar estimation errors across all conditions (up-fast: M=.228, ±.154; up-slow: M=.250, ±.241; down-fast: M=.266, ±.114; down-slow: M=.211, ± .243). In accord, no significant main effect for direction ($F_{(1,15)}$=.003, p=.957, η^2=.000) or velocity ($F_{(1,15)}$=.157, p=.698, η^2=.010), and also no interaction ($F_{(1,15)}$=1.059, p=.320, η^2=.066) was observed.

The results above indicate that, at the behavioural level, participants accurately estimated the stimulus end position, as well as time-to-contact, the latter with a certain yet consistent bias from the reality across all conditions (temporal overestimation).
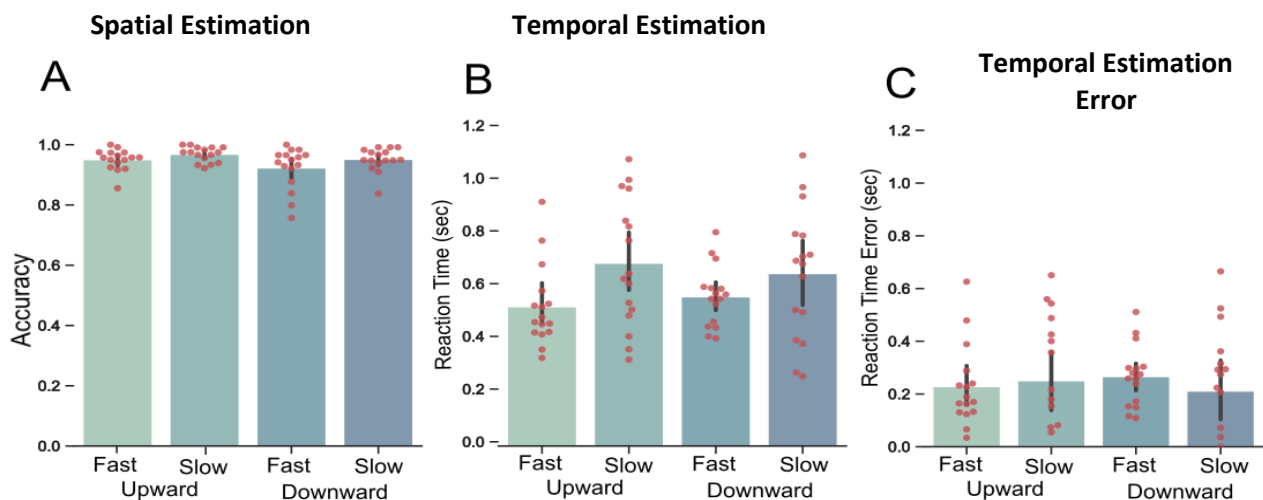
Figure 3 - Behavioural results. In all bar graphs (from left to right), light green bar (1st bar) depicts fast condition, darker green (2nd bar) slow condition in upward direction, light blue bar (3rd bar) depicts fast condition and dark blue bar (4th bar) slow condition in downward direction. Red dots superimposed on each bar represent behavioural results of all individual subjects. (A) Group average accuracy for spatial estimation. (B) Group average reaction times for temporal estimations. (C) Group average reaction times for temporal estimation error (difference between physical stimulus displacement time and estimated time).

Univariate fMRI-results

Subject-specific level

In the first analysis step, we identified modulations in fMRI signal for each individual participant using univariate analysis. Comparisons of the trajectories (upward vs. downward) revealed significant patterns of activity in regions representing upper and lower visual quadrants contralateral to the stimulated hemifield, as expected (see Fig. 4 for an exemplary subject; all other subjects can be found in the Appendix A, Figure 1). In contrast, the comparison of speed levels (fast vs. slow) did not yield any significant modulations of fMRI signals in low-level visual areas.
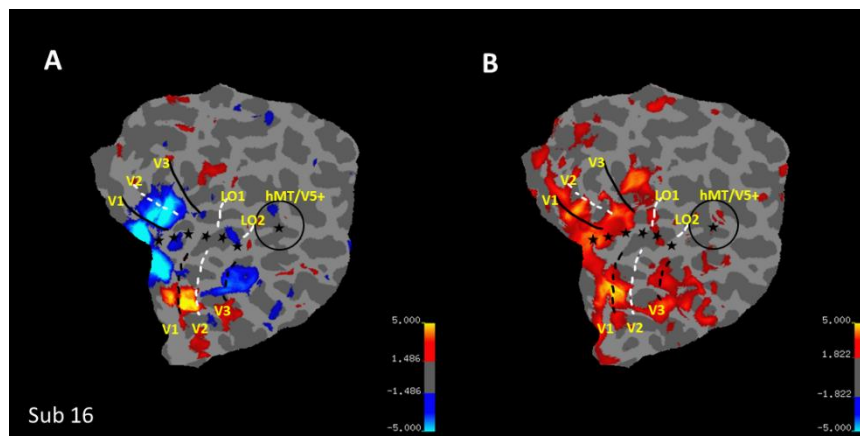
Figure 4 – Univariate analysis results of an exemplary participant during (A) Visible Phase and (B) Occluded Phase, for contrast between upward (warm colours) vs. downward (cold colours) projected on the individual flat map. Retinotopic map delimitations are indicated by stars (central visual field), plus white and black full and dashed lines indicating borders between visual fields (Abdollahi et al., 2014). Results from other participants can be found in the appendix A, Figure 1.

Group level

Statistical comparison of univariate Modulations during Visible & Occluded Phases: From all low-level regions of each individual participant based on retinotopic masks, we extracted beta weights during the visible phase from the local maxima and averaged them across participants (Fig. 4A). To test – in a first manipulation check – if we would be able to differentiate upward and downward trajectories of visible stimuli in V1-V3, we then statistically compared these beta weights. During the presence of the target moving upward in the visible phase, *lower V1, V2 and V3* showed enhanced fMRI-signals compared to downward movements (lower V1-upward: M=8.376, ±3.845 vs. downward: M=2.985, ±2.818; V2-upward: M=7.081, ±3.880 vs. downward: M=1.868, ±2.092; V3-upward: M=6.450, ±3.165 vs. downward: M=1.998, ±2.010), as shown by the paired one-tail Student's T-tests (upward > downward: $t(15)=7.534$, $p_{holm}<.001$; $t(15)=6.655$, $p_{holm}<.001$; $t(15)=5.998$, $p_{holm}<.001$, respectively). During downward movements in *upper V1* compared to

upward movements the analysis revealed similar results (upper V1-downward: M=11.797, ±5.845 vs. upward: M=3.773, ±3.738; V2-downward: M=9.418, ±4.229 vs. upward: M=1.749, ±2.251; V3-downward: M=7.788, ±3.162 vs. upward: M=1.381, ±2.457), (V1-; V2-; V3-), , as revealed by the paired one-tail Student's T-tests (downward > upward: $t(15)=7.944$, $p_{holm}<.001$; $t(15)=6.902$, $p_{holm}<.001$; $t(15)=8.653$, $p_{holm}<.001$, respectively). Together, these findings show that the visual stimulation was salient enough to elicit differential fMRI-signals in accord with motion direction.

The identical locations independently identified during visible stimulation (see above) were then used to analyse activation patterns during occlusion. During the occluded phase, a pattern similar to the visible phase was present for the lower VF (Figure 4B): When participants were asked to temporally and spatially estimate upward movements, enhanced fMRI-signals compared to downward movements were observed in *lower V1* (lower V1-upward: M=16.834, ±6.225 vs. downward-: M=15.696 ±6.428; V2-upward: M=13.057, ±7.234 vs. downward: M=11.806, ± 6.725; V3-upward: M=10.283, ±6.777 vs. downward: M=8.997, ±6.381). Statistical analyses revealed significant differences in all three regions (upward > downward: $t(15)=2.261$; $p_{holm}=.040$; $t(15)=1.990$, $p_{holm}=.040$; $t(15)=2.919$, $p_{holm}=.015$, respectively). Unexpectedly, higher response during upward movements was also registered in the *upper V1* (upper V1-upward: M=21.027, ±11.401 vs. downward: M=20.435, ±10.059); however, this difference was not significant (downward > upwards: $t(15)=-0.851$; $p=.796$). In contrast, we found the hypothesised pattern for upper V2 (upper V2-upward M=14.174, ±5.896 vs. downward: M=14.891, ±5.061) and V3-upward: M=12.426, ±8.558 vs. downward: M=12.986, ±8.072). Yet, these results were not significantly different (downward > upwards – upper V2: $t(15)=1.023$, $p=.161$; upper V3: $t(15)=-0.677$, $p=.254$).

Unfolding interaction between factors: While the t-tests above were pre-planned to directly test our main hypothesis, below we extend our analysis by including the factor velocity, visual area (V1, V2, V3) and visual quadrant (upper VQ = upper V1-3; lower VQ = lower V1-3) using repeated measures ANOVAs. In the visible phase statistical analysis revealed significant interaction between direction and VQ ($F(1,15)=131.862$, $p<.001$, $\eta^2=.898$), plus velocity and direction ($F(1,15)=5.582$, $p=.032$, $\eta^2=.271$) and velocity and VQ ($F(1,15)=30.566$, $p<.001$, $\eta^2=.671$). Post-hoc tests confirmed that fMRI-responses, due to downward direction, were higher than upward direction in the upper VQ (MD= -7.367, SE=.672, t=-10.962, $p_{bonf}<.001$) and responses due to upward directions were higher in the lower VQ compared to downward direction responses in these regions (MD=5.019, SE=.672, t=7.468, $p_{bonf}<.001$), confirming the above t-tests. In addition, slow motion resulted in significantly higher fMRI-signals in upper relative to lower visual quadrant; while no such effect was seen for fast motion (VQ *velocity - slow in upper VQ vs. slow in lower VQ: MD=5.940, SE=0.589, t=4.991, $p_{bonf}<.001$) and the slow motion also differed for upward vs.

downward direction, while no such effect was observed for fast motion (direction*velocity: up-slow vs. down-slow: MD=-2.185, SE=.586, t= -3.726, p_{bonf} =.005). Finally, the distinct pattern of responses yielded main effects for direction (F(1,15) = 8.575, p=.010, η^2=.364), VQ (F(1,15)=5.744 , p=.030, η^2=.277, and visual areas (F(1,15)=9.327, p<.001 , η^2=.383) with higher responses for the downward vs. upward direction, higher responses for upper VF field than lower VF and enhanced responses in V1 compared to V2 (MD=1.704, SE=.558, t=3.053, p_{bonf}=.014) and to V3 (MD = 2.328, SE = .558, t=4.172, p_{bonf} =<.001).

During the occlusion phase, statistical analysis again revealed interactions between direction and VQ (F(1,15)=5.331, p=.036, η^2=.262), supporting the t-test results, direction and velocity (F(1,15)=32.746, p<.001, η^2=.686), velocity and visual areas (F(1,15)=5.371, p=.010, η^2=.264), plus a triple interaction between direction, velocity and visual areas (F(1.22,18.4)=19.087, p<.001 (Greenhouse-Geisser-corrected), η^2=.560). A Post-hoc comparison for the hypothesized interaction indicated marginally significant results for downward motion in the lower visual quadrant compared to upper visual quadrant (MD=3.938, SE=1.412, t=2.788, p_{bonf} =.077). In addition, post-hoc tests for interaction of direction and velocity revealed that fast motion led to enhanced responses compared to slow motion in the upward direction (MD=5.129, SE=1.280, t=4.006, p_{bonf}=.003), while no significant effect for fast vs. slow motion was observed for the downward direction. Post-hoc tests of velocity*visual areas revealed that fast responses compared to slow response were most prominent in V1, whereas the triple interaction with direction revealed that this elevation in V1 was highest for upward motion, while significant differences for downward motion was seen only in V1 compared to V3 for fast condition (see Appendiy A, Figure 2. Finally, main effects revealed results similar to the visible phase with upper visual regions eliciting higher responses than lower visual regions (F(1,15)=5.439, p=.034, η^2 = .266). Moreover, V1, V2 and V3 again expressed differential effects (F(1,15)=16.534, p<.001, η^2=.524). Comparisons showed that V1 presented higher beta values than V2 (MD=5.016, SE=1.302, t=3.851, p_{bonf} =.002) and V3 (MD=7.325, SE=1.302, t=5.624, p_{bonf} <.001).

Together, results of our univariate analysis indicated that activity in low-level visual regions was enhanced by direction at least in one of the VQ during occlusion phase, thus they do in part support our hypothesis. However, the absence of significant effects in one quadrant might be due to the lower sensitivity of univariate analysis approaches as it is well known that multivariate pattern analysis has a higher sensitivity than traditional univariate analysis. Moreover, MVPA allows for drawing conclusions about the representational content within activation patterns (Anzellotti & Coutanche, 2018). To test our research question even more thoroughly, we performed run-wise GLM analysis and used the resulting beta values as input to multivariate pattern analysis.

Multivariate Pattern Analysis results

A series of volume-based MVPA analyses was applied to test for pattern similarity between visible and partially occluded stimulation periods.

Classifying Direction Patterns of Visible from Occluded Phase: This classification analysis was most crucial to test our hypothesis for a common engagement of low-level visual cortex during the presentation of visible and dynamically occluded motion. It was performed with the main purpose of decoding similar activation patterns for visible and occluded phases in upper and lower V1-3. For these multivariate analyses, maps of beta weights for upward and downward motion were calculated run-wise separately for visible and occluded phase and used as input.
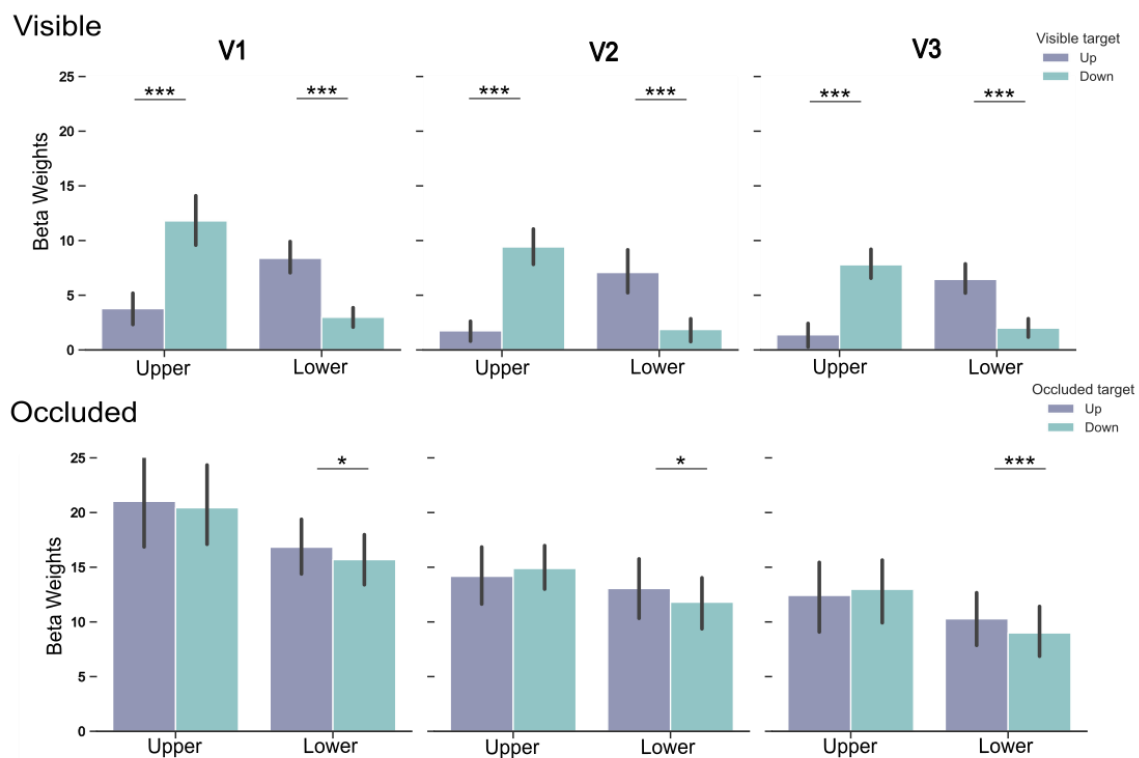
Figure 5 - Univariate beta weights (proportional to percent signal change) during visible phase (upper row) and occluded phase (lower row). Green bars depict average beta weights for downward trajectories, while purple bars average beta weights for upward trajectories. Stars indicate significance between conditions inside each region on interest.

Results (Fig.6 and table 1.A) show that direction-specific informational patterns from the visible phase could be used to decode informational patterns in the occluded phase in the lower AND upper V1, V2 and V3 significantly extending the results from the univariate analysis by showing

the similarity in spatial layout of the informational content of these two phases (see below for a more thorough description of the spatial layout within V1).

Classifying Direction Patterns from Visible & Occluded Phase: As manipulation checks, we performed MVPAs separately for the visible and occluded phase to check for reliability of the classification. For both phases we found direction-specific informational patterns of activity predicting motion trajectory. For these two separate analyses, we also expected accuracy values to be higher when the classifier was trained and tested in the visible phase, once the stimulus was all the time present. Indeed, results (Table 1.B) indicated higher accuracy values for visible phase compared to the cross-phase analysis and to the occluded phase analysis, and higher values of the latter compared to the cross-phase analysis (Fig.6). These results further confirmed that the classifier decoded the relevant direction-specific information and that the information was somewhat diluted during occlusion compared to visible stimulation.

A

DIRECTION	Quadrant	ROI	Accuracy	SE	Permutation p
		V1	0.602	0.005	< .001
	lower	V2	0.611	0.006	< .001
Visible-Occluded		V3	0.611	0.006	< .001
		V1	0.607	0.009	< .001
	upper	V2	0.597	0.006	< .001
		V3	0.608	0.007	< .001

B

DIRECTION	Quadrant	ROI	Accuracy	SE	Permutation p
		V1	0.862	0.022	< .001
	lower	V2	0.817	0.020	< .001
Visible		V3	0.804	0.022	< .001
		V1	0.863	0.019	< .001
	upper	V2	0.857	0.020	< .001
		V3	0.837	0.015	< .001
		V1	0.651	0.009	< .001
	lower	V2	0.660	0.009	< .001
Occluded		V3	0.671	0.010	< .001
		V1	0.668	0.013	< .001
	upper	V2	0.681	0.013	< .001
		V3	0.673	0.013	< .001

Above, we used averaged scores of accuracies across participants. For maximal transparency and to give the reader an impression of the interindividual variability, Fig. 7 shows the two relevant measures average decoding accuracies (top) and number of spheres for each ROI (from which average decoding accuracies are calculated, Fig. 7 bottom), for every subject. We observed a higher interindividual variability in decoding accuracy during the occluded phase, compared to the other phases. The number of spheres included in the 5% sample of most informative voxels adopted also varied across subjects, following a heterogeneous pattern, but did not show a bias towards one analysis. The average of spheres across the three analyses is 84.21 (±30.08) spheres.
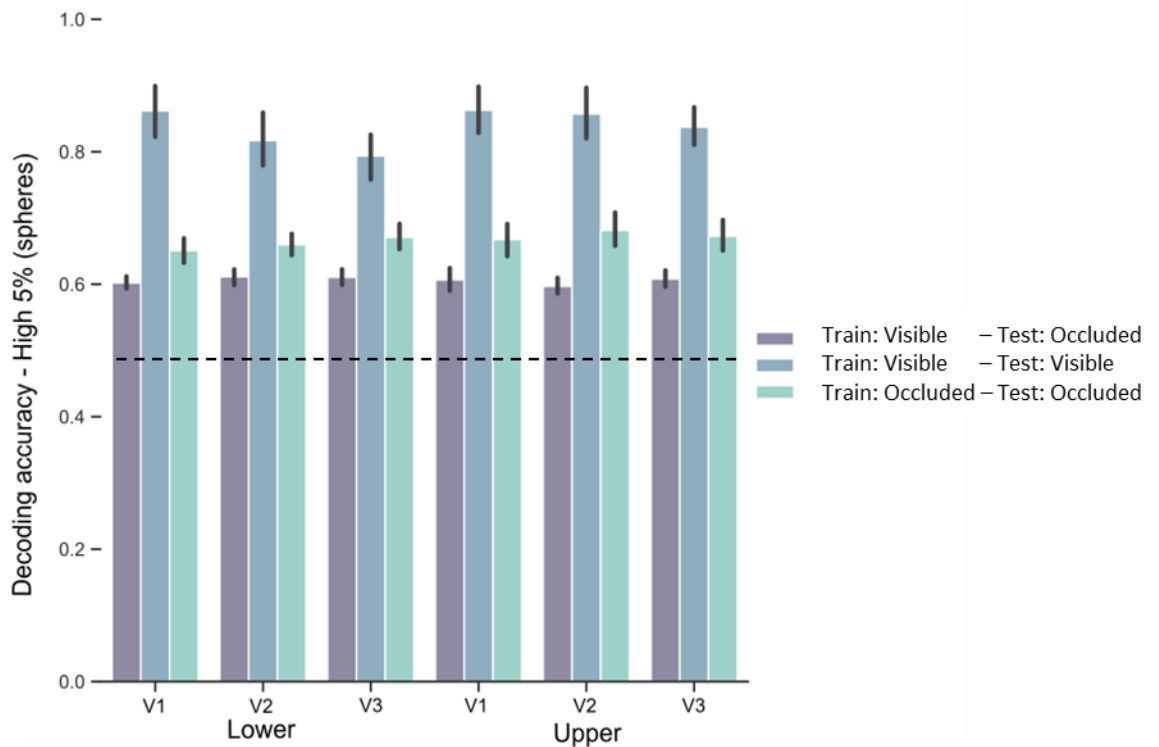
Figure 6 - Decoding accuracies for all classification analyses in upper and lower V1-V3. Dashed line depicts the theoretical chance level, though note that the chance level used for statistical testing was derived from permutations tests. Purple bars show average accuracies for the classification analysis trained on visible data and tested on occluded data. Blue bars show the accuracies for the classification analysis with training and testing the visible phase only and green bars depict average accuracies for the analysis using occluded data also during both training and testing.
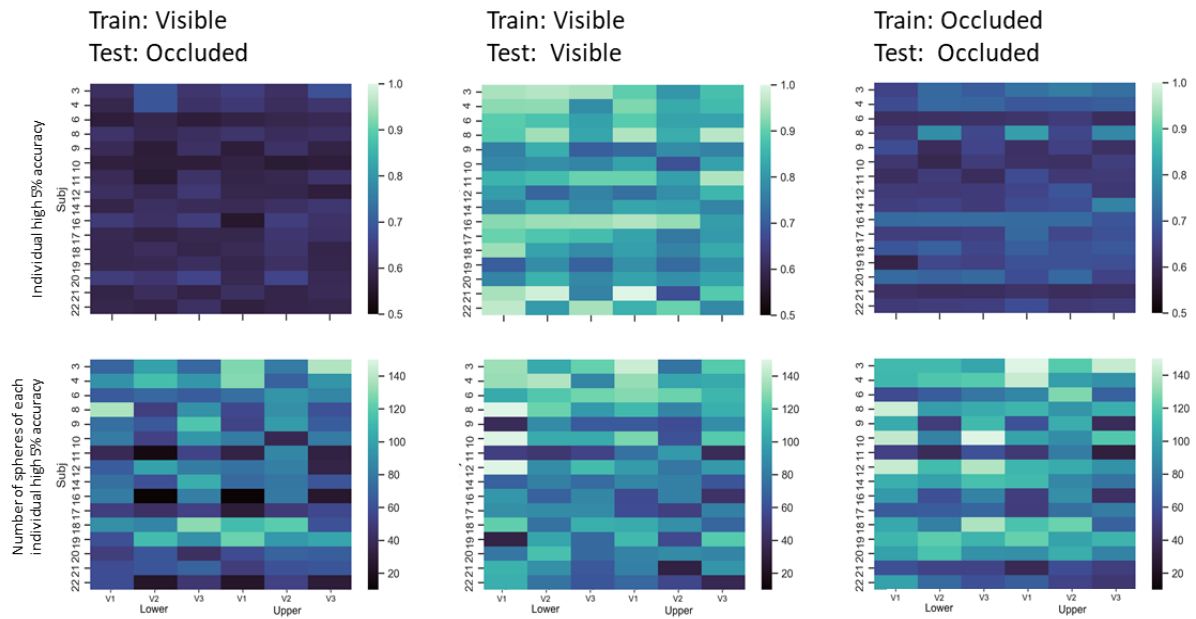
Figure 7 - Upper row depicts average decoding accuracies of each participant in each of the 6 ROIs. The lower row depicts the number of spheres included in the calculation of the 5% highest accuracy values, for each subject in each ROI. The left row represents results from classification analysis in which the classifier was trained in visible phase data and tested in occluded phase data; the middle row show results of analysis in which the classifier was trained and tested in visible phase data; and right row, train and test was carried out in occluded phase data.

Spatial layout of significant spheres across classification analyses: The projection of location of the significant spheres map for each analysis onto the retinotopic maps was carried out to verify their exact anatomical location. Comparing the overlap of spheres maps across analyses will tell us where, within the visual field, the map can be found and what their exact spatial layout would be, i.e. scattered or concentrated. This, in turn, allows us to draw firm conclusions regarding their representational content, especially if they are concentrated in a portion within the visual field which encodes the visible stimulus. For this, we focused in V1 which contains neurons with the highest spatial acuity and projected retinotopic maps on visual field representations (Duncan & Boynton, 2003; Song et. al., 2015). Moreover, we also included the results from the univariate functional localiser as a further manipulation check. For the visual fields subject-specific density maps were computed signifying the concentration of significant spheres within specific regions of the visual field. Figure 8 (top) shows visual field maps of an exemplary subject, in which we observed overlapping density maps for the different statistical tests. Across participants, overlap of the functional localiser (green line) with significant spheres from the visible phase (blue line) was observed for 13 participants in lower V1 and for 8 participants in upper V1, which indicates a robust reliability, once the stimulus is physically present even across multivariate and univariate methods. For visible and occluded phases, the overlap was observed for all 16 in both upper and lower V1, while for visible and visible-occluded, we observed the overlap for 14 participants in the upper V1

and 15 for the lower V1. Finally, for occluded and visible-occluded phases, the overlap was found for 13 in the upper V1 and 14 participants in lower V1. It should be noted, however, that for some subjects we find that parts of the density map fall outside the stimulated visual quadrant. This scattering was most likely caused by the quality of the polarity maps which was not high enough in all parts of visual cortex to allow for an errorless transformation, though note that the delimitation of different visual fields was not affected by these local variations in polar maps. Importantly, when inspecting the location of significant spheres in anatomical space overlaid onto the curvature, polarity and eccentricity maps (see Fig. 8 - bottom), we could confirm that the significant clusters were located in the upper and lower lip of V1, respectively.
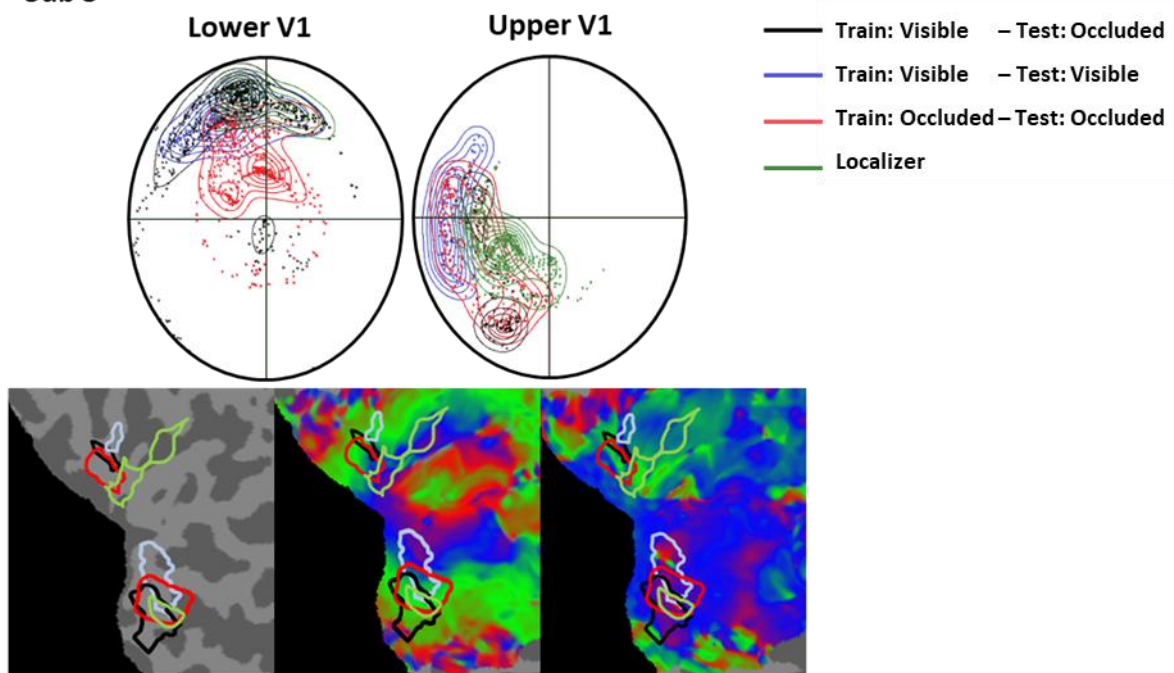
Figure 8 - Significant decoding accuracy maps projected onto retinotopic maps and derived visual field maps of one exemplary subject. Top: Visual fields of lower V1 and upper V1. Black curvatures and dots depict the localization of the vertices with significant accuracies for the visible-occluded classification. Blue and red curvatures and dots represent the localization of the vertices with significant accuracies for the visible and occluded classifications, respectively. Green lines and dots represent the same, but here results from the univariate functional localizer was used. Dots which spread to other quadrants could indicate scattered representations, but might be partly reflect the quality of retinotopic mapping itself. Bottom: Significant decoding accuracy maps overlaid on flattened anatomical maps of occipital cortex (right), the retinotopic eccentricity (middle) and polarity maps (left).

We interpret our findings as evidence that different types of information can be found in similar regions of the visual field within the primary visual cortex. Results for different analyses of spheres, selective for different types of visual stimulation, converge within topographically organized regions within the early visual cortex. Importantly, it should be noted that this pattern

of results is unbiased as the different analyses were spatially unrestricted within visual regions and carried out with independent data sets from different runs, at least for the analysis of the functional localiser, the visual only and occluded only MVPAs. That confirms that the information-based searchlight selection criterion did not randomly pick arbitrary voxels within the visual cortex. Rather, the selection reflected the spatial selectivity of cortical regions representing the very same stimulus throughout different conditions, even during occlusion.

Discussion

Our study tested the involvement of low-level visual regions in continuous motion extrapolation by comparing visible and occluded stimulus trajectories. Our behavioural results demonstrated that participants were highly accurate in judging the target's direction and time of arrival. The general overestimation of time intervals that we observed seems to be related to our specific stimulus settings. Here, short intervals (around 250-800 ms) were employed which are often overestimated (Benguigui et al., 2003; Bennet et al., 2018; Vicovaro et al., 2019). Remarkably, univariate fMRI-results showed that, to some extent, activity in low-level visual regions was tied to estimated motion trajectories. The more sensitive MVPA-analysis revealed that the activity pattern in V1 evoked by visible motion was indeed informative about the direction of the trajectory during occlusion. Finally, the location of informative spheres was consistent across several independent classifications, strongly suggesting that the sub-regions within low-level visual areas, coding the stimulus trajectory, were selectively engaged; and this claim was further supported using fMRI-based receptive field mapping of the informative regions.

Univariate Analysis read-outs

Our *univariate* fMRI-analysis compared velocity and direction in low-level visual areas. Results revealed that velocity did not differentially modulate fMRI-signals in any low-level areas consistently, while the motion trajectory selectively enhanced neural activity during the visible phase and partially during occlusion. We attribute this outcome to the dominance of spatial estimation over temporal estimation, which might be due to the well-known higher spatial acuity of the visual system (Klein et al., 2018, Welch & Warren, 1986). Our motion direction results indicated that low-level visual areas were engaged during the occlusion of the target, thereby extending previous observations on the involvement of the primary visual cortex in apparent motion (Ekman et al., 2017) to continuous motion extrapolation. In particular, the vertical visible trajectory elicited responses in the upper visual area for downward direction and in the lower visual area for upward direction, as expected. During the dynamic occlusion of the stimulus, similar

patterns of activation in the lower quadrants of the visual regions were observed, partly supporting particular theories about the mechanisms of motion extrapolation, which posit that a visual representation of a non-visible object is maintained during occlusion. These results are also in line with previous mental imagery findings which investigated imagery using retinotopic mapping and found activation in both striate and extrastriate cortex for imagined objects (Slotnick, et al., 2005).

However, this similarity in univariate activation patterns was less pronounced for the upper visual areas (lower visual field), rather an overall higher activation in upper V1 relative to lower V1 was observed regardless of visual trajectory. Asymmetry in the upper vs. lower visual quadrants has been previously reported and one possible explanation might be the distribution of 'near-preferring' neurons, which tend to be more frequent in lower VF compared to upper VF (Nasr & Tootell, 2018, 2020; Karim & Kojima, 2017). In general, psychophysiological studies demonstrated that lower visual field seems to be more thoroughly engaged in tasks from different domains, such as motion (Danckert & Goodale, 2001; Levine & McAnany, 2005, Lakha & Humphreys, 2005), colour discrimination and hue sensitivity (Levine & McAnany, 2005). This difference between lower and upper visual field is known as vertical meridian asymmetry which is more pronounced at larger eccentricities (Carrasco et al., 2001, Barbot et al., 2021). Visual field asymmetries have also been reported for the crowding phenomenon (He et al., 1996), the spatial resolution of attention (Intriligator & Cavanagh, 2001), distribution of receptive field properties and orientation preference (Merkel et al., 2020) and may be further amplified by reading habits (Rinaldi et al., 2014). Finally, there might have been an evolutionary advantage preferring downward over upward movements (Previc, 1990), e.g. for catching things falling down than flying away, similar to the preference for looming vs. receding stimuli (e.g. Tyll et al., 2011), which could explain the asymmetry observed for the univariate results.

In addition to the upper vs. lower VF asymmetry observed during the comparison between visible and occluded vertical trajectories, we also observed overall enhanced fMRI-signals during partially occluded relative to the visible phase. Note that participants passively observed the stimulus travelling on the screen during the visible phase, whereas during the occluded phase, they actively had to be engaged with the task. This latter task set may have required a higher level of attention (Zuanazzi & Noppeney, 2020; Klein et al., 2014). On the theoretical level, this difference may be explained in the light of the Rao and Ballard (1999) predictive coding model. In the visible phase, once the stimulus became predictable, less error-correction signals might have been exchanged between lower and higher visual areas, reducing the height of the neural response (Alink et al., 2010). On the other hand, the lack of visual information during the occluded phase might have intrinsically decreased the predictability level, leading to higher activity due to the need

of prediction. On a mechanistic level, the activity in V1 during occlusion may have also been primarily caused by feedback projections from higher cortical regions terminating in supragranular layers, whereas during passive viewing feedforward projections in the infragranular layer may have been primarily engaged. Accordingly, fMRI-responses in supragranular layers was recently found to be enhanced relative to lower cortical layers (de Hollander et al., 2021).

In contrast to our univariate results, previous fMRI studies often failed to reliably observe the recruitment of low-level visual areas during motion prediction (Shuwairi et al., 2007). Olson and colleagues (2003) observed high engagement of inferior parietal sulcus and also reported a strong decrease in fMRI-signal in V1/V2 during occlusion. Our contradictory results could be attributed to the use of techniques such as retinotopy, which allowed us to precisely identify low-level visual areas individually in each participant, targeting the specific low-level visual regions, while accounting for inter-individual anatomical variability (Greenlee, 2000, Amunts et al. 2000). In accord with our results, two recent studies which based their analysis on subject-specific retinotopic mapping were able to observe effects in low-level visual cortex during imagery of motion (Emmerling et al., 2016) and shape predictions (Erlikhman & Caplovitz, 2017). Both studies also used multivariate pattern analysis, which allows to draw conclusions not only on correlative brain-behaviour relationships but on the informational content represented within brain regions.

MVPA read-outs

Our MVPA results further extended our findings by showing that the patterns of activity in upper vs. lower visual field representations could be used to predict encoded motion trajectories during visible stimulation and during occlusion on their own. Most importantly, the data from visual trajectory could also be used for training to predict invisible motion during occlusion. It should be noted that these results significantly extended the univariate results during the occlusion phase by showing that the pattern of activity in low-level visual areas shows some commonalities during visible motion and occlusion. These results are in line with a recent study which suggested that even with no stimulation in these regions, it is possible to decode information based on continuous perception (van Kemenade et al., 2022). Additionally, the successful prediction does not depend on the difference in activation height for upward vs downward tasks, as the lower visual regions did not show enhanced fMRI-signals for occluded upward vs. downward motion in the univariate analysis. Therefore, the pattern of activity, rather than an overall difference in response-amplitude most likely accounts for the results in V1 and also in V5 (see Appendix A), which did not show significant univariate results (see also Wang et al., 2014, for similar results), but yielded significant classification accuracies for motion direction and velocity during occlusion using MVPA.

Despite the similarities in activation pattern, which led to the significant prediction accuracies, it should also be noted that there were some differences in MVPA-results between occluded and visible conditions: group averaged accuracy values were systematically higher for visible classification than occluded classification. This difference may attribute to the fact that the classifier was capturing a more reliable response with visible stimulation compared to stimulus occlusion.

Remarkably, the projection of significant spheres onto the retinotopic maps suggested that the location of the most informative voxels overlapped across the three independent classification analyses (visible and occluded stimuli, plus across category) and the univariate functional localizer. This overlap of visible and occluded informative activity patterns in the visual field may suggest that shared computational circuits in the primary visual cortex do exist, supporting both processes. However, layer-specific fMRI and/or single-cell studies are needed to further corroborate this interpretation. The spatial layout of our results also confirmed the plausibility of our sphere-selection approach, since overlapping results were found across different analyses. Our subject-specific approach was necessary once the target regions show considerable interindividual anatomical variability, thus differing from the standard fMRI-group analysis, which is traditionally based on the assumption of spatial commonalities across participants after spatial transformation of individual brains to a standard reference brain.

Finally, a remarkable outcome from this study is that our results were similar to mental imagery studies (e.g. Albers et al., 2013), despite the fact that no explicit instruction was given to the participants to imagine the stimulation. Instead, we aimed to investigate whether low-level visual regions would engage during the presentation of a dynamically occluded target without the participant having previous knowledge about a specific strategy for performing the task. Future studies could explicitly instruct participants to imagine occluded trajectories and observe if the observed effects vary as a function of task instruction.

To conclude, we investigated the neurobiological processes underlying motion extrapolation as indexed by patterns of activity in low-level visual regions during the presentation of visible and dynamically occluded trajectories. Our data supported the notion that virtually identical regions inside lower and upper V1, V2 and V3 represent information about visual stimulus trajectories in the absence of visual stimulation and suggested that shared neural circuits may be utilized when processing visible and extrapolated trajectories.

This chapter can also be found at Bioarxv (doi: https://doi.org/10.1101/2022.05.26.493554)

Chapter 3 - Investigating prediction of dynamic occlusion under different predictability levels in the primary visual cortex

Abstract

Predictive coding models postulate that high-level visual regions send back projections to low-level areas with high-level predictive information, while the latter compares this information with the incoming one, and sends prediction errors as feedforward information to update the predictions in higher-level areas. Some studies have showed that when the visual system is confronted with low level of predictability, prediction error may enhance activity in low-level visual areas, specifically the primary visual cortex. However, other studies showed that this might not always be the case, meaning that high level of predictability may also enhance activity in this region. One of the explanations for this apparent contradiction is based on the role of attentional mechanisms which might synergistically interact with predictive mechanisms. Our study investigated whether motion extrapolation in high and low predictable contexts could differently modulate fMRI-responses in the primary visual cortex during visible and partially occluded stimulation. To this end, participants performed a modified version of the interception paradigm in visible and occluded phases, in which they observed a stimulus moving horizontally, then vertically at two different velocities. They were instructed to press when and where the stimulus would reach a given point-of-contact. In high predictable context, the velocity would be the same during horizontal and vertical (occluded) trajectory; whereas, in low predictable context, the velocity could change during the vertical (occluded) trajectory. Univariate results showed no difference between high and low predictable contexts neither during visible nor during occlusion phases in low-level visual areas. MVPA results revealed accuracies above chance level for all classification analyses carried out with low and highly predictable context data. Here, we provide evidence that high predictability during motion extrapolation can enhance activity in the primary visual cortex, as much as low predictability, and suggest that attentional mechanisms might have contributed to the consistent enhancement of activity.

Introduction

Completing dynamically occluded information from the environment is among the daily challenges that the brain has to deal with, and for that, predictive mechanisms are essential for cognitive systems. Prediction, as used here, can be understood as the ability of the brain to estimate future input based on the (recent) past information (Alink et al. 2010). This idea that the brain uses top-down information to make predictions about incoming events dates back to Helmholtz. Helmholtz proposed that to build a systematic representation of experiences, the mind uses mental adaptations referred to as "unconscious inferences" (Helmholtz 1866/1962; Patton, 2018), meaning that inferences, or predictions, affect directly our behaviour. More recently, Kahneman and Tversky (1972) extensively investigated how predictions reflect and affect behaviour and postulated that when making predictions and judgements under uncertain circumstances, humans seem to rely on heuristics – mental shortcuts – which may lead either to accurate judgements or systematic errors (Kahneman & Tversky, 1972; Tversky & Kahneman, 1971, 1973).

Early studies developed theoretical models to explain how our brain works in a predictive fashion (Mumford, 1992; Rao and Ballard, 1999; Friston, 2003). One model which gained special attention was the Predictive Coding model from Rao and Ballard (1999). In brief, the model assumes that different levels of a hierarchical model network make predictions and send them to lower levels via feedback connections, while higher levels receive back the information about the error between the prediction and the actual response via feedforward connections. This error is also used by the system to make corrections on the estimation of the input signal. It is further suggested that this process would explain how predictions are coded in visual regions. Lower visual areas learn statistical regularities from the environment and send forward the unpredictable feature of the received input. Besides Rao and Ballard, others also attempted to mathematically explain how different systems works, by varying only how the model is applied to the data and how much the error is minimized (for review, see Spratling, 2017; Aitchison & Lengyel, 2017). The Predictive Coding model has been used to test the mechanisms underlying temporal and spatial predictions in different domains, such as auditory (Baess et al., 2009; Heilbron & Chait, 2018, for review), motor (Shipp, Adams, & Friston, 2013), multisensory integration (Krala et al. 2019) and the visual domain.

In the auditory domain, Baess and colleagues (2009) investigated middle latency response (MLR) in humans, which represents the early brain activity related to auditory information originated from thalamo-cortical feedback loops (McGee et al., 1991). The authors compared three conditions: auditory-motor, in which participants generated their own self-pace sound sequence;

auditory only, in which participants passively heard a sequence of sounds; and motor only, in which participants were instructed to generate their self-pace sequence, but no sound was presented. Electrophysiological results showed that self-paced sound sequences, compared to the other condition, were related to an attenuation of MRLs and a modulation of 40 Hz frequency band, suggesting that self-initiated auditory stimulation may reduce responses in the primary auditory cortex, in accord with Predictive Coding model.

At the multisensory integration level, Krala and colleagues (2019) investigated whether the integration of different domains would follow a predictive coding model. In an fMRI study, participants were asked to estimate their own motion speed in a visual, auditory or bimodal context. Results indicated an increase in response in the respective sensory areas for all three contexts, but a suppression in higher-level cortical regions. These findings suggest that predictions related to these modalities played a role in shaping the information processing organized in a hierarchical order, in accord with other previous studies (Kok et al., 2012; van Kemenade et al., 2017). Additionally, the authors also stated that the prediction of different modalities may affect not only their respective sensory areas, but also higher-level regions in a supramodal fashion.

Finally, in the visual domain, Alink and colleagues (2010) directly tested the predictive coding model, by investigating whether highly predictable moving visual stimulus decreases activity in the primary visual area and whether the stimulus predictability also influences regions which send feedback information to V1, as hMT/V5+ (Vetter et al., 2015). In one experiment, participants observed apparent-motion-inducing bars which could appear along an apparent trajectory at a predictable or unpredictable time (with a large delay). In a second experiment, participants observed a similar environment, but along the trajectory, dots (random-dot motion (RDM) paradigm) could appear, moving in a predictable or unpredictable direction (opposite to the apparent motion direction). In particular, the authors tested whether the unpredictable temporal (delay) or spatial (RDM direction) information increased activity in V1, while predicted stimulation was expected to reduce activity in this region. Results indicated that on the first experiment, highly predictable stimulus onset indeed reduced activity in V1, compared to delayed onset. For the second experiment, they also observed a decrease in response in V1, as well as in hMT/V5+, when the random dot motion direction was predictable. These findings supported the predictive coding model by showing that temporal and spatial predictable visual stimulations reduce activity in V1, while unpredictable visual stimulation enhances activity in this region. Later, Schellenkes and colleagues (2016) extended these findings to V2 and V3, by testing how predictable and unpredictable contrast changes can modulate neural response in low-level visual regions, using random-dot motion at specific locations. Results indicated that when new dots entered the visual

field by being present on new locations, higher responses were registered in V1, V2 and V3 compared to dots which were already displayed in these areas.

Using more complex stimuli Fischer and colleagues (2013) investigated how temporal predictability affects neural processing in the low-level visual areas, during the categorization of predictable and unpredictable moving faces, when primed by an auditory alerting signal. One group of the participants was asked to judge whether the presented moving face was male or female, while the other group judged the direction of the stimuli. In half of the trials, the alerting signal was presented before the visual stimulus. Results indicated that participants' behavioural performance was higher when the stimulus onset was predictable and when the alerting signal was coherent with it. However, a negative correlation was found between activity in V1 and the alerting signal, i.e. the larger the effect of the alerting signal in behavioural performance, the stronger the reduction in the primary visual cortex. These findings suggest, that the increase of temporal predictability reduced the BOLD signal in V1, corroborating previous studies and supporting the importance of temporal information in the prediction of future event.

In contrast to the above-mentioned findings, Coull and colleagues (2008) reported results apparently contradicting the postulates of the predictive coding model. Using a time-to-contact (TTC) paradigm, the authors investigated how fMRI-responses in low-level visual areas were modulated by temporal predictability during egocentric (subjective viewpoint) and allocentric (external viewpoint) viewing. In an ecologically valid driving simulation, participants were instructed to predict whether a car would touch a wall in one task, and in another task whether the colour of the car and the wall matched. It was hypothesized that proper attentional allocation would enhance stimulus detection, considering that spatiotemporal predictability is implicitly related to object-motion TTC task, while temporal predictability is explicitly associated with temporal cueing task. The authors observed increased fMRI-responses in V1 for TTC prediction during the egocentric judgements, likewise a variation in activity as a function of increasing certainty of collision; while allocentric judgements selectively enhanced responses in V5.

These findings were interpreted as an effect of attentionally-induced salience of time-to-contact judgements leading to a modulation in activity in V1. Moreover, this interpretation is in line with the findings of another electrophysiological study, which investigated how temporal and spatial information during dynamically occluded stimulation can expand attentional resources applied during the occlusion period (Doherty et al., 2005). The authors observed that the P1 component, which represent activity in many ventral and dorsal extrastriate visual regions (Di Russo et al., 2002; Foxe et al., 2005), was enhanced when spatial and temporal expectations were

combined, suggesting that temporal predictability of occluded target plays an important role in establishing the efficacy of sensory processing. Moreover, they observed that spatial and temporal predictability work synergistically together and this interaction may affect the attention allocation to the reappearance of the occluded moving stimulus (Doherty and colleagues 2005).

Some researchers have tried to reconcile the contracting views generated by those studies which found evidence that predictability reduces response in the primary visual cortex, with those which found the opposite pattern. For instance, Kok and colleagues (2012) tested two hypotheses related to this contraction: (1) attention and prediction have an opposing relationship, meaning that the excitatory effect related to attention outweighs the inhibitory effect related to prediction by enhancing activity when predicted attended stimulation is presented compared to unattended predicted stimulation; (2) attention and prediction have an interactive relationship, meaning that attention boost the precision of prediction, resulting in an enhanced activity promoted by the predictive error. The authors tested these hypotheses by measuring fMRI-responses in bilateral low-level visual areas (attended and unattended sides), while presenting cues which indicated the likelihood of the side where a Gabor patch would appear. Participants were instructed to indicate the orientation of the Gabor patch on the attended side and to ignore Gabor patches on the unattended side. Results indicated that reduced responses in V1 were observed on the unattended side when they were expected there; compared to enhanced responses in V1, V2 and V3 on the attended side for expected stimuli. The study provided evidence supporting the first hypothesis, which suggested that attention cancels the response reduction during high predictability, as the excitatory response related to attention enhances activity in low-level visual areas, but only on the attended side.

Here, we aim at extending these findings by probing the influence on temporal stimulus predictability in the context of motion extrapolation. To this end, we investigated whether dynamically occluded stimulation presented in high predictable (HP) and low predictable (LP) contexts differently modulate fMRI-signals in V1, by manipulating temporal information. We hypothesized that, according to the predictive coding theory, signal in this region should be smaller during stimulus presentation in the HP context, which requires less attention compared to the more volatile LP context. To test these hypotheses, we used an adapted version of the interruption paradigm (IP - Battaglini & Ghiani, 2021; Box 1), monitored brain activity using fMRI (Box 2) and acquired retinotopic maps (Box 3), in order to identify subject-specific regions of interest. Additionally, multivariate pattern analyses (Box 4) were carried out in right upper and lower V1 and right hMT/V5+, as the stimulation was presented only in the left hemisphere, in order to investigate

the representational pattern of activity in these regions, since the univariate analysis does not allow us to make inferences about the encoded informational pattern.

Materials & Methods

Participants

Eighteen participants (mean age 25.5, ±4.23, eight women) with normal or corrected-to-normal vision, no history of psychiatric or neurological disorders and no regular intake of medicament known to interact with the central nervous system were recruited from the student community of Otto-von-Guericke Universität Magdeburg and gave informed consent to participate in the study according to the local ethics. In a two-day experiment, participants were exposed to eight tasks, four each day, while their brain activity was monitored by fMRI: two training phases (visible stimulation) and two tests phases (occluded stimulation). On a third day participants returned for a retinotopic mapping measurement. Volunteers were rewarded with 10 euros/hour or experiment credits. Two participants were excluded due to absence in one of the days.

High Predictable Context - Visible Phase (training): On a black screen, a white dot moved continuously horizontally (200 px) from the left side to the centre, then vertically upwards (200 px) or downwards (200 px) until it crossed a "X" mark (+120 px) (see Fig.9). The vertical direction would be determined by the velocity was of the horizontal movement, which could be 16.6°/s (fast, 0.250 s; 0.150 s after crossing the "X" mark) or 14.4°/sec (slow, 0.450 s; 0.266 s after crossing "X" mark). [Note that the velocities (or time displacement) used until the stimulus reached the "X" mark were the intervals used for modelling and comparison with participants' response]. Hence, participants could learn associations, such as if the stimulus moves faster horizontally it will move faster upwards, or vice-versa, meaning that, until the point-of-contact, velocity during horizontal and vertical trajectories were identical. The participants were asked to keep their eyes on the fixation cross while attending to the sequence of movements and to indicate where and when the dot would end. We asked them explicitly to avoid pressing after the stimulus crossed the marks. Subjects responded by pressing the left button with their index finger or the right button with the middle finger in case the dot reached the upper "X" mark or lower one, respectively. Thirty trials of each condition were presented in four runs, i.e. 240 trials total (two runs with the configuration: up-fast/down-slow; and two runs: up-slow/down-fast). Intertrial interval was chosen from Poisson distribution with values between 2 and 6 seconds and each run lasted around 8 minutes.
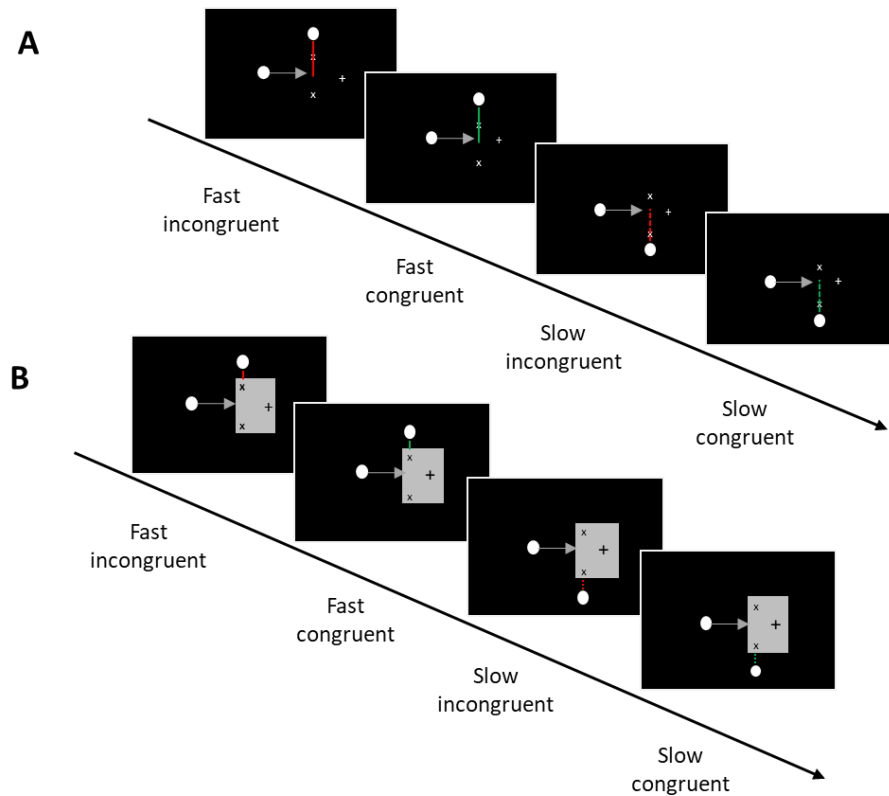
Figure 9 - Experimental Paradigm: The full and dotted grey and red lines (not presented during the experiment) illustrate the two velocities (full = fast; dotted = slow). Different colours represent velocity changes (red = incongruent; green = congruent). The full red line represents fast incongruent trials, in which the stimulus would travel the horizontal trajectory with the fast velocity, but would slow down along the vertical trajectory. The dotted red line represents slow incongruent trials, in which the stimulus would travel the horizontal trajectory with the slow velocity, but would speeded up in the vertical trajectory (A) Visible Phase. Participants observed a white dot moving fast upwards or slow downwards (or vice-versa) and were instructed to estimate when the dot would reach the upper or lower "x" mark, according to the observed velocity. The HP and LP contexts presented the same design, with the difference that in LP context, in 30% of the trials, the velocity-direction pairing would be incongruent, meaning that if they observed the dot going upwards in a fast velocity, in 30% of the trials, the dot would move slowly during the vertical trajectory. (B) Occluded Phase. During the occlusion phase, participants performed the exact same task as during the visible phase, with the difference that the vertical trajectory was occluded by a grey rectangle. The dot reappeared from behind the occluder, so participants could have the feedback of what velocity the stimulus had. For HP context, this was indifferent, as the velocity of the stimulus during the horizontal and vertical trajectory was always the same. However, for LP context, the reappearance was also the indication of whether the participants estimated the time-to-contact correct or not. Participants were explicitly instructed to respond when the target would reach the mark on the occlusion phase, i.e. before the reappearance of the stimulus.

High Predictable Context - Occluded Phase (test): Our adaptation of the IP task was very similar to the visible task described above, with the difference that a grey rectangle, occluding the vertical trajectory, was presented during the whole trial. Participants extracted the temporal information from the horizontal trajectory, in order to make the judgement about the stimulus destination and time of reappearance. Once more, participants were explicitly instructed to avoid pressing the response button after the stimulus crossed the marks, i.e. reappeared. Fifty trials of each condition were presented in four runs, resulting in 400 trials (same configuration as above).

Intertrial interval was chosen from Poisson distribution with values between 2 and 6 seconds and each run lasted around 13 minutes.

Low Predictable Context - Visible Phase (training): In this session, we manipulated the task predictability by introducing different probabilities of the temporal information. For an accurate comparison between high and low predictable context, the paradigm in this phase remained the same as described above with the following exception, if the stimulus moved slowly along the horizontal trajectory, it could change speed in 30% of the trials and move faster along the vertical trajectory, or vice-versa. Seventy-two out of 240 trials were presented with the incongruent displacement time and the number of trials were counterbalanced across conditions. Note that the overall duration of speeding up incongruent trials and slowing down incongruent trials in the vertical trajectory was identical (700 ms), until the point-of-contact.

Low Predictable Context – Occluded Phase (test): The task for this phase remained the same as described in the test phase of the high predictable context with the changes reported above in the visible phase of the low predictable context. The challenge in this phase was to estimate the displacement time without having the visual information of the vertical trajectory, but still being able to use the stimulus reappearance from behind the occluder as feedback. One-hundred out of 400 trials contained the incongruent displacement time and the amount of trials were counterbalanced across conditions.

fMRI Data Acquisition

The scanning sessions were conducted on 3 Tesla Siemens PRISMA MR-system (Siemens, Erlangen, Germany), using a 64-channel head coil. The data of participants were acquired in 16 functional runs divided in two sessions, totalizing 1840 volumes for the training phases and 3144 volumes for the test phases for each subject[3]. Blood oxygenation level-dependent (BOLD) signals were acquired using a multi-band accelerated T2*-weighted echo-planar imaging (EPI) sequence (multi-band acceleration factor 2, repetition time (TR)=2000 ms, echo time (TE)=30 ms, flip angle=80°, field of view (FoV)=220 mm, voxel size=2.2 × 2.2 × 2.2 mm, no gap). Volumes were acquired in interleaved order. Identical slice selection on both days was achieved using Head Scout Localizer whose calculation is based on Autoalign (Siemens, Erlangen).

A high-resolution three-dimensional T1-weighted anatomical map (TR = 2500 ms, TE = 2.82 ms, FoV = 256 mm, flip angle = 7°, voxel size = 1 × 1 × 1 mm, 192 slices, parallel imaging

---

[3] Some subjects had few volumes less due to the adjustment of scanning time and end of the experiment.

with a GRAPPA factor of 2, and 5:18 min scan duration) covering the whole brain was obtained using a magnetization-prepared rapid acquisition gradient echo (MPRAGE) sequence. This scan was used as anatomical reference to the EPI data during the registration procedure.

Retinotopic Mapping

In the third session, retinotopic mapping of participants were measured. The procedure used for measuring the retinotopic maps was the similar to the one used by Warnking et al. (2002) and Bordier et al. (2015). Eccentricity was mapped using a checkerboard ring which slowly contracted or expanded from the fixation dot, while presented on a grey background. The speed of the expansion and the contraction varied linearly with the eccentricity, so that the activation wave kept travelling at an approximate constant speed (Bordier et al., 2015). The ring reached a maximum diameter eccentricity of 6.6 deg and a minimum of 0.2 deg. When the maximum (expansion) or the minimum (contraction) was reached, a new ring would start from the origin. Polarity was mapped using one checkerboard wedge (10 deg) slowly rotating at a constant speed. Specific parameter calculations were similar as the ones described by Warnking and colleagues (2002). The checkerboard stimulation flickered at a frequency of 8 Hz, in 10 cycles of 36 s each. The aspect ratio of the checkboards was kept constant (1.09) by scaling the height linearly with the eccentricity. In order to account for the effects of the hemodynamic delay, the wedges were presented clock- and counter-clockwise, and the rings were presented expanding annuli and contracting annuli (Warnking et al., 2002). In total, eight functional runs were acquired, two for each modality and direction, and each run lasted approximately 6 minutes.

Statistical Analysis

Behaviour

Participants performance was assessed through the averaged correct responses (accuracy), response time and response time error (difference between individual's response time and the presented stimulus duration). We excluded missed trials, trials greater than 1.5 s, i.e. above 3 standard deviations (mean RT=0.864, (SE)± 0.027; mean excluded trials > 3sd = 1.015, ± 0.265 per subjects). Note that the slow stimulus duration of the vertical (occluded) trajectory was 0.450 s, meaning that the mean of the excluded trials was way above this value, meaning that the inclusion of these values could be misleading.

The three measurements were calculated for training and test phases using three different repeated measures (rm) ANOVA: (1) for HP context, we used a 2x2 within-subject design (direction: up-down vs. velocity: fast-slow); (2) for LP context, we used a 2x2x2 within-subject design

(direction: up-down vs velocity: fast-slow vs. congruency: congruent-incongruent); (3) for the comparison of HP vs. LP contexts, we carried out a 2x2x2 within-subject design as well (direction: up-down vs. velocity: fast-slow vs. predictability: high vs. low predictable) using the congruent trials only, as no incongruent trials were present in the HP context. Note that, when presenting the LP context results, we refer to the trials in which the stimulus travelled the horizontal trajectory fast and was slowed-down during the vertical trajectory in the visible or occlusion phases as incongruent fast, whereas the trials in which the stimulus travelled the horizontal trajectory slow and was speeded-up during the vertical trajectory in both phases as incongruent slow, i.e. we use the initial speed for classification. Additionally, for each analysis, we included task order as a between subject factor, however in no statistical analysis any significant effect was observed (all p's > 0.213). All analyses were calculated using JASP (v.0.15.0 - https://jasp-stats.org/). JASP was also used to compute post hoc tests (simple main effects function) and effect sizes (partial η^2).

Retinotopy

We performed a three-dimensional reconstruction of the cortical sheet based on the structural image of each of the 16 subjects using recon-all function from Freesurfer (v.6 - https://surfer.nmr.mgh.harvard.edu/). Retinotopic maps along the polar and eccentricity dimensions were calculated for each of the cortical surfaces using the "selxavg3-sess" function from Freesurfer. Lower and upper primary visual area were delineated manually on the flattened cortical sheets based on the boundaries of phase reversals within the polar angle and eccentricity maps (Abdollahi et al. 2014). Delineation of borders were created based on of Georgieva et al. (2009) and Kolster et al. (2010). The regions were later used to identify the local maxima during the visible phase in HP context. These local maxima were thus used to independently localise the region of interest within the functional region for the occluded phase. Probabilistic map of MT as provided by Freesurfer parcellation for each subject was included in the analyses.

fMRI preprocessing

All data (except retinotopic data) were analysed using SPM12 (www.fil.ion.ucl.ac.uk/spm, Wellcome Trust Centre for Neuroimaging, London, UK). The first five volumes of each run were discarded to allow for steady state magnetization. We performed slice-timing corrected and spatially realignment (registered to the mean image) of all remaining functional volumes. Head motion parameters were later used as nuisance regressors in the general linear model (GLM). Finally, the structural image was coregistered (estimate and reslice) to first functional image of the first run. Resliced images were smoothed with a gaussian kernel of 6 mm.

fMRI data Modelling

Data of individual contexts (HP and LP) were modelled with general linear model (GLM, Friston et al., 1995), which included the run-wise condition parameters, derivatives, and six motion regressors as nuisance covariates. In particular, regressors of each condition (up-fast, down-slow, up-slow, down-fast or up-slow, down-fast, up-fast, down-slow, and respective incongruent conditions of LP contexts) were modelled with the canonical hemodynamic response function (HRF), using the onset of the initial stimulus trajectory of each trial. Temporal and dispersion derivatives of each regressor were added to the model in order to account for variability in the onset response and shape (Friston et al., 1998). Estimated beta weights of the HRF of each participant were extracted using MarsBar 0.44 (Anton et al., 2002) from subject-specific lower and upper V1 masks (see below for details of retinotopic analysis). We performed three rmANOVAs: (1) for HP context, we used a 2x2x2 (direction, velocity, V1 Quadrant), (2) for LP context for, we used a 2x2x2x2 direction, velocity, V1 Quadrant and congruency) and for combined congruent HP and LP, a 2x2x2x2 (direction, velocity, V1 Quadrant and predictability). Task order was included in the analysis as between-subject effect, but no significant analysis was observed (all p's > 0.078). A full rmANOVA (direction, velocity, predictability, V1 quadrant, task order) was run for comparisons in which all tasks were included, however no difference between tasks were observed. Results are presented in the appendix B, table 1. For the MVPA, we modelled single trial GLMs (Least Square Separate a (LSS) approach, Mumford, 2012 – script adapted from https://github.com/ritcheym/fmri_misc/blob/master/generate_spm_singletrial.m).

Multivariate Pattern Analysis

A series of trial-wise multivariate pattern analyses was performed on beta values from GLMs of low and high predictable context for both Visible and Occluded Phases. To this end, trial-wise GLMs were carried out, and for the MVPA, the trials were calculated using Least Square Separate approach (Mumford, et al., 2012). Trial-wise MVPA was chosen here, due to the low number of runs for each task. Two runs are not enough to make valid train and test partitions as we would have only one in each part. For these cases, trial-wise analyses are recommended as the number of trials allow enough data in each partition (Mumford, et al., 2012). For all analyses, we used the searchlight method with a 4.4 mm sphere, a linear discriminant analysis (LDA) classifier and leave-25%trials-out (Etzel & Braver, 2013). All partitions were balanced and repeated 4 times. All analyses were carried out at the single-subject level, as the searchlight analyses were performed inside each individual mask.

We applied a cut-off at the accuracy of 0.5 (chance level) to filter out all the voxels which contained below chance accuracies, and included in the analysis only the values which belonged to the highest 5% values of the distribution. This additional thresholding was done in order to obtain only the most informative voxels of the decoding. This procedure was applied to all the classification analyses below described. The statistical significance of the accuracies of each analysis were accessed using the same procedure as in chapter 2. Permutations were carried out at the subject-level and 1000 iterations which contained randomised data labels per run, keeping the same original dataset. In order to have the spatial comparison, the same searchlight spheres included in the 5% highest accuracy sample were obtained for all 1000 samples of each individual participant. These sampled values were averaged across spheres for the original and permuted dataset permutation. For group level analysis, analyses were done based on Etzel (2017) approach. The null distribution carried the average across participants for each of the 1000 permutations plus the true-labelled group-level average (1001 group-level accuracies). The permutation p value was computed by taking the sum of the permuted accuracies higher or equal to the true-labelled accuracy and dividing by the number of iterations plus 1, as in chapter 2. Each analysis described below served a different purpose, such as decoding spatial, temporal information from both contexts, and congruency information from low predictable context.

Classifying Direction in HP & LP Context: Here, we carried out two classification analysis in which the classifier was trained in the visible phase and tested in the occluded phase using data of each context independently. We attempted to decode spatial visible information - upward vs downward motion trajectory - from occluded phase and compared accuracies from both analyses. We expected accuracies from LP context classification analysis to be significantly lower than HP contexts, due to the presence of incongruent trials, i.e. unpredictability.

Classifying Velocity in HP & LP Context: As the classification analyses above, we trained the classifier on the data of the visible phase and tested on data of the occluded phase within contexts. In this case, we attempted to decode temporal visible information - fast vs slow - from occluded data and compared accuracies from the different contexts. Here, we also expected decoding accuracies from LP context to be smaller than accuracies from HP context, also due to the presence of incongruent trials.

Manipulation checks: To verify whether the classifier was really decoding relevant information, classification analyses were performed on the visible and occluded data separately for both contexts. For HP contexts, direction and velocity were classified from both phases, as well as for LP contexts. Additionally, for the latter, congruent vs. incongruent information were classified.

Here, we expected that decoding accuracies from visible phases were higher than occluded phases, as the longer exposure of the stimulus during the visible phase may allow a more robust representation of the information, whereas during occlusion, participants are expected to mentally represent the trajectory, thus less bottom-up input would drive the response.

We further ran pairwise Student's T-test to compare HP and LP contexts in all conditions in lower and upper V1 quadrants and in V5 to investigate whether conditions in LP context would encode more or less information, hence higher or lower accuracy values, compared to HP context.

Results

Behaviour: *Spatial estimation*

Visible Phase

High predictable context

Results indicated a main effect of velocity, suggesting a higher performance during slow motion ($F(1,14)=44.061$, p <.001, $\eta_p^2=0.759$; fast-slow: mean difference (MD)=-0.058, (SE)±.009, t=-6.638, p_{bonf} <.001) and marginally significant main effect for direction, pointing to a tendency of higher performance during upward direction ($F(1,14)=3.709$, p=.075, $\eta_p^2=.209$; upward vs. downward: MD=.032, ±.016, t=2.926, $p_{bonf}=.075$). No interaction was observed between factors. Figure 10A shows averaged accuracy for all direction-velocity paired conditions during visible period.

Low predictable context

We observed a triple interaction (Figure 10A) between direction, velocity and congruency ($F(1,14)=19.174$, p<.001, $\eta_p^2=.578$; congruent fast vs. incongruent fast in downward: MD=.104, ±.022, t=4.736, p_{bonf}<.001; congruent slow vs. incongruent slow in upward: MD=.102, ±.022, t=4.643, p_{bonf}<.001). Among incongruent conditions (incongruent fast=expected fast, but stimulus slowed down; incongruent slow=expected slow, but stimulus speeded up), we observed differences between both velocities in both upwards and downwards direction (upward fast vs. downward fast: MD=.108, ±.029, t=3.785, $p_{bonf}=.012$, and upward slow vs. downward slow: MD=-0.107, ±.029, t=-3.759, $p_{bonf}=.013$). Within downward direction, performance during incongruent slow motion was significantly higher (downward fast vs. downward slow: MD=-0.128, ±.026, t=-4.871, p_{bonf}<.001). We still found an interaction between direction and velocity ($F(1,14)=5.014$, p=.042, $\eta_p^2=.264$; fast vs. slow in downward: MD=-0.068, ±.021, t=-3.219, $p_{bonf}=0.024$). Additionally, results indicated main effect of congruency ($F(1,14)=10.721$, p=.006, $\eta_p^2=.434$, congruent vs. incongruent: MD=.037, ±.011, t=3.274, $p_{bonf}=.006$) and a main effect of velocity ($F(1,14)=6.914$,

p=.020, η_p^2 =.331, fast-slow: MD=-.026, ±.010, t=-2.630, p_{bonf}=.020). Figure 10B depicts averaged accuracy for all conditions.

High x Low Predictability

In the comparison of congruent results from both high and low predictable phases during the visible task, we observed a triple interaction between direction, velocity and predictability (F(1,14)=6.481, p=.023, η_p^2 =.316). Significant differences were observed in LP context between upwards fast and slow motion (MD=-0.056, ±.016, t=-3.498, p=.028); in HP context between downward fast and slow motion (MD= -0.077, ±.016, t=-4.777, p<.001) and between HP and LP contexts during downward fast motion (MD= -0.059, ±.015, t=-3.829, p=.010). Results also pointed to interactions between predictability and velocity (F(1,14)=6.800, p=.021, η_p^2 =.327), with differences between fast and slow motion in HP context (fast vs. slow: MD=-0.058, ±.010, t=-5.945, p<.001) and LP context (fast vs. slow: MD=-0.032, ±.010, t=-3.278, p=.020), indicating higher performance during slow motion. An interaction between predictability and direction (F(1,14)=7.167, p=.018, η_p^2 =.339) pointed to a marginally significant difference in HP context between upward and downward conditions (MD=.034, ±.013, t=2.574, p=.094). Finally, we observed a main effect of velocity (F(1,14)=28.794, p<.001, η_p^2 =.673; fast vs. slow: MD=-0.045, ±.008, t=-5.366, p<.001).

<u>Occluded Phase</u>

High Predictable Context

As in the HP visible phase, here we observed only a main effect of velocity, again revealing higher performance during slow motion (F(1,14)= 15.996, p<.001, η_p^2 =.533; fast vs. slow: MD=-0.050, ±.013. t=-4, p_{bonf}<.001). No interaction was observed. Figure 10B shows averaged accuracy for all direction-velocity paired conditions during occlusion period.

Low Predictable Context

During this phase, analyses pointed to a triple interaction between direction, velocity and congruency (Figure 10B), indicating that higher performance during congruent trials compared to incongruent trials (F(1,14)= 23.749 p<.001, η_p^2 =.629; congruent fast vs. incongruent fast in downward: MD=.124, ±.024, t=5.140, p_{bonf} <.001; congruent slow vs. incongruent slow in upward: MD=.100, ±.024, t=4.162, p_{bonf} =.004). For incongruent trials different pattern of results were observed (incongruent fast in upwards vs. incongruent fast in downward: MD=.130, ±.028, t=4.670, p_{bonf} =.001; incongruent fast vs. incongruent slow in upward: MD=.115, ±.029, t=3.910, p_{bonf} =.009; incongruent fast vs. incongruent slow in downward: MD=-0.127, ±.029, t=-4.340, p_{bonf}=.002; incongruent slow in upwards vs. incongruent slow in downward: MD=-0.112, ±.028, t=-4.028,

p_{bonf}=.007). An interaction between direction and velocity (F(1,14)= 4.731 p=.047, η_p^2=.253; post-hoc failed to show significant results). A main effect of congruency was also revealed by the analysis (F(1,14)= 7.856 p =.014, η_p^2=.359; congruent-incongruent: MD=.034, ±.012, t=2.803, p_{bonf} =.014).
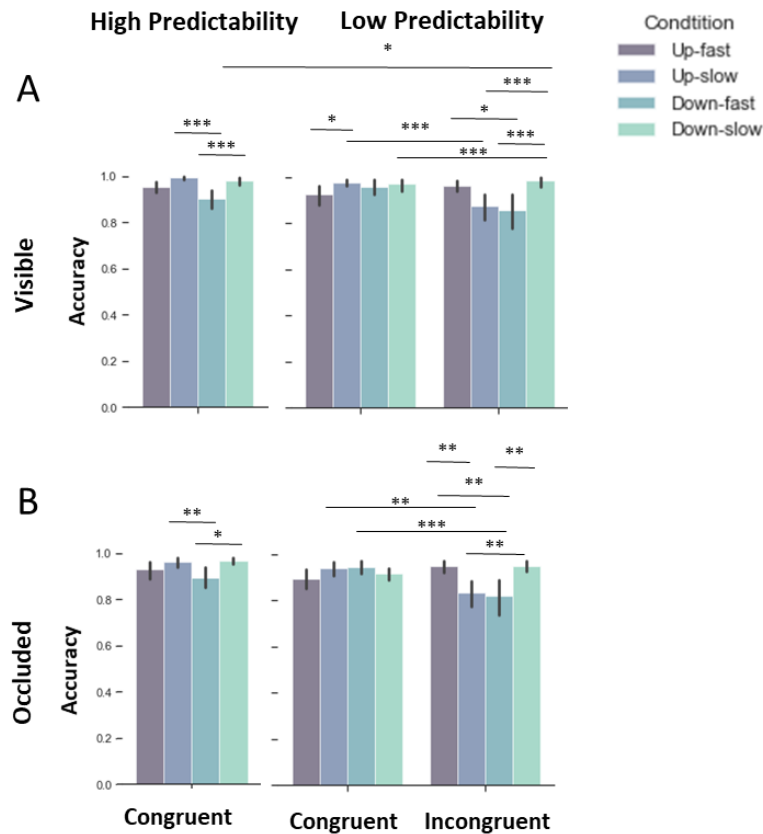
Figure 10 - Averaged accuracy across conditions. Dark purple bars depict results of fast motion in upward trajectory, blue bars depict results of slow motion in upward trajectory, dark green bar, fast motion in downward direction and light green, slow motion in downward trajectory. Note that the accuracy results were highly similar for occluded and visible motion trajectories. (A) Results of visible period during HP (left) and LP contexts (right) show differences between conditions. Differences were observed between congruent fast and slow in downward condition in HP context, and also difference between the concurrent conditions up-slow/down-fast (condition presented within the same task). Analysis also yielded differences between congruent and incongruent conditions in LP contexts, as well as a significant difference between HP and LP, indicating that slow in downward trajectory in LP presented higher accuracy than slow during downward trajectory in HP. (B) Results of occluded period during HP (left) and LP contexts (right) showed differences between slow and fast in downward trajectory during HP, and also difference between the concurrent condition up-slow/down-fast (condition presented within the same task), as in visible phase. During occluded phase in LP contexts, differences between congruent and incongruent conditions were observed, as during the visible phase.

High x Low Predictability

Here we compare the congruent results from both high and low predictable phases during the occluded task. Results indicated a triple interaction between direction, velocity and predictability, suggesting higher performance during slow motion in downward direction in HP context (F(1,14)=16.085, p=.001, η_p^2=.535; downward slow in LP context vs. downward slow in HP context: MD=-0.052, ±.015, t=-3.429, p_{bonf} =.035; downward fast vs. downward slow in HP context: MD=-0.070, ±.019, t=-3.598, p_{bonf} =.021). We also observed an interaction between velocity and

predictability (F(1,14)=18.557, p<.001, η_p^2=.570; slow in LP vs. slow in HP context: MD=-0.038, ±.010, t=-3.849, p_{bonf} =.005; fast vs. slow in HP context: MD=-0.050, ±.012, t=-4.213, p_{bonf} =.002). Besides a main effect for velocity (F(1,14)=6.684, p=.002, η_p^2 =.323; fast vs. slow: MD=-0.028, ±.011, t=-2.585, p_{bonf} =.022) was observed, as well as a marginally significant main effect for predictability (F(1,14)=3.337, p=.083, η_p^2 =.192).

Temporal Estimation

Visible Phase

High predictable context

Statistical analysis revealed main effects of velocity (F(1,14)=78.964, p<.001, η_p=.849; fast vs. slow: MD=-0.112, ±0.013, t=-8.886, p_{bonf} <.001) and direction (F(1,14)=15.200, p =.002, η_p^2 =.521; upward vs. downward: MD=-0.023, ±.006, t=-3.889, p_{bonf} =.002), indicating that participants answered slower to slow motion, as expected, and also to downward direction. No interaction was observed. Figure 11A shows averaged reaction time for all conditions during visible phase.

Low predictable context

Results revealed a triple interaction between direction, velocity and congruency (Figure 11A), which indicated slower response time during incongruent in both directions, and for congruent slow in upward direction (F(1,14)=5.882, p=.029, η_p^2=.296; congruent fast vs. incongruent fast in upward: MD=-0.106, ±.014, t=-7.539, p_{bonf}<.001; congruent fast vs. incongruent fast in downward: MD=-0.073, ±.014, t=-5.168, p_{bonf}<.001; congruent slow vs. incongruent slow in upward: MD=.061, ±.014, t=4.313, p_{bonf}=.002). We also observed an interaction between velocity and congruency (F(1,14)=52.895, p<.001, η_p^2=.791; congruent fast vs. incongruent fast: MD=-0.089, ±.011, t=-8.292, p_{bonf} <.001, and congruent slow vs. incongruent slow: MD=.040, ±.011, t=3.709, p_{bonf} =.006). As well as in spatial estimation, difference between incongruent fast and slow was significantly high (MD=.080, ±.010, t=8.072, p_{bonf}<.001). Main effects were seen for congruency (F(1,14)=16.446, p=.001, η_p^2=.540, congruent-incongruent: MD=-0.025, ±.006, t=-4.055, p_{bonf}=.001) and velocity(F(1,14)=12.269, p=.004, η_p^2=.467, fast-slow: MD=.015, ±.004, t=3.503, p_{bonf}=.004).

High x Low Predictability

In these analysis, only congruent trials were analysed, from both high and low predictable phases during the visible task, we observed a triple interaction (Figure 11A) between direction, velocity and predictability (F(1,14)=5.340, p=.037, η_p^2 =.276). Significant differences were observed in HP context between upwards fast and slow motion (MD=-0.091, ±.013, t=-7.087, p_{bonf}<.001) and

downward fast and slow motion (MD=-0.114, ±.013, t=-8.892, p_{bonf}<.001). However, differences between downward and upward trajectories were also observed during slow motion (MD=-0.043, ±.012, t=-3.540, p_{bonf}=.027). In LP context, differences were seen between upward fast and slow motion (MD= -0.065, ±.013, t=-5.065, p<.001). Reaction time was also significant difference in HP compared to LP context during downward slow motion (MD= .073, ±.011, t=6.457, p_{bonf}<.001). We further observed an interaction between predictability and velocity (F(1,14)=28.829, p_{bonf}<.001, η_p^2 =.673), with differences between fast and slow motion in HP context (fast-slow: MD=-0.103, ±.008, t=-13.345, p_{bonf}<.001); in LP context (fast-slow: MD=-0.049, ±.008, t=-6.409, p_{bonf}<.001), and between HP and LP context, indicating higher reaction time during slow motion in HP (fast-slow: MD=.039, ±.009, t=4.501, p_{bonf}<.001). An interaction between predictability and direction (F(1,14)=23.795, p<.001, η_p^2 =.630) pointed to a significant difference in HP context between upward and downward direction (MD=-0.032, ±.007, t=-4.787, p_{bonf}<.001); and between HP and LP during downward direction (MD=.033, ±.008, t=3.956, p_{bonf}=.004). Additionally, we observed a main effect of velocity (F(1,14)=167.373, p<.001, η_p^2 =.923; fast vs. slow: MD=-0.076, ±.006, t=-12.937, p_{bonf}<.001) and direction (F(1,14)=4.996, p=.042, η_p^2 =.263; upward vs. downward: MD=-0.012, ±.005, t=-2.235, p_{bonf}=.042).

Occluded Phase

High Predictable Context

Results with response time indicated main effect of velocity (F(1,14)= 78.964, p<.001, η_p^2 =.849; fast vs. slow: MD=-0.112, ±.013. t=-8.886, p_{bonf} <.001), as well as of direction (F(1,14)= 15.200, p= .002, η_p^2 =.521; upward vs. downward: MD=-0.023, ±.006. t=-3.899, p_{bonf} =.002), pointing to higher response time to slow motion and downwards direction, such as during HP visible phase. No interaction was observed. Figure 11B shows averaged reaction time for all direction-velocity paired conditions during occluded phase.

Low Predictable Context

Analysis did not yield significant results for reaction time during low predictable context. Instead a marginally significant triple interaction was observed (direction, velocity and congruency: F(1,14)= 3.473, p=.083, η_p^2 =.199). No significant or marginally significant differences were observed in the post-hoc analyses.
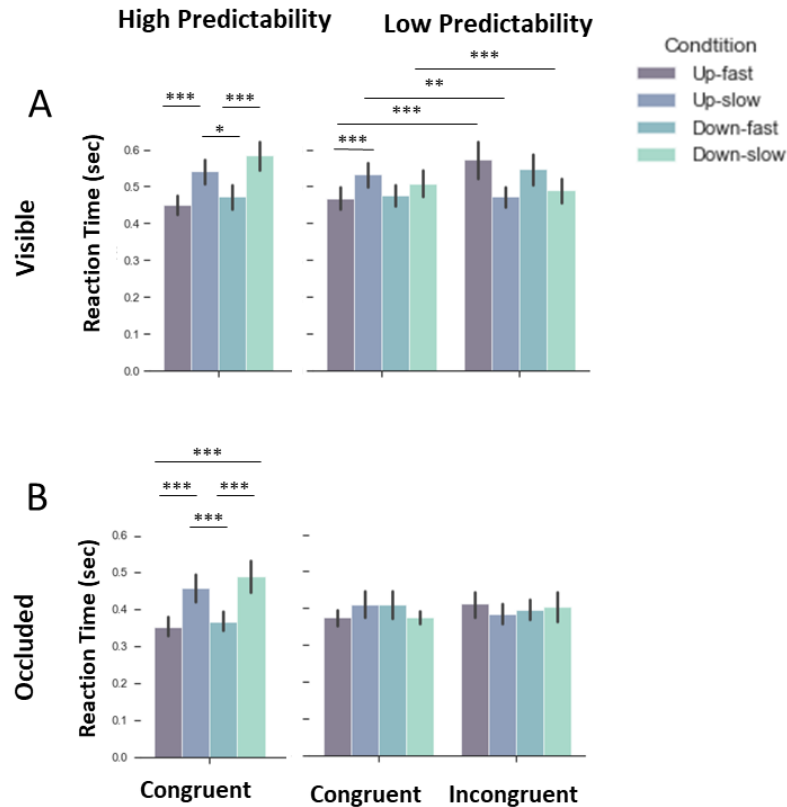
Figure 11 - Averaged reaction time across conditions. Dark purple bars depict results of fast motion in upward trajectory, blue bars depict results of slow motion in upward trajectory, dark green bar, fast motion in downward direction and light green, slow motion in downward trajectory. (A) Results of visible period during HP (left) and LP contexts (right) show differences between conditions. We observed differences between fast and slow conditions in up- and downward trajectories, indicating that participants were estimating the time-to-contact accordingly (answering fast when the stimulus was fast and answering slow when the stimulus was slow). This pattern can be clearly observed during visible condition in HP and LP, but not during occluded condition in LP (B). In Figure B, we could observe, for instance, that participants responded slower during incongruent compared to congruent fast, as in incongruent fast, the stimulation indeed reappeared slower.

High x Low Predictability

Response time results indicated an interaction for direction and predictability (F(1,14)=10.252, p=.006, η_p^2 =.423; upward vs. downward in HP context: MD=-0.023, ±.005, t=-4.822, p$_{bonf}$ <.001) and velocity and predictability (F(1,14)=83.224, p<.001, η_p^2 =.856; fast vs. slow in HP context: MD=-0.112, ±.010, t=-10.817, p$_{bonf}$<.001; slow in HP vs. slow in LP context: MD=.079, ±.013, t=6.015, p$_{bonf}$ <.001), suggesting higher response time for estimation for slow velocity during HP context, but lower response times for fast velocity in the HP context. This suggests that participants may have chosen a different strategy, as response times for the congruent trials showed a central tendency. We also observed significant main effects for direction (F(1,14)=13.216, p=.003, η_p^2=.486; upward vs. downward: MD=-0.012, ±.003, t=-3.635, p$_{bonf}$=.003), velocity (F(1,14)=45.490, p<.001, η_p^2=.765;

fast vs. slow: MD=-0.057, ±.008, t=-6.745, p_{bonf}<.001) and a marginally significant effect for predictability (F(1,14)=4.136, p=.061, η_p^2 =.228; HP vs. LP context: MD=-0.024, ±.012, t=2.034, p_{bonf}=.061). Interaction between direction and velocity did not reach significance, but post-hocs show significant differences between conditions, indicating that participants were estimating time-to-contact accordingly.

Temporal Estimation Error

Visible Phase

High predictable context

Results showed main effect of velocity (F(1,14)=137.095, p<.001, η_p^2=.907; fast vs. slow: (MD=.098, ±.008, t=11.709, p_{bonf} <.001) and direction (F(1,14)=16.309, p=.001, η_p^2 .538; upward vs. downward: MD=-0.032, ±.008, t=-4.038, p_{bonf} =.001), revealing an overestimation for fast motion and upward direction. Analysis did not reveal significant interaction. Figure 4A depicts averaged reaction time error for all conditions during visible phase.

Low predictable context

We observed again the triple interaction between direction, velocity and congruency (Figure 12A), suggesting that errors were smaller during fast incongruent trials than during congruent trials in upward direction, but not downward direction (F(1,14)=12.269, p=.004, η_p^2 =.467; congruent fast vs. incongruent fast in upward: MD=.159, ±.012, t=13.660, p<.001; congruent fast vs. incongruent fast in downward: MD=.125, ±.012, t=10.686, p<.001); congruent slow vs. incongruent slow in upward (MD=-0.142, ±.012, t=-9.904, p<.001; congruent slow vs. incongruent slow in downward: MD=-0.115, ±.012, t=10.686, p<.001). Results still revealed an interaction between velocity and congruency (F(1,14)=231.417, p<.001, η_p^2 =.943; congruent fast vs. incongruent fast: MD=.142, ±.010, t=14.611, p_{bonf}=.001; congruent slow vs. incongruent slow: MD=-0.129, ±-0.129, ±.010, t=-13.259, p_{bonf}<.001). Main effects were observed for direction (F(1,14)=16.445, p=.001, η_p^2=.540, up vs. down: MD=-0.019, ±.008, t=-2.425, p_{bonf}<.001), and velocity (F(1,14)=5.882, p=.029, η_p^2 =.296; fast vs. slow: MD=-0.019, ±.008, p_{bonf}=.029).

High x Low Predictability

Analysis of congruent trials of HP and LP contexts from pointed to an interaction between predictability and velocity (F(1,14)=4.930, P=.043, η_p^2 =.260), similar to results from reaction time. Differences were observed between fast and slow motion in HP (MD=.097, ±.011, t=8.881, p_{bonf}<.001) and LP (MD=.117, ±.011, t=-10.663, p_{bonf}<.001). Main effects were observed for direction

(F(1,14)=10.229, p=.006, η_p^2 =.424; upward vs. downward: MD=-0.027, ±.008, t=-3.209, p_{bonf}=.006) and velocity (F(1,14)=113.799, p<.001, η_p^2 =.860; fast vs. slow: MD=.107, ±.010, t=10.668, p_{bonf}<.001).

Occluded Phase

High Predictable Context

Main effect was observed for velocity (F(1,14)= 44.235, p<.001, η_p^2 =.747; fast vs. slow: MD=-0.086, ±.013. t=-6.651, p_{bonf} <.001) and direction (F(1,14)= 16.420, p=.001, η_p^2 =.523; up vs. down: MD=-0.024, ±.006. t=-4.052, p_{bonf} =.001), showing an overestimation, this time, during fast motion as well as during downward direction. No significant interactions were observed. Figure 12B depicts averaged reaction time error for all conditions during occluded phase.

Low Predictable Context

We observed an interaction between velocity and congruency, indicating an overestimation during congruent fast and incongruent slow (speeded-up stimulus)(F(1,14)=483.345, p<.001, η_p^2 =.972; congruent fast vs. congruent slow: MD=.0172, ±.014, t=11.879, p_{bonf} <.001; congruent fast vs. incongruent fast: MD=.193, ±.010, t=19.806, p_{bonf}<.001; congruent slow vs. incongruent slow: MD=-0.190, ±.010, t=-19.525, p_{bonf} <.001; incongruent fast vs. incongruent slow: MD=-0.212, ±.014, t=-14.658, p_{bonf}<.001). A marginally significant triple interaction (Figure 12B) was observed (direction, velocity and congruency: F(1,14)=4.248 , p=.058, η_p^2 =.233). Post-hoc comparisons pointed to differences between congruent fast vs. congruent slow in upward (MD=.168, ±.019, t=8.904, p_{bonf}<.001); congruent fast vs. congruent slow in downward (MD=.175, ±.019, t=9.260, p_{bonf}<.001); congruent fast vs. incongruent fast in upward (MD=.198, ±.011, t=17.939, p_{bonf}<.001); congruent slow vs. incongruent slow in upward (MD=-0.200, ±.011, t=-18.065, p_{bonf}<.001); congruent fast vs. incongruent fast in downward (MD=.188, ±.011, t=17.009, p_{bonf}<.001); incongruent fast vs. incongruent slow in upward (MD=-0.230, ±.019, t=-12.148, p_{bonf}<.001); and incongruent fast vs. incongruent slow in downward (MD=-0.194, ±.019, t=-10.299, p_{bonf}<.001).
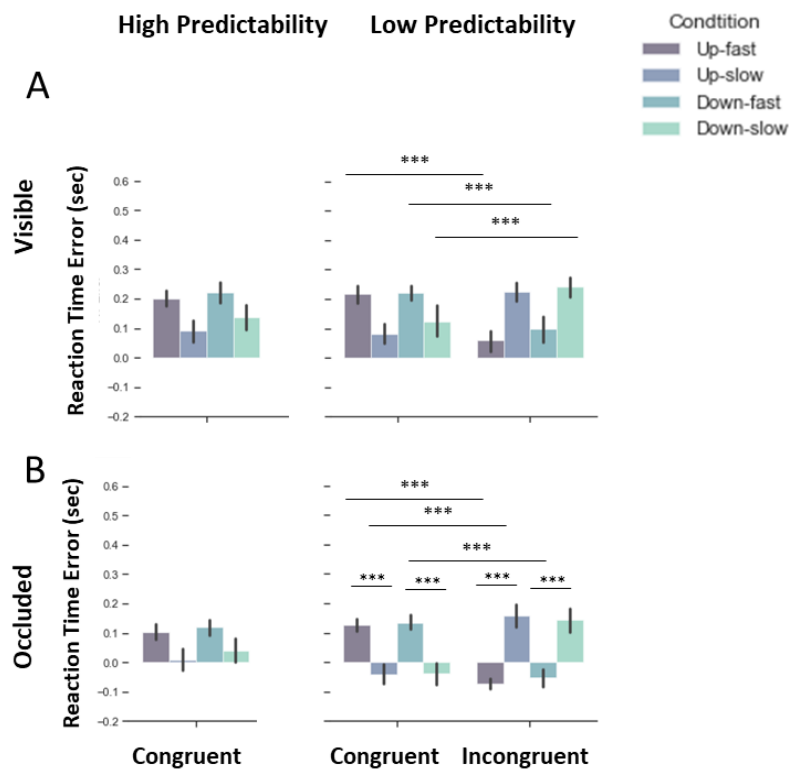
Figure 12 - Averaged reaction time error across conditions. Dark purple bars depict results of fast motion in upward trajectory, blue bars depict results of slow motion in upward trajectory, dark green bar, fast motion in downward direction and light green, slow motion in downward trajectory. Although the conditions were clearly (and significantly) different in HP context during visible (A-left) phase and occluded (B-left), the analysis did not show interaction between direction and velocity. (A) Differences were observed in LP context during visible phase and occluded phases (B) when congruent and incongruent trials were compared. Note that the bars in fast congruent conditions are similar to the slow in incongruent conditions, showing that participants were trying to estimate according to the congruent velocity of the stimulus. During the slow conditions (and incongruent fast), we could observe an underestimation, while during fast (and incongruent slow) condition we see that participants overestimated their responses. In appendix B, it is possible to observe a plot of reaction time error of incongruent condition during occlusion in the LP context calculated based on the expected velocity subtracted from participants' response. Interestingly, we observed the same pattern of response seen in congruent condition during occlusion in the LP context, suggesting that participants were not estimating according to the feedback, rather they were responding according to the learned velocity-direction association.

High x Low Predictability

Reaction time error analysis yielded similar results compared to reaction time. We observed an interaction for direction and predictability ($F(1,14)=5.069$, $p=.041$, $\eta_p^2=.266$; upward vs. downward in HP context: $MD=-0.023$, $\pm.006$, $t=-3.914$, $p_{bonf}=.003$), velocity and predictability ($F(1,14)=38.000$, $p<.001$, $\eta_p^2=.731$; fast vs. slow in HP context: $MD=.088$, $\pm.013$, $t=6.873$, $p_{bonf}<.001$; slow in HP vs. slow in LP context: $MD=.063$, $\pm.013$, $t=4.890$, $p_{bonf}<.001$; fast vs. slow in LP context: $MD=.172$, $\pm.013$, $t=13.420$, $p_{bonf}<.001$). We also observed significant main effects for direction ($F(1,14)=10.491$, $p=.006$, $\eta_p^2=.428$; upward vs. downward: $MD=-0.014$, $\pm.004$, $t=-3.239$, $p_{bonf}=.006$), velocity

(F(1,14)=143.372, p<.001, η_p^2=.911; fast vs. slow: MD=.130, ±.011, t=11.974, p_{bonf}<.001) and a marginally significant effect for predictability (F(1,14)=3.783, p=.072, η_p^2=.213).

Univariate fRMI-results

Visible Phase

High predictable context

Analysis of beta weights during visible stimulation presented in HP context indicated an interaction between direction and V1 Quadrant (Figure 13A), which suggests that the vertical stimulations were salient enough to elicit higher responses in the opposite quadrant (F(1,14)=76.090, p<.001, η_p^2=.845; upward vs. downward in the upper V1: MD=-2.485, ±.511, t=-4.865, p_{bonf} <.001; upward vs. downward in lower V1: MD=2.230, ±.511, t=4.364, p_{bonf} <.001). We also observed a triple interaction between direction, velocity and V1 quadrant (Figure 14A), mainly pointing to higher fMRI-responses during fast motion in downward direction in upper V1 (F(1,14)=6.761, p=.021, η_p^2=.326; downward fast vs. downward slow in upper V1: MD=5.019, ±1.442, t=3.480, p_{bonf} =.043; downward fast in upper V1 vs. downward fast in lower V1: MD=4.200, ±1.155, t=3.636, p_{bonf} =.031, upward slow vs. upward fast in lower V1: MD=5.252, ±1.442, t=3.642, p_{bonf} =.028). A main effect of velocity was also seen (F(1,14)=35.717, p<.001, η_p^2=.718; fast vs. slow: MD=3.690, ±.617, t=5.976, p_{bonf}<.001). No effect for task order was observed for any of the conditions.

Low predictable context

During visible stimulation presented in low predictable context, we observed again direction and V1 Quadrant interaction (Figure 13B - F(1,14)=26.231, p<.001, η_p^2=.652), which demonstrated that, the insertion of the noise through the incongruent trials still led to higher responses in the opposite quadrant; this effect was significant for upper V1 (MD=-2.630, ±.472, t=-5.573, p_{bonf} <.001), but marginally significant for lower V1 (upward vs. downward in lower V1: MD=1.304, ±.472, t=2.764, p_{bonf} =.063). Further interactions between velocity and congruency (Figure 15A) was also seen, interestingly presenting higher fMRI-signal during congruent fast motion and incongruent slow motion (F(1,14)=99.931, p<.001, η_p^2=.877; congruent fast vs. slow: MD=4.240, ±.374, t=11.329, p_{bonf} <.001; congruent fast vs. incongruent fast: MD=3.319, ±.455, t=7.286, p<.001; congruent slow vs. incongruent slow: MD=-1.706, ±.455, t=-3.746, p_{bonf} =.006).

We further observed an interaction between direction and velocity (F(1,14)=4.694, p=.048, η_p^2=.251; downward fast vs. downward slow: MD=4.212, ±1.180, t=3.570, p_{bonf} =.016), and a marginally significant triple interaction between direction, velocity and V1 Quadrant (Figure 14B), which yielded significant post-hoc comparisons (F(1,14)=4.240, p=.059, η_p^2=.232; upward fast vs.

downward fast in upper V1: MD=-5.799, ±1.284, t=-4.517, p_{bonf} =.005; downward fast vs. downward slow in upper V1: MD=4.766, ±1.237, t=3.852, p=.031). Main effects for direction (F(1,14)=5.841, p=.030, η_p^2=.294; upward-downward: MD=-0.663, ±.274, t=-2.417, p_{bonf} =.030), velocity (F(1,14)=38.808, p<.001, η_p^2=.735; fast-slow: MD=1.727, ±.277, t=6.230, p_{bonf} <.001) and marginally significant effect for congruency (F(1,14)=4.504, p=.052, η_p^2=.243; congruent-incongruent: MD=.806, ±.380, t=2.122, p_{bonf} =.052) were also seen in the results.
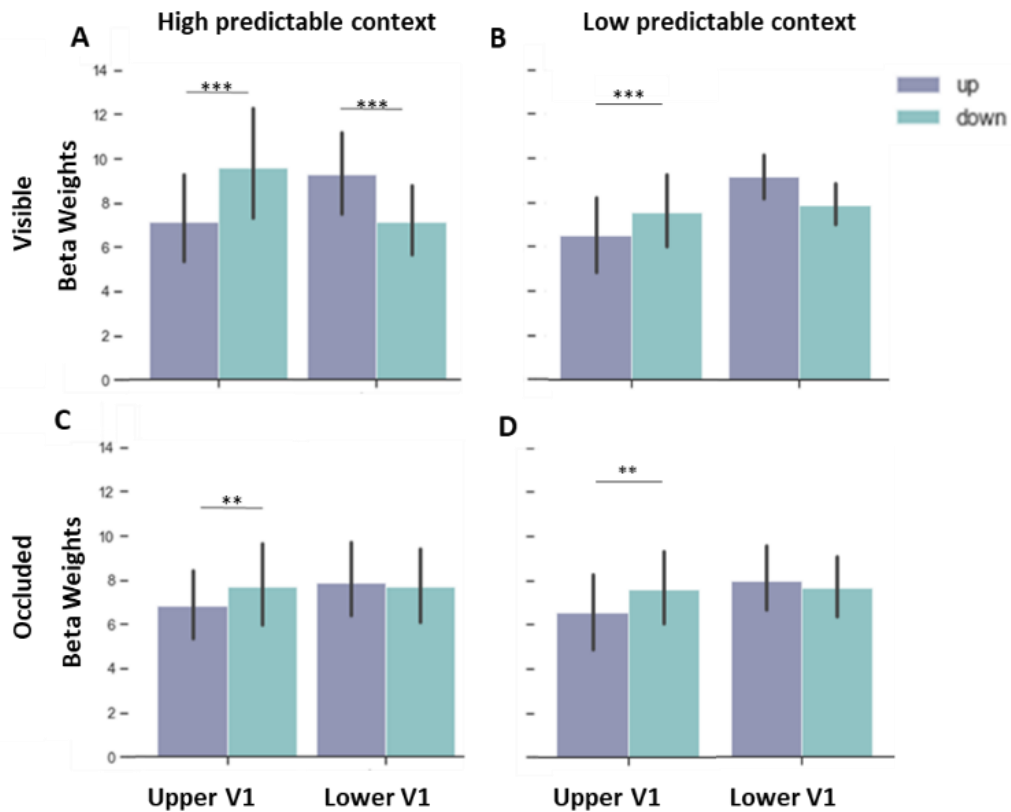
Figure 13 - Beta weights of HP and LP contexts during (A) visible and (B) occluded phase, indicating an interaction between direction and V1 Quadrant. Purple bars represent upward trajectory and green bars represent downward trajectory. (A) During visible phase in HP context, as expected, we observed that downward trajectory modulated higher responses in upper V1, compared to upward trajectory, whereas upward trajectory elicited higher responses in lower V1 compared to downward trajectory. (B) During visible phase in LP context, we observed the same pattern as in HP context, however, significant results were seen only in upper V1, while results in lower V1 were just marginally significant.

High x Low Predictability

When comparing congruent beta values from both contexts, we observe interactions between direction and V1 Quadrant (F(1,14)=54.439, p<.001, η_p^2=.795; upward vs. downward in the upper V1: MD=-2.777, ±.456, t=-6.087, p_{bonf} <.001; upward vs. downward in lower V1: MD=1.515, ±.456, t=3.320, p_{bonf} =.016), which indicated that the vertical stimulations were salient enough to elicit

higher responses in the opposite quadrant. Additionally, triple interactions were seen between direction, velocity and V1 Quadrant (F(1,14)=12.864, p=.003, η_p^2=.479; upward fast vs. upward slow in lower V1: MD=4.075, ±1.137, t=3.585, p_{bonf} =.004; upward fast vs. downward fast in upper V1: MD=-4.965, ±1.118, t=-4.441, p_{bonf}=.005; downward fast vs. downward slow upper V1: MD=6.158, ±1.137, t=5.418, p_{bonf}<.001) and velocity, V1 quadrant and predictability (F(1,14)=6.408, p=.024, η_p^2=.314; post-hoc comparisons were not observed for factors between different contexts). A main effect was observed for velocity (F(1,14)=78.946, p<.001, η_p^2=.849; fast vs. slow = MD=3.965, ±.446, t=8.885, p_{bonf} <.001).

<u>*Occluded Phase*</u>

High predictable context

Beta weights during high predictable occluded phase indicated an interaction between direction and V1 Quadrant (Figure 13C), which demonstrated that during occlusion, downward direction elicited a similar pattern of response in upper V1, but not lower V1, compared to visible phase, in which the stimulus was visible (F(1,14)=10.927, p=.005, η_p^2=.438; upward vs. downward in upper V1: MD=-0.945, ±.285., t=-3.315, p_{bonf}=.016). Further, it was observed a main effect of velocity (F(1,14)=42.861, p<.001, η_p^2=.754; fast vs. slow: MD=4.013, ±.613, t=6.547, p<.001). Although no difference was observed for the triple interaction between direction, velocity and VF (Figure 14C), but for the sake of comparison, we ran post-hocs and found significant differences between upward fast vs. upward slow in lower V1 (MD=4.013, ±.613, t=6.547, p=.044); downward fast vs. downward slow in lower V1 (MD=4.230, ±1.054, t=4.015, p=.009); upward fast vs. upward slow in upper V1 (MD=3.667, ±.1.054, t=3.480, p=.039); downward fast vs. downward slow in upper V1 (MD=4.531, ±1.054, t=4.301, p=.004).

Low predictable context

During low predictable context, we once more observed interaction between direction and V1 quadrant (Figure 13D - F(1,14)=19.683, p<.001, η_p^2=.584; post-hoc comparisons revealed the difference only when incongruent trials were not included in the analysis: F(1,14)=14.691, p=.002, η_p^2=.517; upward vs downward in the upper V1: MD=-1.532, ±.436, t=-3.511, p=.014). Additionally, it was seen interactions between velocity and congruency (Figure 15B - F(1,14)=30.281, p<.001, η_p^2=.684; congruent fast vs. congruent slow: MD=3.953, ±.602, t=6.561, p_{bonf}<.001; congruent vs. incongruent fast: MD=2.767, ±.461, p_{bonf}<.001), and direction and congruency (F(1,14)=15.575, p=.001, η_p^2=.527; congruent vs. incongruent downward: MD=1.462, ±.349, t=4.192, p_{bonf}=.003). Further, results revealed a marginally significant interaction between direction and velocity

(F(1,14)=4.016, p.065, η_p^2=.223; downward fast vs. slow: MD=4.119, ±1.101, t=3.743, p_{bonf}=.007). We have also seen main effect for velocity (F(1,14)=18.184, p<.001, η_p^2=.565; fast vs. slow: MD=2.162, ±.507, t=4.264, p_{bonf} <.001) and congruency (F(1,14)=8.946, p=.010, η_p^2=.390; congruent vs. incongruent: MD=.976, ±.326, t=3.000, p_{bonf}=.010). Here as well, for the sake of completeness, we ran post-hocs related to the triple interaction between direction, velocity and VF (Figure 14D) and observed significant difference between downward fast vs. downward slow in upper V1 (MD=4.288, ±1.171, t=3.610, p_{bonf}=.035).
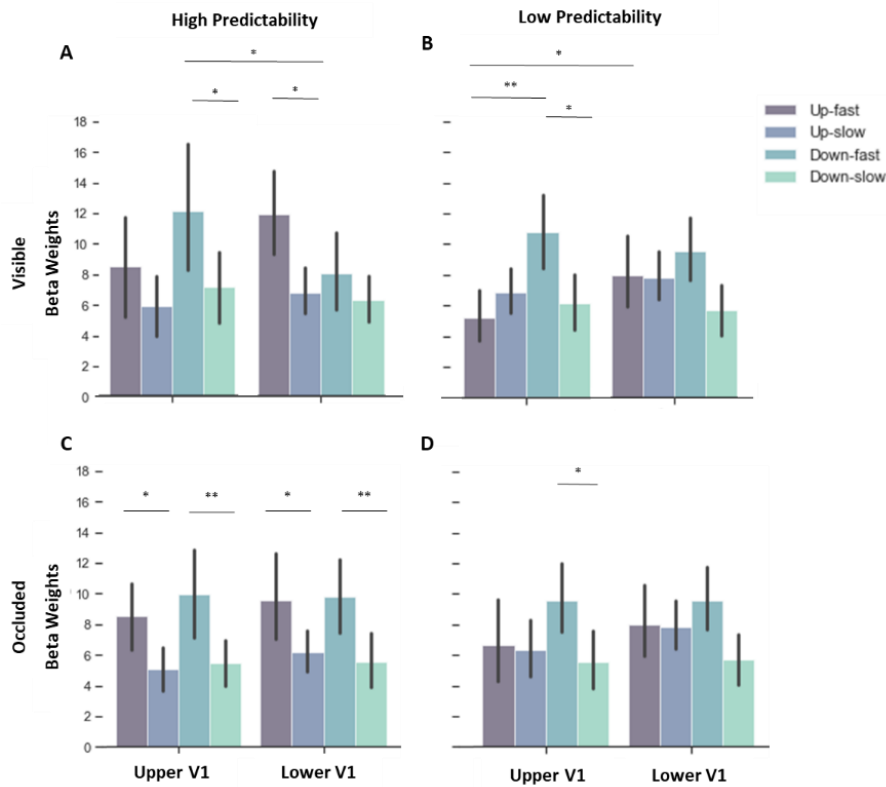
Figure 14 - Beta weights of HP and LP contexts during visible and occluded phase, indicating interaction between direction, velocity and V1 Quadrant. Purple bars represent upward trajectory and green bars represent downward trajectory. (A) During visible phase in HP context, we observed higher responses for fast compared to slow motion in downward trajectory in upper V1, which was also higher compared to fast downward in lower V1. In lower V1, responses during fast motion was higher than slow motion in upward trajectory. (B) During visible phase in LP context, fast motion compared to slow motion seemed to have modulated higher responses in downward trajectory in upper V1, which was also higher compared to fast motion in upward trajectory. However, fast upward motion was higher in lower V1 compared to upper v1. (C) During occlusion phase in HP context, differences were observed with the same quadrant only. Fast motion in upward, as well as in downward trajectory elicited higher responses compared to slow motion in the respective trajectories. (D) In LP context, during occlusion phase, fast motion compared to slow motion in downward trajectory modulated higher responses in upper V1.

High x Low Predictability

During occlusion, comparison between both contexts yielded interaction between direction and V1 quadrant (F(1,14)=18.134, p<.001, η_p^2=.564; upward vs. downward in the upper V1: MD=-1.238, ±.301, t=-4.116, p_{bonf}=.003), revealing a marginally significant interaction between direction and velocity (F(1,14)=3.451, p=.084, η_p^2=.198; upward fast vs. upward slow: MD=2.701, ±.894, t=3.020, p_{bonf}=.033; downward fast vs downward slow: MD=5.265, ±.894, t=5.889, p_{bonf}<.001). We further observed a main effect of direction (F(1,14)=5.489, p=.034, η_p^2=.282; upward vs. downward: MD=-0.616, ±.263, t=-2.343, p_{bonf}=.034) and velocity (F(1,14)=49.106, p<.001, η_p^2=.778; fast vs. slow: MD=3.983, ±.568, t=7.008, p_{bonf}<.001), but no main effect or interaction with predictability.
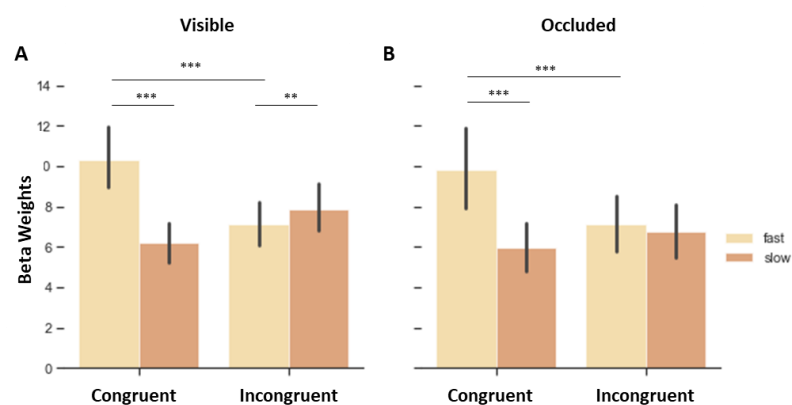
Figure 15 – Congruent and Incongruent comparison in visible and occlusion phases. Fast congruent trials showed higher fMRI-responses in both V1 quadrants during (A) visible and (B) occluded phases, compared to slow congruent and incongruent conditions. Note, however, that slow incongruent (speeded-up stimulus in the vertical trajectory) elicited higher responses compared to fast incongruent (slowed-down stimulus in the vertical trajectory), meaning that fast, though expected slow, trials showed higher responses during visible, but not during occlusion phase, suggesting that fast motion engage higher response in V1, compared to slow motion.

Multivariate Pattern Analysis results

We performed a series of trial-wise volume-based MVPA analyses to investigate the representational pattern of activity during visible and occlusion phases in HP and LP contexts, separately, in lower and upper V1 quadrants and in rhV5. Additionally, a comparison between both contexts were carried out to investigate whether LP context encoded more information, i.e. predictive error, than HP context. Table 1 and 2 depict the accuracy values of all analyses, of which we decoded spatial information, i.e. upward and downward trajectory; and temporal information, i.e. fast and slow motion, respectively

Spatial Information

Classifying Direction Patterns of Visible Phase from Occluded Phase in HP and LP contexts. In these analyses we trained the classifier in the visible phase and tested in the occluded phase data using upward and downward conditions as labels regardless of predictability. Here we expected to decode visible information from the occluded data, as we have seen in the previous study (chapter 2) that the different modalities can share the same spatial layout in low-level visual areas. In order to obtain the most informative voxels, we averaged the highest 5% most informative spheres (range of 45 to 112 selected spheres), similar to the previous chapter. Results showed accuracies above chance level (Fig. 16: "Visible-Occluded", and table 2), suggesting that we could successfully decode direction-specific informational patterns from the visible phase in the occluded phase in the lower and upper V1 and V5. Additionally, all analyses with the true labels yielded significantly higher accuracies compared to the permutation analyses (table 2A). Together, these findings indicate that MVPA significantly extended the results from the univariate analyses by showing that both phases share similar informational pattern in the primary visual area and V5. Furthermore, these classification analyses replicate the results of our previous study, in which we demonstrated a common engagement of low-level visual cortex during the presentation of visible and dynamically occluded motion.
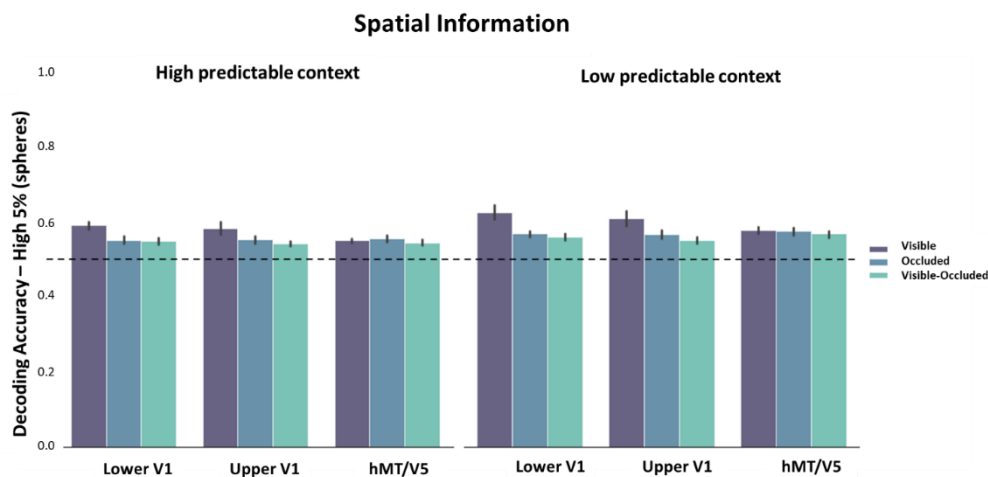
Figure 16 – Classifying Spatial Information: Decoding accuracies of all classification analyses in different ROIs when classifying directions. The decoding accuracies represent the averaged values of the 5% most informative spheres of the searchlight analyses. Purple bars depict averaged accuracy of classification analyses in which the classifier was trained and tested in visible phase ("Visible"), blue bars depict the averaged accuracy of classification analyses in which the classifier was trained and tested in occluded phase ("Occluded"); and green bars show averaged accuracy of analysis in which the classifier was trained in visible phase and tested in the occluded phase ("Visible-Occluded"). The three triple bars from the left (showing analyses on Lower V1, Upper V1 and hMT/V5, respectively) represent the averaged accuracies of the analyses with HP context data, whereas the three triple bars from the right represent the averaged accuracies of the analyses with LP context data. The dashed line on 0.5 represent the cut-off of accuracies below chance level

As a manipulation check, we tested the classifier in visible and occlusion phases separately. Results indicated that accuracies from the classification analysis in which we trained and tested in visible phase data were higher compared to the two other classification analyses (Figure 16 - "Visible", "Occluded, table 2B-C). Such results were expected, as during the visible period more visual information is available to be encoded by the visual system. In contrast, the other two analyses presented very similar averaged decoding accuracies. Note that the decoding accuracies of this analysis were generally smaller compared to the first experiment as we used trial-wise rather than run-wise estimates as input to the MVPA, which includes an increased noise level.

When comparing accuracies of HP and LP context (table 2), we observed significantly higher accuracies decoded from LP context data compared to accuracy decoded from HP context data in all analyses, this may suggest that the incongruent condition might have led to an encoding of more information. Further, we present results of congruent and incongruent decoding.

Spatial Information: Direction

ROI	Predictability	Accuracy	SE	Permutation p-value	N spheres (average)	Paired T-Test
Lower V1		High	0.551	0.005	<.001	100 (±42.93)	t=-2.501.
		Low	0.564	0.005	<.001	96 (±42.84)	p = .024
Upper V1	Visible-Occluded	High	0.545	0.004	<.001	71 (±46.59)	t=-2.579.
		Low	0.554	0.005	<.001	77 (±48.21)	p = .021
V5		High	0.548	0.004	<.001	66 (±21.61)	t=-5.628.
		Low	0.571	0.005	<.001	72 (±23.80)	p <.001

ROI	Predictability	Accuracy	SE	Permutation p-value	N spheres (average)	Paired T-Test
Lower V1		High	0.594	0.005	<.001	101 (±44.52)	t=-4.303.
		Low	0.629	0.010	<.001	112 (±48.75)	p <.001
Upper V1	Visible	High	0.585	0.009	<.001	73 (±57.19)	t=-3.373.
		Low	0.612	0.011	<.001	83 (±56.88)	p = .004
V5		High	0.553	0.003	<.001	49 (±24.03)	t=-5.378.
		Low	0.581	0.005	<.001	59 (±20.77)	p <.001

ROI	Predictability	Accuracy	SE	Permutation p-value	N spheres (average)	Paired T-Test
Lower V1		High	0.554	0.005	<.001	74 (±39.94)	t=-4.763.
		Low	0.571	0.004	<.001	88 (±38.88)	p <.001
Upper V1	Occluded	High	0.556	0.005	<.001	45 (±33.92)	t=-2.548.
		Low	0.569	0.006	<.001	62 (±43.10)	p = .023
V5		High	0.558	0.004	<.001	51 (±23.52)	t=-3.740.
		Low	0.578	0.005	<.001	58 (±21.17)	p = .002

Table 2 – Decoding accuracy of spatial information: Accuracy values of all analyses of all conditions are displayed on the table above, together with the standard error of the mean (SE). Permutation p-values demonstrate that the permuted accuracy distributions were highly significant different from the true label accuracy distribution. The average number of spheres included in the sample of 5% most informative spheres can be seen in the range of 45 to 112.

Temporal Information: classifying velocity

Classifying Velocity Patterns of Visible Phase from Occluded Phase in HP and LP contexts. Here, we carried out the same analyses as in the previous session by training the classifier in the visible phase and tested in the occluded phase data, but using fast and slow conditions as labels. We expected to decode motion information in the primary visual area and V5. As well as in the previous analyses, decoding accuracies, obtained from the sample of the 5% most informative spheres (range of 81 to 132 spheres) were above chance level (Figure 17: "Visible-Occluded", table 3), suggesting that temporal information may be also encoded in visual areas and may share similarity patterns during visible and occluded phases.
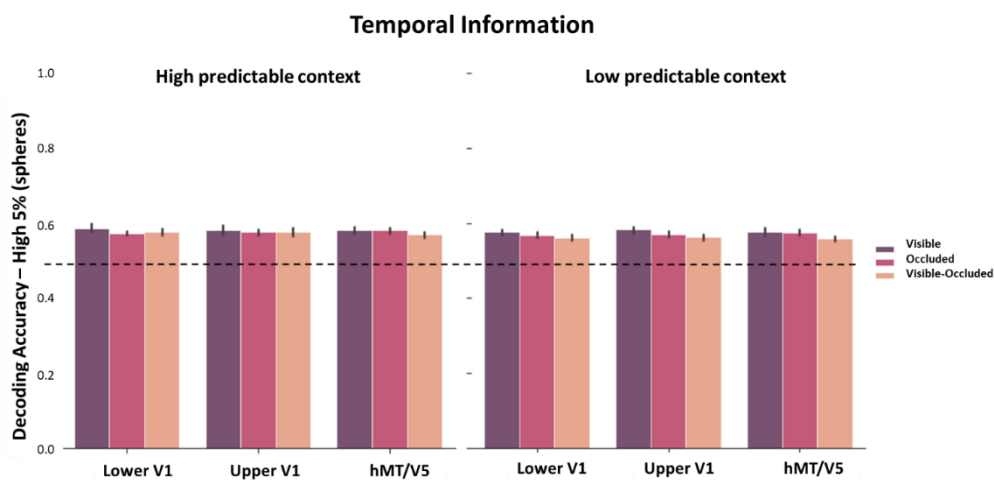
Figure 17 - Classifying Temporal Information: Decoding accuracies of all classification analyses in different ROIs when classifying velocity. The decoding accuracies represent the averaged values of the 5% most informative spheres of the searchlight analyses. Purple bars depict averaged accuracy of classification analyses in which the classifier was trained and tested in visible phase ("Visible"), pink bars depict the averaged accuracy of classification analyses in which the classifier was trained and tested in occluded phase ("Occluded"); and orange bars shows averaged accuracy of analysis in which the classifier was trained in visible phase and tested in the occluded phase ("Visible-Occluded"). The three triple bars from the left (showing analyses on Lower V1, Upper V1 and hMT/V5, respectively) represent the averaged accuracies of the analyses with HP context data, whereas the three triple bars from the right represent the averaged accuracies of the analyses with LP context data. The dashed line on 0.5 represent the cut-off of accuracies below chance level.

Manipulation checks were carried out also here (Figure 17: "Visible", "Occluded"), by analysing visible and occluded phases separately. Note, however, that, in comparison with the decoding of spatial information, we did not observe higher accuracy for visible phase analysis compared to the other two analyses. This may indicate that the pattern of temporal information was encoded similarly independently of the availability of the stimulus (visible or occluded). In contrast with the comparison of spatial information decoding accuracies from HP and LP context, in which we observed higher accuracies for the latter, accuracies from analyses with LP context data were not higher than accuracies from analyses with HP context data (Table 3). Instead, classification analyses with visible phase only or occluded phase only did not yield significant

different results between both contexts; whereas analyses in which the classifier was trained in visible and tested in occluded HP context data yielded higher accuracies than the same analysis with LP context data. These findings might suggest that temporal information can be better decoded when the encoding is not affected by some noise, such as the incongruency factor.

Temporal Information: Velocity

ROI	Predictability	Accuracy	SE	Permutation p-value	N spheres (average)	Paired T-Test
Lower V1		High	0.577	0.005	<.001	132 (±52.52)	t = 3.487.
		Low	0.561	0.004	<.001	125 (±50.57)	p = .003
Upper V1	Visible-Occluded	High	0.577	0.005	<.001	100 (±63.11)	t = 3.208.
		Low	0.562	0.004	<.001	95 (±61.80)	p = .006
V5		High	0.569	0.005	<.001	81 (±18.38)	t=3.390.
		Low	0.558	0.004	<.001	73 (± 20.93)	p = .004

ROI	Predictability	Accuracy	SE	Permutation p-value	N spheres (average)	Paired T-Test
Lower V1		High	0.586	0.006	<.001	112 (±44.48)	t=1.352.
		Low	0.576	0.004	<.001	94 (±42.10)	p = .196
Upper V1	Visible	High	0.581	0.007	<.001	86 (±51.98)	t=-0.192.
		Low	0.582	0.005	<.001	75 (±46.26)	p = .850
V5		High	0.580	0.005	<.001	73 (±20.16)	t=0.484.
		Low	0.577	0.005	<.001	58 (±20.87)	p = .636

ROI	Predictability	Accuracy	SE	Permutation p-value	N spheres (average)	Paired T-Test
Lower V1		High	0.573	0.003	<.001	124 (±47.70)	t=1.120.
		Low	0.568	0.005	<.001	107 (±45.36)	p = .280
Upper V1	Occluded	High	0.576	0.004	<.001	94 (±60.94)	t=1.054.
		Low	0.571	0.004	<.001	86 (±59.31)	p = .308
V5		High	0.581	0.005	<.001	76 (±18.42)	t=1.359.
		Low	0.575	0.004	<.001	67 (±18.63)	p = .194

Table 3 –Decoding accuracy of temporal information: Accuracy values of all analyses of all conditions are displayed on the table above, together with the standard error of the mean (SE). Permutation p-values demonstrate that the permuted accuracy distributions were highly significant different from the true label accuracy distribution. The average number of spheres included in the sample of 5% most informative spheres can be seen in the range of 81 to 132.

Congruent Information in LP context

Classifying Incongruent trials of Visible Phase and Occluded Phase in LP context: These analyses were carried out by training the classifier in the visible and occluded data separately, using congruent and incongruent conditions as labels. Results indicated that averaged accuracies (average of the number of the 5% most informative spheres is 75, ±41.05) were significantly above chance level compared to permutation analyses of visible phase in lower V1 (mean (M) = 0.572,

±.024, permutation p (p_{perm}) <.001; upper V1 (M=.566, ±.019, p_{perm}<.001) and V5 (M=.571, ±.022, p_{perm}<.001), as well as of occluded phase in lower V1 (M=.554, ±.015, p_{perm}<.001), upper V1 (M=.552, ±.014, p_{perm}<.001) and V5 (M=.580, ±.023, p_{perm}<.001). These results indicated that incongruent trials were successfully classified differently from congruent trials, suggesting that different information was encoded during the tasks with lower temporal predictability. Additionally, these findings significantly extend the univariate analysis which also showed different pattern of activity between congruent and incongruent conditions.
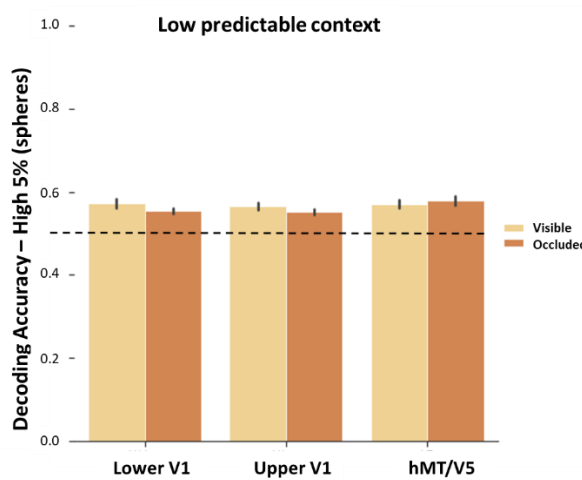
Figure 18 - *Classifying congruent and incongruent information: The decoding accuracies represent the averaged values of the 5% most informative spheres of the searchlight analyses. Yellow bars depict averaged accuracy of classification analyses in which the classifier was trained and tested in visible phase ("Visible"), Orange bars depict the averaged accuracy of classification analyses in which the classifier was trained and tested in occluded phase ("Occluded"). The two bars from the left, middle and right (showing analyses on Lower V1, Upper V1 and hMT/V5, respectively) represent the averaged accuracies of the analyses with LP context data. The dashed line on 0.5 represent the cut-off of accuracies below chance level*

Overlap of sphere centres

To evaluate that our approach of choosing the 5% highest accuracy values is robust and free of bias, we calculated the number of spheres which share the same centres across different classification analyses. Interindividual results indicated that all participants d shared spheres across different analysis in different probability context in all masks. Heatmaps with individual results can be seen in the appendix B. The averaged overlapped spheres centre for all classification analyses performed here can be seen in tables 1 and 2. The overall average of all analyses is 83.19 (sd: ±21.63). Note that this value is similar to the number of sphere centres reported in the previous study (chapter 2). This similarity between overall averages of both studies may be a result of the down-sampled space, as the analyses were carried out in the reduced space of ROI masks. Together, these results suggested that our approach of selecting the 5% highest informative voxels are robust, supporting

the interpretation that when different decoding analyses share the same sphere centre, the decode pattern is truly informative, rather than random noise.

Discussion

Our study investigated whether motion extrapolation mechanisms presented in high and low predictable contexts, throughout the manipulation of the temporal information, could differently modulate fMRI-responses in the primary visual cortex during visible and occlusion period. Our behavioural results demonstrated that during visible phase, differences were observed between HP and LP contexts, indicating that performance was higher for HP compared with LP especially for slow motion in downward trajectory. Moreover, accuracies were also higher during congruent trials compared to incongruent trials presented in LP context. In contrast, during occlusion phase participants performed equally well in both HP and LP contexts. However, we observed differences between velocities. Performance was better during slow motion compared to fast motion stimulation. These results are in line with the notion of evidence accumulation proposed by the Theory of Magnitude (ATOM), which assumes that different magnitudes, here temporal and spatial, interfere with one another and predicts relatable but not always symmetrical interaction between the magnitudes (Lambrechts et al., 2013). Moreover, participants might just have had more time to respond more accurately.

Reaction time results during visible stimulation showed that participants attempted to estimate the time-to-contact of the stimulus accordingly (faster responses during fast motion, slower responses during slow motion), in HP and LP context, following the expected pattern, corroborating our first study (chapter 2; Agostino et al., under revision). However, we, further, observed an interaction between velocity and predictability which indicated that participants responded faster during LP context. During occlusion, temporal estimation in LP context did no longer follow the same pattern, meaning that faster trials were not estimated faster and slower trials were not estimated longer. Rather, reaction time was similar across conditions in LP context, suggesting that temporal estimation indeed was hindered by lower predictability. This effect could be explained by post-error adaptations (Danielmeier & Ullsperger, 2011; King et al., 2010), which mainly happen in frontal areas, such as medial frontal cortex (MFC). Post-error adaptations alter future behaviour, leading to potential improvements, such as faster reaction times or higher accuracies. One of these adaptations is known as post-error speeding and it was showed that it is related to an enhancement of performance after a given threat (Caudek et at, 2015) and an increase of activity in task-relevant visual areas (King et al., 2010). However here, we didn't observe the improvement of fast stimulus estimation, as participants were still trying to adequately respond

according to the learned pattern. This was also found in a reversal of responses for incongruent relative to congruent trials during occlusion, pointed by reaction time error, which demonstrated that participants applied the learned congruent direction-velocity change. In appendix B, it possible to see this effect when reaction time error is calculated based on the velocity that the participants are expecting subtracted from their response time. The plots showed that for incongruent condition during occlusion, congruent and incongruent trials followed the same pattern.

Univariate analysis read-outs

At the neural level, results of our univariate analysis indicated no significant differences between HP and LP context, neither during visible nor during occlusion phase. This finding is not in line with our initial hypothesis that we should see enhanced fMRI-signals in the LP context which should have required a greater amount of attention. However previous studies which observed an enhancement in activity in the primary visual cortex during the processing of dynamically occluded stimulation due to attention did not modulate attentional demands parametrically (Kok et al., 2012; Coull et al. 2008; Doherty et al., 2005), thus it is conceivable that a certain amount of attention, present in HP and in LP contexts, increased the signal to the maximum. Hence, attention would affect prediction processing not gradually but categorically and the manipulation of attentional demands would not further modify fMRI-responses. Moreover, it is important to emphasize that during occlusion participants did not make a simple time-to-contact judgement, but rather they were required to make a more complex prediction due to the velocity-direction association. Potentially the reappearance of the stimulus may have automatically captured attention and thus may have generated a response high enough to cancel the pattern of activity related to the predictive error, thus equalizing the response pattern in HP and LP contexts.

We further observed that upwards trajectories enhanced responses in lower V1 and downward trajectories enhanced responses in upper V1, not only during the visible phase, but also and most importantly, during occlusion phase. These results corroborated the univariate results of our previous study presented on chapter 2, which demonstrated that the mechanisms related to visualizing and extrapolating a moving stimulation indeed engage activity in low-level visual areas. However, here observed that the expected pattern was seen in visible and occlusion phase in HP and LP contexts in upper V1, hence lower visual field. Differences between vertical hemifields are robust. The literature of the so-called vertical meridian asymmetry (Carrasco et al., 2001; Rijsdijk et al., 1980; Previc, 1990) indicates a dominance of the lower visual field over the upper visual field in different tasks, such as spatial resolution (Talgar & Carrasco, 2002), visual acuity (Skrandies, 1987), motion (Levine & McAnany, 2005), among others (Karim & Kojima, 2010, for review). An

ecological explanation for this difference between vertical meridians was given by Previc (1990), who proposed that the dominance of the lower visual field comes from the primordial of the primate visual system, which was functionally more developed due to forelimb manipulatory skills. Later, studies indicated that the lower VF contains a larger amount of "near-preferring" neurons most commonly found in the latter compared to the first (Nasr & Tootell, 2018, 2020; Karim & Kojima, 2017). These findings could explain the difference between this and our previous study, given that in this study we introduced the reappearance of stimulus, which might also have led to an automatic capture of attention (Lakha & Humphreys, 2005). It is important to mention once more that the portion (voxels) in the respective quadrants which could have been modulated by the reappearance of the stimulus was carefully excluded from the analyses to avoid misleading conclusions.

While in the spatial domain the stimulation modulated different patterns of activity, in the temporal domain univariate results were unanimous. The presentation of fast stimulation consistently enhanced activity in both upper and lower visual quadrants. Interestingly, even during incongruent conditions of visible stimulation, there was a tendency for the incongruent slow (speeded-up stimulus) to follow the same pattern of enhanced activity observed during the presentation of congruent fast. One possible explanation for these findings is that velocity might be coded based on neural mechanisms engaged in the memory of speed (Pasternak & Greenlee, 2005). Another is that V1 may be more promptly receiving feedback projections from V5 during fast motion (Edwards et al. 2017; Sterzer et al., 2006; Muckli et al. 2005), which could increase the response signal, while processing of slow motion would be taking longer to reach V5 and reach V1 back.

Note that the univariate results partially oppose to the behaviour results in which we observed that a major effect for slow, rather than fast motion. However, during LP context, the reversal pattern seen during incongruent trials in reaction time, could be seen as a tendency in the univariate results. Accordingly, MVPA results also pointed to decoding differences between congruent and incongruent trials, which we discuss in the next section. Note, as well, that in the next chapter we follow-up on this observation and investigate causal relation between the primary visual cortex and velocity discrimination.

MVPA read-outs

The series of multivariate pattern analyses extended the results of the univariate analyses throughout a different perspective. Although in the latter analyses, no difference was observed between fMRI-response signal in V1 during HP and LP contexts stimulation, the decoding analyses

indicated that the encoded representational pattern of activity differ between both contexts. First, we observed that representational patterns of activity from visible phase could be decoded from occluded phase in upper and lower V1, suggesting that both types of information share similar representational pattern in the very same voxels, replicating the results from the first study (chapter 2; Agostino et al., under revision). The robustness of this decoding and the sphere selection that we used was further confirmed by computing the overlap of sphere centres. This overlap indicated that a significant number of spheres, regarding the ROI size, shared the same centre in upper or lower V1 across different types of classification (train in visible, test in occluded; train and test in visible; and train and test in occluded), suggesting that the algorithm was decoding relevant information rather than noise, and also corroborating our previous study. The effect was observed in HP and LP predictable contexts. Remarkably, we observed higher values when classification analyses were carried out using the LP context data compared to HP context data. These results suggested that the decoding captured a relevant pattern of information, and this pattern may be related to the incongruent trials, which was not captured by the univariate analyses when the factors were modelled together, but separately. We did, though, observe a difference between congruent and incongruent trials when we analysed the difference between them, as well as we successfully classified congruent and incongruent trials from visible and occluded data separately, confirming that the representational patterns of both trial types were significantly different. Future high-field fMRI-studies with increased resolution could disentangle the effects of congruent and incongruent trials by segregating the areas of V1 which represent the horizontal and vertical trajectory in greater detail and would thus be able to separately test the similarity of responses for fast and slow velocities in congruent and incongruent trials.

Furthermore, we mentioned above that computations involved in post-error adaptations are located in medial frontal areas. Therefore, this difference between congruent and incongruent trials observed in the univariate results and in the decoding analysis might be explained by feedback from higher level regions (Noesselt, et al., 2002; Summerfield et al., 2006). For instance, Summerfield and colleagues (2006) investigated how decision-making neurons may access predicted information from lower-level regions, in order to compare with sensory information. In this study, the authors presented face and non-face stimulation and asked participants to discriminate between both, while measuring fMRI. Results indicated that face stimulation does not directly elicit response in MFC, as synchronization between activity in this region and stimulus presentation was not robust enough, suggesting that the information is coming from visual regions. They further observed that when face-type information is implicit ("top-down-generated"), activity in ventral MFC is enhanced. To extend the investigation, the authors carried out a connectivity

analysis and observed enhanced feedback signal, during top-down processing, from MFC to amygdala and fusiform area, region related to face recognition (Nars & Tootell, 2012), but no feedforward enhanced activity during bottom-up processing. Although, we focus our analysis on low-level visual regions, it is conceivable that the hierarchical organization related to predictive coding may be also engaging frontal regions during the processing of dynamic occluded stimulation (top-down information) and error-monitoring in the low predictability context. Future studies could analyse functional connectivity, for instance with psychophysiological interactions (Friston et al., 1997) or dynamic causal modelling (Friston et al., 2003), to directly investigate connectivity between high- and low-level regions during motion extrapolation in higher and lower predictability contexts.

In conclusion, we tested whether visible motion processing or motion prediction would differentially modulate fMRI-responses in the primary visual cortex in higher or lower predictability contexts. According to the predictive coding model, it was expected that stimulation presented in low predictable context would enhance activity in V1 compared to high predictable contexts. However, alternatively, activity during high predictable context would also increase activity in this region if any amount of attention outweighs predictive mechanism in an all-or-nothing rather than a gradual way. Our results provided evidence supporting the latter hypothesis, by showing no difference in fMRI-response signal of high and low predictable context tasks. In contrast, our MVPA results indicated that, although response signal in both cases did not differ, the decoded representational pattern of activity was significantly different, and this difference may be due to the incongruent stimulation. Future experiments are needed to directly test the effect of attention in motion extrapolation by parametrically modulating attentional demands and compare whether the effect remains unchanged. Finally, it is worth mentioning that we replicated the results from the previous experiment, which revealed shared informational patterns for visible and extrapolated changes in motion direction in the primary visual cortex.

Chapter 4 - Finding causal relation between temporal information of dynamic occlusion, V1 and V5

Abstract

Predictive coding models proposes that the visual system follows a hierarchical architecture, in which the low-level visual areas, such as V1, feed forward errors from feedback predictions. During the processing of motion, for instance, higher-level regions of visual system and beyond send and receive information input from V1. However, early studies with cortical blindness patients suggested that V1 might not always be engaged in motion processing, depending on the velocity of the moving stimulus, giving rise to the dynamic parallelism theory; whereas studies with Riddoch patients present opposing results. Here we investigated the role of the primary visual cortex in motion processing, specifically velocity discrimination, by examining possible pathways that motion information of different velocities may take to reach V5. To this end, we used a double-pulse TMS to examine causal evidence of the involvement of V1, and compared to the role of V5 in this process using behavioural read-outs. Results did not provide evidence to establish a robust conclusion. We discuss possible methodological confounds that led us to inconclusive results and suggest improvement for future studies.

Introduction

The amount of information available in the environment constantly challenges the brain to extract and process the relevant information fast and efficiently. It has been proposed that the brain utilizes a hierarchical architecture with predictive top-down signals sent from higher levels and compared to incoming sensory information at lower levels. The difference between this comparison, i.e. the predictive error, is sent back via feedforward loops to higher levels (Rao and Ballard, 1999, Mumford, 1992, Friston, 2003). In this so-called predictive coding models in visual domain, the low-level visual areas, such as V1 sends forward the error from feedback predictions (Alink, 2010). For instance, during the process of motion, higher-level regions of visual system, such as hMT/V5+, sends and receives projections from V1 (Koivisto, Mäntylä, Silvanto, 2010). However, early studies with cortical blindness patients suggested that V1 might not always be engaged in the visual processing, depending on the speed of the moving stimulus (Ffytche, Guy and Zeki, 1995,1996). Given the differences in behavioural and brain read-outs in the earlier studies, here we investigated possible pathways that motion information of different velocities may take to reach V5 by using a double-pulse TMS to examine causal evidence of the involvement of V1, and compare with the role of V5 in this process.

Previous studies have shown the engagement of V5 in primates (Born & Tootell, 1992; Fellemann & Van Essen, 1991; Born & Bradley, 2005, for review) and in humans (Goebel, et al., 1998; Kolster et al., 2010; Muckli et al., 2002; Hampson et al., 2004) during motion processing. The moving visual information takes a path to reach higher levels of processing which starts in the retina and travels all along the optical nerve until it reaches the thalamus. From there, the magnocellular layers of the lateral geniculate nucleus (LGN) forward most of the motion information to V1 (Fellemann & Van Essen, 1991), which feedforward it to higher-level regions, such as V5. In accord, Hampson and colleagues (2004) compared brain activity during resting state and processing of moving stimuli and found a network of functionally connected areas involving thalamus, dorsal cuneus, lingual gyrus, middle occipital gyrus and hMT/V5. Other studies also reported that V5 sends back projections to V1 (Laycock et al., 2007) and this feedback information was seen to be related to awareness of visual motion (Pascual-Leone & Walsh, 2001; Bullier, 2001; Lamme, 2001). In line with that, studies with patients suffering from blindsight and healthy individuals provided robust evidence for the engagement of V1 in conscious motion perception.

Blindsight is a term used to describe patients with cortical blindness who can still use visual information to guide their actions (Pöppel et al., 1973; Cowey, 2010). The first studies which investigated visual-cortical-lesioned patients reported that, even though patients were blind to the

presented stimulation, they were still able to guess its location (Pöppel et al., 1973; Sanders et al., 1974). These findings raised questions about the engagement of low-level visual cortex, specifically V1, in conscious and unconscious visual motion perception. Conscious vision is defined as the visual perception which is supported by subjective experience, while unconscious vision refers to the lack of subjective experience of a certain visual stimulation, although this input may still guide individual's behaviour in some circumstances (Railo & Hurme, 2021, for review). For instance, Hurme and colleagues (2017), in a TMS study, investigated the direct influence of V1 on both processes by inhibiting activity in V1 in two different time intervals (60 ms and 90 ms), while participants responded to detect the appearance of one or more stimuli, as fast as they could. After their response they were asked to indicate how many stimuli they detected, followed by a confidence rating scale, in which they evaluate how certain they were about their response. The authors observed that stimulating V1 in different time intervals result in different visual processing. TMS to V1 delivered at the late interval affected the detection of the visual stimulus, i.e. unconscious vision, but still influenced reaction time, suggesting that the unconscious stimulus affected participants' behaviour. However, TMS to V1 delivered at the early interval was enough to affect conscious vison, but it did not modulate behaviour, indicating that V1 plays different roles in different processing phases. These findings corroborated the study from Koivisto and colleagues (2010), in which they also observed that TMS pulse delivered to V1 at different time windows (20 ms and 60 ms) can impair visual awareness. This study also indicated that this critical time window can be found during TMS delivered to V5, consequently impairing back projections to V1 (Vetter et al., 2015).

In contrast to Blindsight patients, Riddoch patients, who also have lesion in the primary visual cortex, still report visual consciousness, especially during motion perception (Schönfeld et al., 2002a; Zeki & Ffytche, 1998). Studies have shown that moving information can take other pathways to reach V5 without necessarily engaging activity in V1. Studies in primates have supported that V5 also receives information from subcortical regions, such as pulvinar (Baldwin, Balaram, Kaas, 2017) and superior colliculus (Berman & Wurtz, 2010, 2011; Lyon, Nassi, & Callaway, 2010; Schönfeld et al., 2002b). The seminal work of Ffytche, Guy and Zeki (1995) postulated that motion can be processed through different pathways, depending on the speed of the stimulus. The motivation for this hypothesis came from clinical study cases in which patients had either V1 or V5 lesioned. For the patient with lesion in V1, it was observed that only fast-moving (>15°/sec) stimulation could be detected. In contrast, when another patient with lesion in V5 was tested, it was seen that only very slow speed (<6°/sec) could be discriminated, suggesting that this motion was processed by intact regions of the cortex, including V1. From these observations, Ffytche and

colleagues suggested the theory of dynamic parallelism, proposing the existence of two pathways recruited for motion processing: a slow-motion pathway (LGN→V1→V5), and a fast motion pathway (SC→V5). In support to this theory, electrophysiological evidences demonstrated that when participants observed a moving checkerboard stimulus, early visual evoked potentials (VEP) could be registered with an onset before 30 ms and with a peak at approximately 45 ms in V5 (Buchner et al., 1997). However, the authors also observed a second VEP which happened around 50 ms with the peak at 70 ms in V1, suggesting that V5 received a visual input without necessarily engaging V1.

To directly test the dynamic parallelism theory, Grasso and colleagues (2018) applied TMS for provoking a virtual lesion in healthy participants, by disrupting V5 and V1, while participants performed a 2AFC random dot motion task. An inhibitory double-pulse TMS was delivered in different time windows and after each trial, participants were required to rate their perception. Results indicated that, when V5 was disrupted, participants' performance was impaired for both fast and slow motion, in different time windows (~30ms and ~80ms, respectively). In contrast, TMS over V1 was related to a general decrease of motion discrimination performance, unrelated to velocity or time window compared to SHAM stimulation. The authors suggested that this overall performance decrease might be related to the impairment of visual processing. However, results did not offer a robust support for the theory.

The presented literature suggests the involvement of V1 in two different processes in a normally developed brain: general conscious (and unconscious) visual processing and visual motion processing. Here, we focus on the latter to investigated the two possible pathways that motion information might take to reach higher levels in the hierarchical visual cortical organization. Although previous studies already showed some evidence of the engagement of V1 in motion, to our knowledge no study measured directly velocity discrimination in a continuous motion context, which is also more ecologically valid compared to other tasks such as random dot motion (RDM). In this study, we tested the dynamic parallelism theory by mainly disrupting V1. To this end, participants were instructed to discriminate between a baseline velocity compared to a faster and a slower, while we delivered a double-pulse TMS to V1, a SHAM double-pulse TMS to V1, and for replication and control purposes, a double-pulse to V5. According to the dynamic parallelism theory, we expected that (1) disrupting V1 should impair performance during slow velocity discrimination but not fast, as slow-motion information may be conveyed from LGN to V5 through V1, while fast-motion information may take direct pathway potentially from SC to V5; (2) TMS over V5 should result in a general velocity discrimination impairment, as this region is well-known to be

related to motion processing (Vetter et al., 2018); (3) perception ratings should decrease for TMS during early time windows (Hurme et al., 2017).

Materials & Methods

Participants

Fifteen participants (mean age 24.06 ±5.40, 12 women) volunteered to take part in a three-day experiment and were recruited from an MRI compatible participant list and after filling a selection criteria questionnaire (Appendix C). Six participants were excluded from the analyses: four of them did not return on the third day; one was excluded due to technical problems during the stimulation and one participant was excluded due to below chance accuracy in one of the task blocks. Therefore, nine participants (mean age 23.45 ±5.14, 9 women) were included in the analyses. All participants were naïve to the purpose of the experiment, had normal or corrected-to-normal vision, presented no history of psychiatric or neurological disorders and followed all the criteria to take part into a TMS (Box 5) study (Rossi, Hallett, Rossini, Pascual-Leone & Safety of TMS Consensus Group, 2009). All procedure was approved by the local ethical committee of Otto-von-Guericke Universität. Note that, due to the COVID-19 pandemic, it was not possible to recruit and measure more participants.

Neuronavigation

In order to locate the regions of interest as precise as possible a neuronavigation system was used. The system counts with a software (ANT Neuro Visor2-Version 2.4.4.45541; https://www.ant-neuro.com/products/visor2) and an infrared camera used to localize reflective spheres strategically positioned on the participant's head with the use of a band. Individuals' anatomical image (T1) were acquired in a separate session, uploaded on the neuronavigation PC and a model of the brain was created for ROI localization. Markers were set on right M1, using the central sulcus as reference; right V1, using the calcarine sulcus as reference; and right V5 using the middle temporal gyrus as reference. The M1 marker was used as starting point to find the motor threshold, markers on V1 and V5 were used as starting point for eliciting phosphenes to guarantee that we were stimulating the regions of interest.

Motor Threshold

Single pulse TMS applied to the motor cortex is commonly used to evoke contralateral motor potentials, i.e. muscle contractions, at a visible level, in order to establish a stimulation threshold based on a smallest level of stimulation capable of still causing some muscle twitch. This smallest

level of stimulation is known as motor threshold (McConnell, et al., 2001) and it is usually identified using the contralateral thumb (abductor pollicis brevis, Pascual-Leone, et al 1992). In this study, motor threshold was searched on the right M1, so we observed movements on the left thumb, using an initial intensity of 40%, which is below the safety value commonly used (Rossi et al., 2009) and increasing until we observed the first movements. This procedure was used with the only intention of having an initial safe stimulation intensity based on each subject's threshold, meaning that, as soon as we observed and the participant reported a muscle twitch 3 out of 5 times, we used this intensity to start stimulating the occipital cortex to elicit phosphenes.

Phosphene Threshold

The perception of illusionary small light spots when the occipital cortex is stimulated are called phosphenes (Brindley & Lewin, 1968; Marg and Rudiak, 1994, Kammer, 1999; Kammer & Baumann, 2010). Single-pulse TMS is commonly used to elicit phosphenes on participants in order to identify the region of interest inside the occipital cortex; and subject-specific intensity stimulation threshold are used to adequately excite or inhibit the neurons (Harllet, 2000; Merabet et al., 2003). In this study, we identified V1 using the neuronavigation marker as reference and the elicitation of phosphenes. To guide our search and to avoid stimulating areas outside V1, we made sure to be around a region 2 cm above the inion and 2 cm to the right (Grasso et al., 2018). When participants reported seeing phosphenes 3 out of 5 times, we registered the intensity and used 90% of the value for the main experiment. All participants reported seeing a small spotlight during a very short amount of time in the central or left upper visual field or foveal. If foveal phosphene was reported we moved the coil until they reported seeing it more lateral in the visual field. The same procedure was done over V5, however there we expected participants to report moving phosphenes. For some participants, the stimulation intensity had to be adjusted for phosphene induction in V5, meaning that intensity was increased until they reported seeing moving phosphenes. All participants reported seeing a moving phosphene like a "thin white line".

Experimental Design

The experiment followed a within-subject design (Fig. 19A). On day 1, participants performed 6 blocks of the main task, without any stimulation, for training purposes (Pre-test). After this pre-test, we adjusted the neuronavigation to localize the participant's head (see Neuronavigation session, for details) and to identify the first region to be stimulated: M1. Over M1 we measured individual's motor threshold, followed by the phosphene threshold measurement over V1, and, consecutively, the main experiment with the double-pulse TMS application. This procedure was common for all participants, only the order of real and sham stimulation over V1 was

counterbalanced across subjects. On day 2, participants performed additional 6 blocks of the main task as training, followed by the neuronavigation and phosphene threshold over V1. The same TMS intensity used on the first day was also used on the second day, but we repeated the phosphene threshold procedure to confirm that the same intensity could be used. After that, the counterbalanced version of the main task was performed by the participants. As sham condition (Fig. 2B), the coil orientation was used in the vertical position, as studies show that stimulation over V1 should be done with the coil in the horizontal position, i.e. perpendicular to the columnar organization of neurons in the visual cortex, meaning that coil orientation is fundamental for a successful stimulation (Jansen et al., 2015; Gomez-Tames et al., 2018; de Goede, Braack & Putten, 2018). Changing the coil orientation allowed us to keep all the other parameters of the stimulation, giving the participant the same haptic and auditory sensations. On day 3 (Fig. 19A), participants performed the main task, while double-pulses were delivered over V5. The region of interest was again localized with the help of the neuronavigation, and once it was identified, phosphene threshold was measured (for details, see Phosphene Threshold session).

Stimuli

The stimulus consisted of a white dot (0.14°) moving from the left to the centre of the screen in three different velocities: baseline (14°/s - 500 ms motion time), fast (35°/s - 200 ms) or slow (8.7°/s - 800 ms). After the presentation of the moving stimuli, a rating scale containing five sentences was displayed on the screen. A white square framing the first sentence could be moved towards to the right or back (Fig. 19C) by using the same arrows, and to confirm their choices, the upper arrow was pressed. No time limit was imposed during rating. The stimuli were displayed on an Asus RogPG258Q monitor (200 Hz, 1920x1080 px) and ran on Matlab 2020b (MatWorks) under a 64-bit Linux distribution (Ubuntu 20.04.2).

Task

Participants were placed 70 cm away from the monitor and instructed about the experiment. Their task consisted of fixating on a cross, while covertly observing the two dots moving consecutively from left to the centre, and judge if the second dot was faster or slower than the baseline, by using the left and right arrow of the keyboard, respectively. After their response, a rating scale containing five sentences displayed on the screen, in which they could choose the sentence that best represented their perception about the previous trial (Fig.19C). The statements, adapted from Grasso et al. (2018), were: 1 = "I did not perceive any motion at all after the first stimulus"; 2 = "I perceived a motion, but did not perceive any difference"; 3 = "I perceived a difference, but I cannot say if it was faster or slower"; 4 = "I perceived a motion and the difference and I am almost confident

of my answer"; 5 = " I perceived a motion and the difference and I am extremely confident of my answer". The task was presented in a training and test sessions (with TMS). The training phase consisted of 6 blocks of 36 trials each, and the test phase, 12 blocks also of 36 trials each. While participants performed the tasks, we monitored the eye movement online with an eye-tracking device (Eyelink: https://www.sr-research.com/eyelink-1000-plus/).
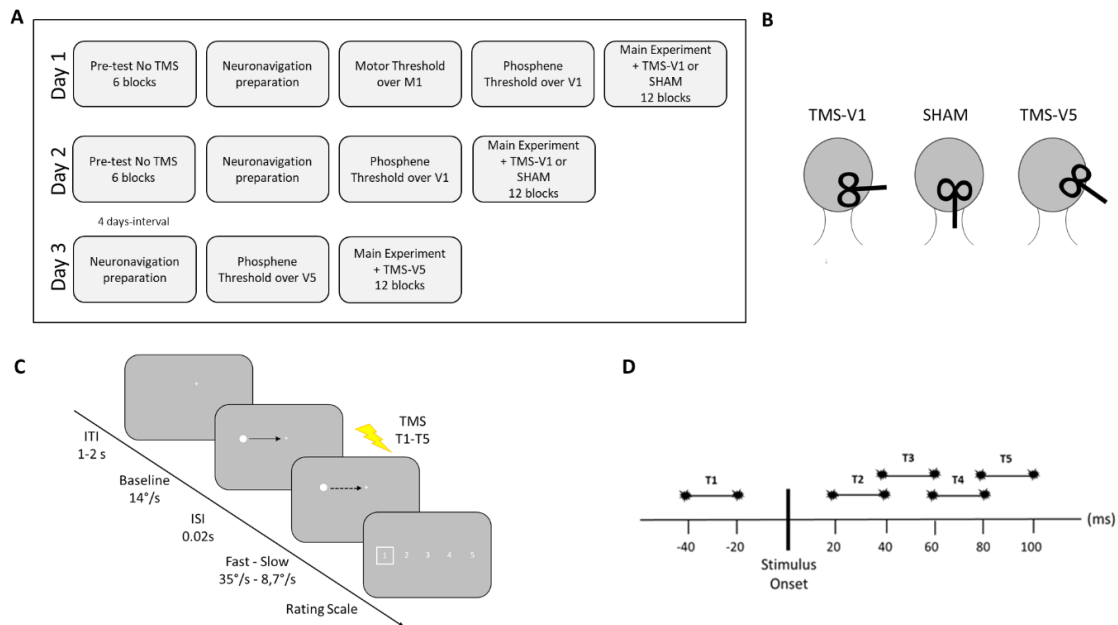
Figure 19 - Overview of the Experiment. (A) Experimental Design: Participants performed a three-day experiment, in which a double-pulse TMS was delivered to their visual cortex. On day 1, they performed a training phase (Pre-test), which was identical to the main experiment, but only half of the blocks were available, the other half was performed on day 2. The Pre-test was followed by the neuronavigation set up, in which we anatomically localized M1, V1 and V5 of each individual participant. After that, the motor threshold was acquired, using the localized M1 on the neuronavigation system as a reference for the search of the muscle movement of the Abductor pollicis brevis (ABP, i.e. thumb muscle). When we observed the movement 3 out of 5 times, we registered the motor threshold. After the threshold was established, the coil was placed over V1 as localized by the neuronavigation system and the motor threshold intensity was used to start eliciting phosphenes. Intensity was adjusted until participants reported 3 out of 5 times that they saw one or more phosphenes. Following the phosphene threshold, participants performed the main experiment. On day 2, participants went through a similar sequence of events, but without the motor threshold acquisition. The order of real and SHAM stimulation over V1 was counterbalanced across subjects. The third session happened four days after day 2, when participants returned for stimulation over V5. Before the stimulation task, we prepared again the neuronavigation for using the localized V5 and elicited phosphenes on this region, expecting participants to report seeing phosphenes in movement. The intensity was adjusted until they reported 3 out of 5 times that they could see the virtual stimulus. (B) Coil orientation and localization according to the stimulation. The first image from left to right depicts the coil rotated in 90° for real stimulation over V1. The centre of the figure-8 coil was touching the region of interested in order to provide the best stimulation condition. The middle image depicts the coil oriented in 0° for SHAM stimulation. Changing just the coil orientation gave us the possibility to keep the same parameters of the stimulation, without perturbating the neurons in V1, as it should happen when the coil is perpendicular to the columnar organization of the visual neurons. The rightmost image shows the coil oriented around 45° to stimulate V5. This orientation could slightly vary across participants. (C) Experimental Task: Participants were asked to fixate their eyes on a fixation cross, while two dots moved consecutively (interval of 20 ms) from the left to the centre and were instructed to respond if the second dot moved faster (dashed line) or slower (dashed line) compared to the baseline velocity (full line) of the first dot. Double-pulse TMS was always delivered after the first stimulation. After the response was given, a screen displaying a rating scale with five sentences (here represented by numbers) was presented, and participants chose the sentence that best represented their motion perception. (D) SOAs for the stimulation triggers in ms: Double-pulse TMS could be delivered before the onset of the second stimulus (double pulse: T1=-40 -20) or after the onset of the stimulus (T2=20, 40; T3=40, 60; T4=60, 80; T5=80, 100), for the same proportion of trial there was no TMS pulse.

The double-pulse TMS could be delivered in different time intervals (Fig.19 D). These intervals were chosen, to establish a series of SOAs, as there is no consensus in the literature about the ideal intervals, in which double-pulse TMS should be delivered during the experiment. The double-pulse TMS could be delivered before the onset (T1= -40, -20), after the onset (T2= 20, 40; T3= 40, 60; T4=60, 80; T5=80, 100) or it could not be delivered (T0 = no pulse), as an additional control condition.

Statistical Analyses

Behaviour measurements were accuracy, reaction time and the responses of a perception rating scale. We computed accuracy by averaging the proportion of correct responses and reaction time (RT) by averaging the response time locked to the disappearance of the second stimulus. Trials with RT exceeding 1.5 s were excluded from the analyses, as well as trials greater than 3 sd. Two exclusion criteria were here used to avoid long reaction times what would no longer allow us to make inferences about the effect of the stimulation, given that the disruption should have a short effect. For the perception rating scale, the median of the rating values was also computed. A 2x3x6 repeated measures ANOVA with within-factors Velocity (fast motion, slow motion); Stimulation (TMS-V1, SHAM-V1, TMS-V5); TMS trigger SOA (T0=no pulse, T1= -40 -20; T2= 20 40; T3= 40 60; T4= 60 80; T5= 80 100) and task order as between subject factor was carried out on JASP (v.0.15.0.0 - https://jasp-stats.org/) for all measurements. Additionally, we averaged the 12 task blocks performed before the TMS application on day 1 and day 2, and used a pairwise Student T-test to compare the averages of accuracies and reaction time for fast and slow conditions, in order to verify if participants were able to discriminate the stimulus velocity.

Results

Training phase

Results of accuracy (figure 20A) indicated a marginally significant difference between fast (mean=.985 ±.023) and slow (mean= .959 ±.037) conditions (t=2.066, df=8, p=.073), suggesting that participants discriminated fast condition from the baseline slightly easier than slow condition. For reaction time (Figure 20B) during training phase, no significant difference was observed between fast (mean=.571 ±.239) and slow (mean=.606 ±.185) conditions (t=-0.464, df=8, p=.655).
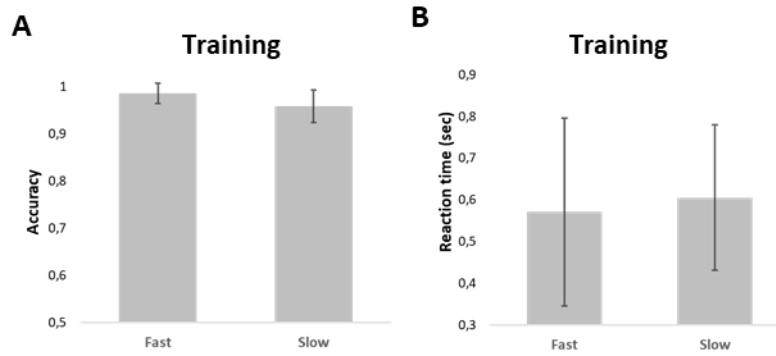
Figure 20 - Accuracy and reaction time during training sessions before stimulation. (A) No differences in accuracy were observed during discrimination between fast and baseline, as well as, between slow and baseline. (B) Results of reaction time were in accord with accuracy, no difference was observed. Error bars represent standard deviation in both measures.

Test phase

Accuracy: Figure 21. A1 depicts the accuracies for fast and slow motion as a function of trigger onset. Results indicated an interaction between velocity and trigger onset (Figure21. A2 - $F(5,35)=4.235$, $p=.004$, $\eta_p^2=.378$). Post-hoc pointed to significant differences for slow condition during T1 and T2 (MD=-0.055, SE=.016, t=-3.527, p_{bonf}=.051), T1 and T3 (MD=-0.064, SE=.016, t=-4.076, p_{bonf} =.009), T1 and T4 (MD=-0.057, SE=.016, t=-3.627, p_{bonf} =.037), and T1 and T5 (MD=-0.033, SE=.016, t=-4.162, p_{bonf} =.006). We expected to observe differences between stimulation conditions, but no further significant main effect or interactions were observed, moreover no significant task order effect was found.

Reaction Time: Figure 21. B1 depicts reaction time for fast and slow motion as a function of trigger onset. We observed again an interaction between velocity and trigger (Figure 21. B2F - $(5,35)=5.847$, $p<.001$, $\eta_p^2=.455$) and between stimulation and trigger ($F(10,70)=1.992$, $p=.047$, $\eta_p^2=.222$). For the first interaction, post-hoc indicates significant differences for fast condition during T0 and T1 (MD=-0.102, SE=.025, t=-3.990, p_{bonf} =.011); T0 and T2 (MD=-0.091, SE=.025, t=-3.570, p_{bonf} =.045); T0 and T3 (MD=-0.093, SE=.025, t=-3.671, p_{bonf} =.032); T0 and T5 (MD=-0.123, SE=.055, t=-4.821, p_{bonf} <.001), and for slow condition T0 and T4 (MD=0.091, SE=.025, t=3.588, p_{bonf} =.042). No further significant main effect or stimulation was observed, as well as no difference for task order.

Rating: Figure 21.C1 depicts perception rating scale for fast and slow as a function of trigger onset. The statistical analysis revealed an interaction between velocity and trigger once more (Figure 21.C2 - $F(10,35)=3.148$, $p=.019$, $\eta_p^2=.310$), and stimulation and velocity ($F(2,14)=4.067$, $p=.041$, $\eta_p^2=.367$). Post-hoc analysis showed differences for the first interaction during slow

93

condition for T1 and T3 (MD=-0.558, SE=.135, t=-4.142, p_{bonf} =.006), T1 and T4 (MD=-0.558, SE=.135, t=-4.142, p_{bonf} =.006), and T1 and T5 (MD=-0.567, SE=.135, t=-4.93, p_{bonf} =.005), in accord with the accuracy results. For the second interaction, significant differences were found between TMS-V1 and TMS-V5 during slow condition (MD=0.333, SE=.097, t=3.450, p_{bonf} =.034). Additionally, a main effect of trigger ($F(5,40)$=2.494, p=.049, η_p^2=.263) was observed, with marginally significant difference between T0 and T1 (MD=.279, SE=.094, t=2.977, p_{bonf} =.079).
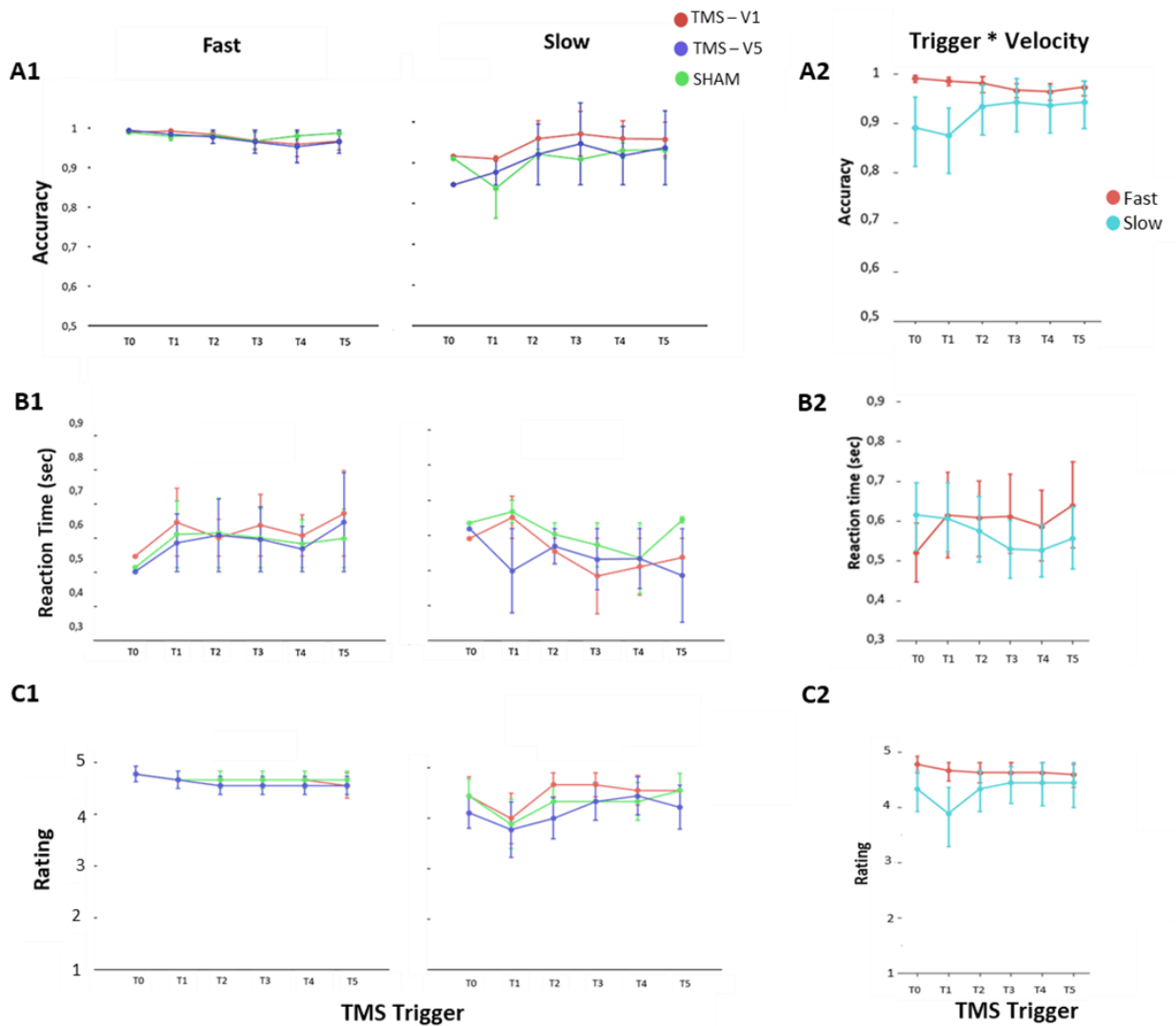
Figure 21 - Results of behavioural measurements. For A1, B1 and C1, red line and dots depict the TMS condition over V1, green line and dots depict results of the sham condition over V1 and blue line and dots, the TMS condition over V5. Plots on the left column depict results from the discrimination between baseline velocity and fast velocity, while plots on the middle column represent results from the discrimination between baseline velocity and slow velocity. Error bars show the difference between T0 (no pulse) and the other triggers. (A1) Accuracies, based on the proportion of correct responses, did not differ between stimulation neither during discrimination of fast nor slow motion. However, we observed a difference between TMS trigger SOA during discrimination of slow motion. Figure A2 shows the interaction between trigger and velocity, suggesting difference in T1 (TMS trigger before the onset of the moving stimulus) compared to all other triggers. (B1) No difference between stimulation was observed during discrimination of both velocities, but an interaction between velocity and trigger (Figure B2). Figure C1 depicts the rating scale representing participants'

perception of the moving stimulus. During discrimination between fast and baseline movement, participants were confident about their perception and their answer during all TMS triggers, while during discrimination between slow and baseline, they were less confident during T1. A significant interaction between velocity and trigger (Figure C2) was observed also for this measure (see main text).

Individual Differences

Among many challenges that a TMS experiment brings, individual differences are the most important one, as individuals differ not only in their macronatomical gyral-sulcal layout (Amunt et al., 2000), but also in their functional and cognitive organisation (Gießing et al., 2020; Nicolo, Ptak & Guggisberg, 2015). For this reason, here we present individual results from all three measures in all three conditions during training (Figure 22) and test (Figure 23) phases. It is evident that some of the results were caused by one subject (59) which behaved as an outlier in all stimulation conditions during discrimination of slow motion. Therefore, we carried out the analysis again, without this outlier. However, besides the exclusion of one more subject, the interaction between trigger and velocity was consistently present across the three measures, with differences between T1 compared to other triggers, suggesting that TMS pulses delivered before the onset of the visual stimulation indeed affected the behaviour.

Training Phase
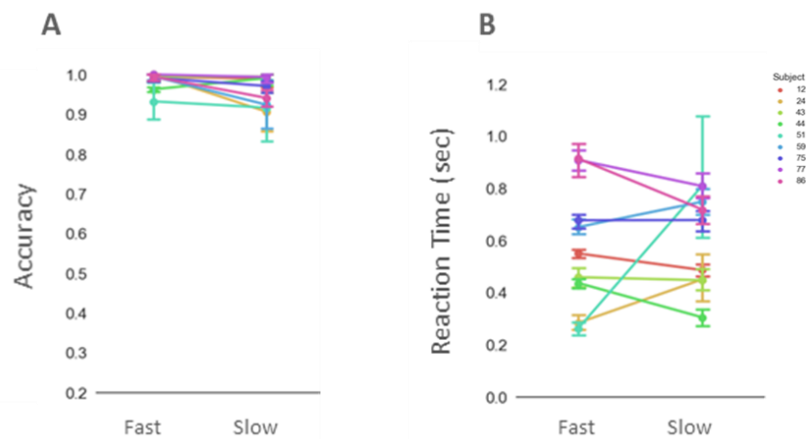
Figure 22 - (A) Accuracy during training session showed consistency between subjects. (B) Reaction time varies considerably between subjects, but not within subject, except for subject 51 (light green). Points on the left indicate results for fast condition and on the right, for slow condition in figures A and B. Error bars depict standard deviations.

Results after removal of outlier

Accuracy: Analysis of the proportion of correct responses indicated an interaction between velocity and trigger ($F(5,30)=3.666$, $p=.010$, $\eta_p^2=.379$). Post-hoc comparisons pointed to significant differences in slow motion discrimination when stimulation was delivered in T0 compared to T3

(MD=-0.056, SE=.015, t=-3.784, p_{bonf} =.024); and T1 compared to T3 (MD=-0.057, SE=.015, t=-3.826, p_{bonf} =.021). A main effect of velocity was also observed ($F_{(1,6)}$=8.527, p=.027, η_p^2=.587), showing that accuracy was greater for fast than slow motion (MD=.014, SE=.005, t=2.920, p_{bonf} =.027).

Test Phase
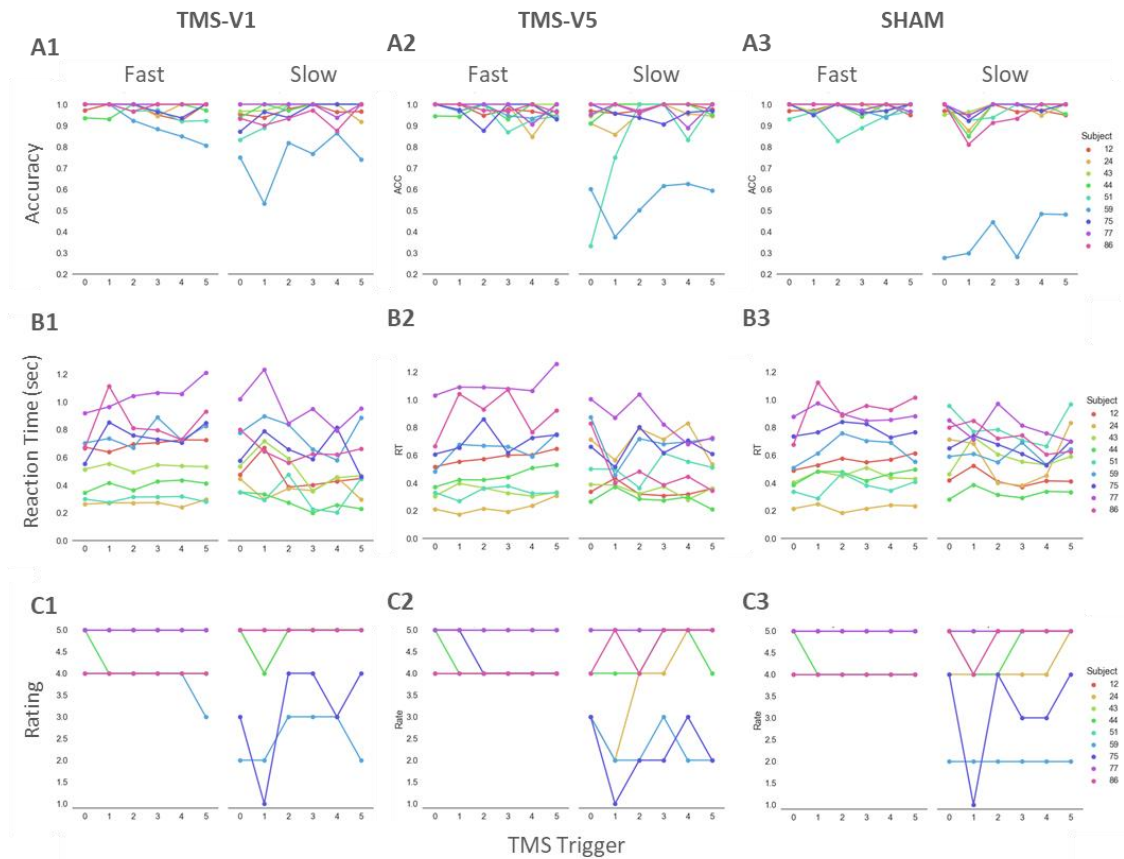
Figure 23 - Individual behavioural responses in each measure for each TMS trigger. (A1) Accuracy during TMS over V1. Each line represents one subject. We can observe, for slow condition (right column), one outlier, subject 59. This subject behaved differently from the others also during TMS over V5 (A2) and SHAM (A3). Reaction time during TMS over V1 (B1), V5 (B2) and SHAM (B3) varied considerably across subjects, but it is possible to see that subjects behaved consistently across different stimulations. Figures C1 to C3 depict once more subject 59 (light blue) as an outlier, but also subject 75 (dark blue).

Reaction Time: Analysis of reaction time showed a triple interaction between stimulation, trigger and task order ($F_{(10,60)}$=2.227, p=.028, η_p^2=.271), as well as interactions between velocity and trigger ($F_{(5,60)}$=4.461, p=.004, η_p^2=.426) and trigger and task order ($F_{(5,60)}$=2.793, p=.035, η_p^2=.318), and a marginally significant interaction between stimulation and trigger ($F_{(10,60)}$=1.813, p=.078, η_p^2=.232). Post-hoc of the triple interaction indicated that subjects starting with sham condition when TMS was applied over V1 showed smaller reaction time when pulse was delivered in T1 compared to when no pulse was delivered (MD=-0.161, SE=.036, t=-4.421, p_{bonf} =.018), as well as T1 compared to T3(MD=.151, SE=.036, t=4.165, p_{bonf} =.046) and marginally significant difference

between T1 and T4 (MD=.145, SE=.036, t=3.990, p_{bonf} =.086). Post-hoc of the interaction between velocity and trigger pointed to differences between T0 and T5 in fast condition (MD=-0.115, SE=.027, t=-4.209, p_{bonf} =.006); while for trigger and task order, the differences, in subjects which started with sham condition, were found between T0 and T1 (MD=-0.086, SE=.023, t=-3.762, p_{bonf} =.048) and T1 and T4 (MD=.107, SE=.023, t=4.648, p_{bonf} =.004). Comparisons between stimulation and trigger interaction showed a marginally significant difference between stimulation over V1 delivered in T1 and T3 (MD=.093, SE=.026, t=3.636, p_{bonf} =.071).

Ratings: Similar to the accuracy and reaction time measures, analysis of perception rating also showed double interaction for velocity and trigger (F(5,30)=2.661, p=.042, η_p^2=.307). Additionally, an interaction between stimulation and trigger was observed (F(2,12)=4.053, p=.045, η_p^2=.403). Post-hoc of the first interaction pointed to differences for slow motion condition during triggers T1 and T3 (MD=-0.542, SE=.148, t=-3.654, p_{bonf} =.036), T1 and T4(MD=-0.583, SE=.148, t=-3.935, p_{bonf} =.014) and T1 and T5 (MD=-0.625, SE=.148, t=-4.216, p_{bonf} =.006). For the second interaction, differences were found also for slow condition during stimulation of V1 and V5 (MD=.354, SE=.104, t=3.392, p_{bonf} =.049).

Discussion

In this study, we investigated the causal relation of V1 with the processing of motion, by probing participants' velocity discrimination, while disrupting V1 with a double-pulse TMS paradigm, compared to SHAM condition over the same region. We further delivered TMS pulses over V5, in order to have a control condition, when attempting to disrupt general motion perception. When TMS is applied over V1, we expected to observe an impairment in the discrimination of the slow-moving target, but not fast, compared to the baseline motion. In contrast, when applying TMS over V5, we expected to observe a general impairment in the velocity discrimination. Our results did not show significant difference between conditions, including the SHAM, which does not allow us to draw conclusions about velocity discrimination and the stimulated regions. Although, results did not show consistent significant differences, we could be observed a pattern of a general decrease in the proportion of the correct responses (accuracy) when the pulse was delivered before the onset of the stimulus (T1: -40, -20 ms). This decrease in accuracy was intensified by one outlier, however other subjects showed the same tendency. The inverted pattern was also seen in this time window, as response time of the participants increased as well as the rating scale decreased. As a matter of fact, we see interaction between trigger pulse and velocity in all three measures, indicating that the pulse before the onset was significantly

different from some of the other triggers. Below we present possible explanations for the outcome of our study.

Stimulus

Our study differed from previous ones in terms of the velocity/display time of our moving target. Most of the studies which investigated the involvement of V1 with motion processing, presented paradigms with very fast stimulation, such as random-dot motion (Silvanto et al., 2005; Grasso et al., 2018; Laycock et al., 2007; Koivisto et al., 2010; Silvanto & Muggleton, 2008), in which the stimulus duration was below 80 ms. It is important to emphasize that we chose a single moving target, because we aimed to test the dynamic parallelism theory adapting the paradigm used in previous studies[4] without decreasing dramatically the target display time, therefore keeping a consistency among the studies. For the same reason, we kept the stimulus appearance the same, although, a stimulus with a higher size and contrast, such as a checkerboard pattern could have yielded better effect for stimulating V5. Nonetheless, even our faster moving, i.e. shorter target may have been simply too long (200 ms of display time), meaning that, even if there was a disruption in the V1 or V5, the stimulus was long enough to enable participants to still perceive it after the disruption period. This would also explain why we see a pattern of impairment in behaviour and perception of motion (rating scale) when the trigger is sent before the pulse, whereas, any pulse after the onset, which could cause a disruption, thus an impairment in behaviour, might not have a long-lasting effect capable of accounting for the continuity of the moving stimulus. It is worth-noting that studies which delivered TMS pulses before the onset of the moving target focused on testing the dynamic parallelism theory (Grasso et al., 2018; Laycock et al., 2007), while studies which investigated the role of V1 in visual consciousness and unconsciousness presented the pulse trigger intervals exclusively after the offset of the stimulation (Silvanto et al., 2005; Koivisto et al., 2010; Silvanto & Muggleton, 2008). This means that, not the processing, but the judgement of the stimulus would be compromised, which was not our goal.

Future studies could account for that in two ways. First, the target velocity could be decreased down to 100 ms, so the last trigger of the double-pulse would be sent together with the offset of the stimulus and judgment wouldn't be impaired, as it was seen that the earliest time window related to visual unconsciousness is approximately 20ms (Koivisto et al., 2010). The second is the TMS paradigm itself. By choosing to have a longer motion stimulation, maybe for a more ecological validity (Boulinguez et al., 2009; Thompson et al., 2009; Thompson et al., 2016), a long-

---

[4] Studies presented on chapters 2 and 3.

lasting TMS effect would be preferable, such as repetitive TMS (rTMS), which will be discussed ahead.

TMS Paradigm

The choice of the TMS paradigm was based on the use of double-pulse TMS following two previous studies which investigated the dynamic parallelism theory (Grasso et al., 2018; Laycock et al., 2007). Other studies also suggested that double-pulse is to be preferred, as it enables a stronger modulation of the visual network (Kammer & Baumann, 2010; Moliadze et al., 2005). In contrast, single-pulse protocols show weaker effects though they can also be effective for inhibitory activity (Amassian et al., 1998; Sack et al., 2006; Hurme et al., 2017, Hurme et al., 2019; Koivisto et al., 2017). However, as above mentioned, for longer visual stimulation, neither single- nor double-pulse TMS seem to be well suited.

Inhibitory rTMS is performed with 1Hz or less (Kosslyn et al., 1999; Thompson et al 2009; Thompson et al., 2016) and it know to last up to 15 min (Thompson et al., 2009), depending, of course, on the session duration. For instance, Thompson and colleagues (2016) tested whether the hypothesis that pairs of stimuli moving in the opposite direction suppress activity in V5, but not V1. In this study, participants received a 1Hz rTMS over V1 and V5 prior to the experimental task. After the rTMS session, they performed the task which consisted of moving paired-dots with duration of 200 ms of display time after. Results indicated that the rTMS over V5 impaired discrimination accuracy for paired-dots moving in the same direction, while, rTMS over V1 hindered discrimination accuracy for stimuli moving in the opposite direction. Another early study using 1 Hz rTMS to investigate the relation between the primary visual cortex and imagery also reported relevant findings. Kosslyn and colleagues (1999) monitored activity in V1 using PET imaging, while participants performed an imagery task, in which first they were instructed to observe and memorize quadrants containing different stripes orientations and sizes. Next, participants closed their eyes and received an auditory instruction to imagine a specific feature of the stripes in two of the quadrants, such as length, and reported in which quadrant there were stripes with the larger feature (e.g. "quadrant 1 has longer stripes compared to quadrant 2"). After the PET scan, participants received rTMS pulses over V1, as well as a SHAM stimulation for control purposes, while performing the same perception and imagery tasks as before. It was observed that, behaviourally, response time increased when TMS was delivered over V1, compared to sham condition, in both perception and imagery tasks, suggesting that rTMS caused a disruption in this area.

In contrast, other studies also showed that higher frequencies can also inhibit the stimulated region of interest. A TMS-fMRI study investigated the causal relation between virtual lesion and brain networks focusing on the interconnexion between V1 and V5+ (Raffin et al., 2022). Using short trains of 10 Hz TMS on healthy participants over the two regions of interest, the authors observed their behaviour during a motion discrimination task. Results indicated that when TMS bursts were delivered over hMT/V5+ at around 130 ms, a decrease in general motion discrimination occurred together with a deterioration in the performance awareness compared to no TMS condition. Similarly, motion discrimination was also disturbed when TMS bursts were applied over V1 and the same effect was, once more, seen for motion awareness, i.e. a certain number of moving stimuli was perceived as static. Moreover, imaging results observed BOLD signal change when TMS bursts were applied to both regions, suggesting that a perturbation not only in the regions independently, but also in the V1-hMT/V5+ network related to motion discrimination. Taken together, future studies could opt for a higher frequency, such as 10Hz for stimulating V1 and V5, but application should be done in short trains or even double-pulse. In contrast, 1Hz-rTMS could also be an option, but as the effect is stronger, it is important to consider that a temporary blindness might occur, so it is not adequate to all kinds of visual experimental design.

Individual Differences

In addition to interindividual macroscopic differences in brain structures, functional regions, such as the primary visual cortex, can still vary substantially with respect to their exact positioning on the microanatomical gyral-sulcal pattern (Amunts et al., 2000). To account for macroscopic variability, we used participants' anatomical images (T1) to create a model for the neuronavigation system. To account for the functional variability, we measured static and moving phosphene threshold in V1 and V5, respectively, to make sure that we were stimulating the right region using the right intensity. Although we tried to control for structural and functional differences, additional retinotopic mapping and functional localisation of V5 could be used to improve the precision of the neuronavigation. Moreover, functional connectivity can also be different between subjects (Gießing and colleagues, 2020; Nicolo, Ptak, Guggisberg, 2015, for review). In a recent study, Gießing and colleagues (2020) investigated inter-individual differences in connectivity between parietal regions and other areas, before and after rTMS over the first. Participants took part in a resting state and a visuospatial detection task, while brain activity was monitored using fMRI, followed by a 1Hz rTMS and sham stimulation. The authors observed that behavioural results were significantly associated with individual functional connectivity states of each brain region, particularly the ones which were not directly stimulated. Furthermore, the stimulation over parietal regions caused significantly different individual changes in the accuracy of the visuospatial

detection task, depending on the current state of the brain network. In accord, Nicolo and colleagues (2015) also stated that inhibitory or excitatory TMS does not only depend on the combination of parameters, but also the cortical excitability and baseline activity of each individual, and even cognitive attributes, as attention, which might have played a role on task of this study. We observed that some participants demonstrated a huge drop for all three measures (sub.59) or mainly for the rating scale (sub.77), hence, we did not discard the possibility that the attentional level of these participants might have been compromised. Moreover, after the exclusion of subject 59 and reanalysis of the data, changes in the results were observed, however the interaction between trigger and velocity remained consistently across measurements, suggesting, once more, that stimulation before the onset affected participants' behaviour.

In conclusion, we aimed at testing the dynamic parallelism theory, by investigating the role of V1 with velocity discrimination, compared to V5, while participants compared the velocity of two stimuli moving consecutively on the screen. Our findings do not support the hypothesis that disrupting V1 impairs the processing of slow stimulus compared to fast stimulus. We also observed no impaired in the general motion discrimination when double-pulse TMS is applied over V5, as it is established by the common literature. Here, we discussed potential reasons why we obtained inconclusive results, such as the duration of the stimulation and the choice of the TMS paradigm, which were chosen, based on our previous studies and the literature, respectively. Future studies could test this continuous motion paradigm with rTMS, as its long-lasting effect may accounts better for long stimulus duration.

Chapter 5 - General Discussion

In the beginning of this thesis, I presented some examples of daily situation which require complex prediction processes from the brain. For instance, when crossing the streets, our brain automatically estimates the time and space of a car in order to perform the next action safely. To add another level of complexity, our brain also makes these estimations if a car becomes dynamically occluded by a larger vehicle. Throughout this thesis I aimed at investigating the mechanisms behind this process focusing on the visual cortex to answer the question as: Is the primary visual cortex instrumental in the processing of dynamic occluded objects? Does the primary visual cortex respond differently when the temporal predictability of occluded targets is manipulated, as proposed by the predictive coding model? Is there a causal relation between the primary visual cortex and processing of the temporal information of a moving object? To address these questions, I conducted here three studies, used fMRI (Box 2) and TMS (Box 5) techniques and analysed the data using univariate and multivariate pattern analyses (Box 4). Below, I will discuss the findings, relate the common aspects between the three studies, present limitations of the studies and offer future perspectives on the topic under investigation.

In chapter 2, I answered the first question about the relationship of the primary visual cortex and the processing of dynamically occluded objects by showing evidence that simultaneously predicting temporal and spatial information from occluded stimulus enhanced fMRI responses not only in V1, but also in V2 and V3. These findings were particularly important, because to my knowledge this was the first study which used a Prediction Motion task with a higher level of complexity, as the participants had to perform two estimation at once, and showed the high engagement of low-level visual cortex during partially occluded stimulation. These findings are extending previous studies which often failed to find modulation in V1 in the context of stimulus occlusion. The positive outcome may be attributed to the level of specificity applied to the analyses, which covers two main approaches: Subject-specific definition of functional regions and subject-specific statistical analysis. For the definition of functional regions, masks for functionally defined low-level visual regions were created based on individual's retinotopic map. This is relevant because studies have showed immense anatomical differences across subjects (Greenlee, 2000; Amunts, 2000), so controlling for these differences should be of utmost important when it comes to investigation in these regions. Second, all analyses – univariate and MVPA – were performed at single-subject level, which allowed a huge spatial specificity advantage compared to other studies, which used normalized voxel-based analyses (Olson et al., 2003; Shuwairi et al., 2007; O'Reilly, Mesulam, & Nobre, 2008).

Extending and supporting the univariate results, the MVPA results indicated that informational pattern of activation of the stimulus presented during the visible phase could be decoded from the occlusion phase. Moreover, it was observed that regions inside the low-level visual areas are common across both domains, suggesting that the same regions can encode and possibly integrate both bottom-up and top-down information. To complement this analysis, we projected the spatial accuracy maps onto retinotopic maps and observed an overlap across different modalities, i.e. visible and occlusion, supporting the notion that the informative patterns were located along the stimulus-trajectory. Future studies could investigate the involvement of the primary visual cortex during the presentation of visible and dynamically occluded stimulation by using layer-specific fMRI.

In chapter 3, I demonstrated that using a similar paradigm, but with a "feedback" mechanism, in which the stimulus reappeared, I answered the second question about a possible difference in responses of the primary visual cortex when temporal predictability of occluded objects is manipulated. The findings indicated that, in contrast with what is assumed by the predictive coding model, no difference in fMRI-response was observed in V1 when task stimulation was presented with a higher or lower level of temporal predictability. This suggests that either the difference between the predictability levels was not large enough, so the predictive error could modulate stronger responses in V1, or attentional mechanisms were cancelling the effect of predictive error, as postulated by Kok and colleagues (2012). The findings of this study supported the second hypothesis. It is worth-mentioning that the task used in this study may have engaged a high level of attentional resources, as the participants had to make two estimations, temporal and spatial, before the reappearance of the stimulation. Moreover, the reappearance of the stimulus might also have automatically captured attention promoting an increase of response. Thus, attentional resources may have led to high fMRI-response modulation in V1. Future studies could modulate attention during occlusion phase and see if the effect remains.

Expanding the univariate results, the MVPA results demonstrated that informational pattern presented at higher and lower predictability could be decoded in all classification analyses performed in this study. However, accuracy values of decoding performed with low predictable context data were higher than the with high predictable context data. This difference may be due to the processing of the incongruent trials, which, in a separate classification analysis, were seen to be differently classified compared to the congruent trials. Potentially, incongruent trials did not only affect the processing of the temporally unexpected stimuli within the incongruent trials but changed the processing of congruent trials following incongruent trials. Similar effects have been reported for auditory and visual omission responses in ERP-research (e.g. Dercksen et al., 2022)

and often trials following stimulus omissions were not analysed there. Future analyses, beyond the scope of this thesis, could investigate the responses to congruent trials following incongruent trials. Moreover, future studies could also modulate the volatility of trials in low predictable context and investigate connectivity patterns of low-level visual areas with high-level regions, such as MFC.

Finally, one of the most relevant aspect of this second study is that it corroborates the first study. At the univariate level in both studies, not only visible but also, and most importantly, occlusion phase enhanced fMRI-responses in the primary visual cortex. Moreover, MVPA results revealed the same pattern of decoding accuracy values. For instance, higher values were observed when the classifier was trained and tested in the visible phase, compared to the accuracy values from the analysis in which the classifier was trained and tested in the occluded phase, which, in turn, were higher than the values from the analysis carried out by training the data in visible phase and testing in occluded phase. However, in addition to the many similarities there were a few differences between the two studies which I will discuss one by one below.

In the first study, the V1 quadrant showed similar response pattern during visible and occluded stimulation phase was the lower one, while in the second study, it was the upper one. This difference can be explained by an effect known as vertical meridian asymmetry, discussed in both second and third chapters (see also below next section). Another difference concerns the difference in response height of the activity pattern of visible and occluded in the first study, which was not the same observed in the second one. In the first study, beta weights were higher for occluded phase compared to visible phase. It is conceivable that this difference might be related to the predictability level of the task, i.e. due to the lack of novelty during the visible phase, the system did not compute many predictive errors, decreasing the response in V1, V2 and V3. However, during occlusion, the stimulus did not reappear and this could be related to a lower level of predictability, thus an increase of the signal. This effect would be in line with the predictive coding model. However, when predictive coding model was tested on the second study, this effect disappeared and response enhancement was similarly observed in visible and occlusion phase and might be due to attentional load related to the task performance and/or the reappearance of the stimulus, as mentioned above.

Visual Asymmetry

Differences between lower and upper V1, thus upper and lower visual fields (VF), respectively, were seen in both studies and can be explained by the vertical meridian asymmetry. This phenomenon indicates that the difference between upper and lower VF is due to the amount of "near-preferring" neurons most commonly found in the latter compared to the first (Nasr & Tootell, 2018, 2020;

Karim & Kojima, 2017). A recent study also showed that presaccadic attention – the preparation of saccadic eye movement for the future eye position – increases the sensitivity in the lower but not at the upper vertical hemifield (Hanning et al., 2022). Participants were asked to fixate on the middle point and perform a saccadic eye movement towards the direction indicated by a small blue line which could appear on right, left, above or below the fixation point. Results indicated that presaccadic attention does not alter asymmetries in visual performance. The authors, hypothesized that the distribution of cortical surface region in the primary visual cortex might be responsible, as V1 contains considerably less cortical sheet assigned to the processing of information in the upper vertical (lower quadrant) compared to the lower vertical (upper quadrant) hemifield (Benson et al., 2021; Himmelberg et al., 2020; Himmelberg et al., 2021 a,b).

In contrast, another recent study which investigated redundancy masking – a phenomenon in which individuals are asked to report items presented in one of the hemifields and they fail to report one or more item – found divergent results (Yildirim, Coates & Sayim, 2022). In this study, participants were presented to three parallel lines, which could appear in different positions all over the vertical hemifields, and were asked to indicate the number of perceived lines. The authors observed similar results for upper and lower vertical hemifields, meaning that no asymmetry was found there, opposing to the redundancy masking phenomenon. Nonetheless, the vast majority of studies present evidence that lower visual field has advantages over the upper visual field in many aspects, such as spatial resolution (De Lestrange-Anginieur & Kee, 2020; Greenwood et al., 2017), motion (Danckert & Goodale, 2001; Levine & McAnany, 2005, Lakha & Humphreys, 2005), colour discrimination and hue sensitivity (Levine & McAnany, 2005), and accumulation of speed information (Carrasco et al., 2004). Carrasco and colleagues (2004) demonstrated that covert attention cancels the vertical asymmetries in temporal performance. This suggests that during the temporal estimation required for performing the tasks, results should not differ across quadrants, which is in line with the velocity effect observed in the second study of this thesis.

To avoid any quadrant-specific or any laterality effects future studies could introduce a few changes and present the stimulation only in one quadrant. Potentially, in a first step, cortical magnification stimuli should be used to account for the size of cortical sheet activated as a function of eccentricity, while the task would remain the same, in which the direction-velocity association would still be present. In a second step, the task could be also modified. The current task used in the fMRI experiments builds on several mechanisms: spatial and temporal estimation to perform the task, and velocity discrimination to judge the direction change. In follow-up experiments, these parts, instrumental in task performance, should be disentangled and compared with the results presented here. One could see if the fMRI-response height would still keep being high or would

decrease, as now participants would have only one estimation to perform. Additionally, one could observe potential laterality effects of motion extrapolation by presenting them in different hemispheres.

Predictive coding model and attention

The first study found notorious differences regarding fMRI-response height between visible and occluded phases. As mentioned before, one possible explanation for that is that the high predictability of the stimulus during visible phase may have decreased the response signal, while the intrinsic lower predictability caused by the lack of stimulation during the occlusion phase may have increased responses in low-level visual area. This effect, which can be explained by the predictive coding model, was further tested on the second study, which, however, did not, in this regard, corroborate the first one. The second study did not find a selective increase of activity in the primary visual cortex in the lower predictable context, which would be expected given the results of enhanced learning in high volatility contexts should also recruit more attentional resources. One could, however argue, that the interaction of attention and prediction happens in an all-or-nothing way and not gradual, boosting the response in both high and low levels of predictability. These findings are in line with Rao' simulation study (Rao, 2005). Rao developed a model to account for attention in predictive coding using Bayesian models. While modelling neurons of primate visual cortex, he observed that stimulation of feedback connections coming from higher levels may simulate the effects of attention by generating a modulatory tuning behaviour and decreasing uncertainty in the presence of a complex scenario. Later, Feldman and Friston (2010) suggested that attention is a phenomenon that naturally emerges in a Bayesian-optimal model and improves synaptic gain to boost the precision of the predictive error, what was later tested by Kok and colleagues (2012).

However, in the study from Kok and colleagues (2012), attention and prediction could not be properly disentangled. Participants were primed with a prediction cue, indicating the likelihood of the side in which the stimulus would appear, followed by an attentional cue indicating the side that they should attend. The problem with this paradigm is that both cues are entangled into each other, meaning that both explicitly relate to the direction (word "right" or "left", for the prediction cue, and arrow pointing to one of the directions, for the attentional cue). To account for that, future studies could test the relation between attention and predictive coding, by using a different cue and just one, such as colour, and adopt tasks with different levels of difficulty for comparison. To test temporal prediction, the first and control task could be the simple paradigm introduced above. In the second task a fixation cross, which changes the colour, could be presented to indicate which

velocity, consequently the direction as well, the stimulus would move, given the learned association. Taken together, I propose future studies to characterize the interplay of attention in greater detail.

Backward and Forward projections: from V5 to V1 and back

We have seen that the predictive coding model assumes that top-down information is sent backwards from higher areas to lower areas, where the information will be compared to bottom-up one, and the error between this comparison is forwarded to higher areas. Many studies showed that this interaction occurs between the motion area hMT/V5+ and the primary visual cortex (Vetter et al., 2015; Edwards et al. 2017; Sterzer et al., 2006; Muckli et al., 2005). However, these studies investigated mainly apparent motion, and not continuous motion. Therefore, in the third study of this thesis, I simplified the tasks from the studies one and two, by presenting the stimulus travelling only in the horizontal trajectory and eliminating the occlusion, meaning that participants just needed to discriminate between velocities. Specifically, I aimed at investigating the relation between the primary visual cortex and temporal information discrimination, by using TMS to stimulate V1 and V5, as additional control condition, under the perspective of the dynamic parallelism theory (Grasso et al., 2015). This theory assumes that motion information can take two pathways to reach V5, depending on the velocity. Fast moving stimulus would go from LGN, pass through superior colliculus or putamen and reach V5, while slow moving stimulus would engage V1 to reach V5. By disrupting V1, I would expect to see an impairment in the discrimination of slow, but not fast stimulation. However, results did not provide robust evidence to support this theory, as no difference was observed between both fast and slow motion.

In the chapter 5, I presented some reasons why these results were not consistent to the theory. Two of the reasons was the type of TMS stimulation paradigm and the other was the duration of the stimulus. Therefore, here I suggested that future studies, by opting for the same, thus long, stimulus duration, could choose repetitive TMS paradigm. This paradigm over V1 would be correspondent to a virtual lesion in which participants would not be able to see the stimulus, but still be able to judge the stimulus velocity, simulating the phenomena of Blindsight (Cowey & Stoering, 1991) or Riddoch (Zeki, 1998; Riddoch, 1917) syndrome. Alternatively, future studies could opt for using a shorter stimulus duration, which would be within the double-pulse interval window. Finally, TMS could also be combined with fMRI (Bergmann et al., 2021; Raffin et al., 2022) to directly measure changes in local activity and interregional connectivity when participants perform temporal estimations.

Final remarks

In conclusion, the studies presented in this thesis show robust evidence that voxels in V1 - activated when predicting dynamically occluded stimulation - do not only overlap with active voxels during visible stimulation, but that the activity patterns evoked by visible stimulation can be used to accurately predict the extrapolation of occluded changes in motion trajectory, hence both representations share a common informational pattern. This observation was found in two independent experiments with different tasks and across different sets of subjects. The engagement of V1 is of special relevance, as it points at a visual-spatial format of predictions. Moreover, previous studies which investigated this type of stimulation failed to show the engagement of lower-level visual regions, most likely due to methodological issues. This brings us to the next important contribution of this thesis. Here a combination of methods was presented, such as the use of retinotopic maps, multivariate analyses, and the option of single-subject level over group-level analysis, which most likely contributed to the robust results in the first study, replicated on the second study. Results of the second study also presented evidence of the intrinsic engagement of attention and its relation with prediction, potentially hinting at the possibility that, independently of the predictability level and thus independent of the size of attentional engagement, attention might boost the perception of the occluded moving stimulus and outweigh the predictive signal, which should reduce activity in sensory areas. Finally, future high-field studies are needed, focusing on the laminar profile of activations during visible motion processing and occluded motion extrapolation to shed light on the fine-grained activation pattern during visible motion processing and motion extrapolation. In this thesis I showed that V1 might be a worthy target for these future investigations.

References

Abdollahi, R. O., Kolster, H., Glasser, M. F., Robinson, E. C., Coalson, T. S., Dierker, D., Jenkinson, M., Van Essen, D. C., & Orban, G. A. (2014). Correspondences between retinotopic areas and myelin maps in human visual cortex. *NeuroImage*, *99*(100), 509–524. https://doi.org/10.1016/j.neuroimage.2014.06.042.

Adams, R. A., Shipp, S., & Friston, K. J. (2013). Predictions not commands: active inference in the motor system. *Brain structure & function*, *218*(3), 611–643. https://doi.org/10.1007/s00429-012-0475-5

Aitchison, L., & Lengyel, M. (2017). With or without you: predictive coding and Bayesian inference in the brain. Current opinion in neurobiology, 46, 219–227. https://doi.org/10.1016/j.conb.2017.08.010

Albers, A. M., Kok, P., Toni, I., Dijkerman, H. C., & De Lange, F. P. (2013). Shared representations for working memory and mental imagery in early visual cortex. *Current Biology*, 23(15), 1427-1431.

Aleman, A., Sommer, I. E., & Kahn, R. S. (2007). Efficacy of slow repetitive transcranial magnetic stimulation in the treatment of resistant auditory hallucinations in schizophrenia: a meta-analysis. *The Journal of clinical psychiatry*, *68*(3), 416–421. https://doi.org/10.4088/jcp.v68n0310

Alink, A., Schwiedrzik, C. M., Kohler, A., Singer, W., & Muckli, L. (2010). Stimulus predictability reduces responses in primary visual cortex. The Journal of neuroscience : the official journal of the Society for Neuroscience, 30(8), 2960–2966. https://doi.org/10.1523/JNEUROSCI.3730-10.2010

Amassian, V. E., Cracco, R. Q., Maccabee, P. J., Cracco, J. B., Rudell, A. P., & Eberle, L. (1998). Transcranial magnetic stimulation in study of the visual pathway. Journal of clinical neurophysiology : official publication of the American Electroencephalographic Society, 15(4), 288–304. https://doi.org/10.1097/00004691-199807000-00002

Amunts, K., Malikovic, A., Mohlberg, H., Schormann, T., & Zilles, K. (2000). Brodmann's areas 17 and 18 brought into stereotaxic space-where and how variable? *NeuroImage*, 11(1), 66–84. https://doi.org/10.1006/nimg.1999.0516.

Anzellotti, S., & Coutanche, M. N. (2018). Beyond Functional Connectivity: Investigating Networks of Multivariate Representations. *Trends in cognitive sciences*, 22(3), 258–269. https://doi.org/10.1016/j.tics.2017.12.002.

Assad, J. A., & Maunsell, J. H. (1995). Neuronal correlates of inferred motion in primate posterior parietal cortex. *Nature*, *373*(6514), 518–521. https://doi.org/10.1038/373518a0

Atsma, J., Koning, A., & van Lier, R. (2012). Multiple object tracking: anticipatory attention doesn't "bounce". *Journal of vision*, 12(13), 1. https://doi.org/10.1167/12.13.1.

Baess, P., Widmann, A., Roye, A., Schröger, E., & Jacobsen, T. (2009). Attenuated human auditory middle latency response and evoked 40-Hz response to self-initiated sounds. The European journal of neuroscience, 29(7), 1514–1521. https://doi.org/10.1111/j.1460-9568.2009.06683.x

Baldwin, M., Balaram, P., & Kaas, J. H. (2017). The evolution and functions of nuclei of the visual pulvinar in primates. The Journal of comparative neurology, 525(15), 3207–3226. https://doi.org/10.1002/cne.24272

Barbot, A., Xue, S., & Carrasco, M. (2021). Asymmetries in visual acuity around the visual field. *Journal of vision*, 21(1), 2. https://doi.org/10.1167/jov.21.1.2.

Battaglini, L., & Ghiani, A. (2021). Motion behind occluder: Amodal perception and visual motion extrapolation. *Visual Cognition*, 29(8), 475-499. https://doi.org/10.1080/13506285.2021.1943094

Battaglini, L., Campana, G., & Casco, C. (2013). Illusory speed is retained in memory during invisible motion. *i-Perception*, 4(3), 180–191. https://doi.org/10.1068/i0562.

Battaglini, L., Campana, G., Camilleri, R., & Casco, C. (2014). Probing the involvement of the earliest levels of cortical processing in motion extrapolation with rapid forms of visual motion priming and adaptation. *Attention, perception & psychophysics*, 77(2), 603–612. https://doi.org/10.3758/s13414-014-0795-z.

Baurès, R., Maquestiaux, F., DeLucia, P. R., Defer, A., & Prigent, E. (2018). Availability of attention affects time-to-contact estimation. *Experimental brain research*, *236*(7), 1971–1984. https://doi.org/10.1007/s00221-018-5273-8

Behrens, T. E., Woolrich, M. W., Walton, M. E., & Rushworth, M. F. (2007). Learning the value of information in an uncertain world. Nature neuroscience, 10(9), 1214–1221. https://doi.org/10.1038/nn1954

Benguigui, N., Ripoll, H., & Broderick, M. P. (2003). Time-to-contact estimation of accelerated stimuli is based on first-order information. *Journal of experimental psychology. Human perception and performance*, 29(6), 1083–1101. https://doi.org/10.1037/0096-1523.29.6.1083.

Bennett, S. J., Uji, M., & Baurès, R. (2018). Asymmetrical time-to-contact error with two moving objects persists across different vertical separations. *Acta psychologica*, *185*, 146–154. https://doi.org/10.1016/j.actpsy.2018.02.003.

Benson, N. C., Kupers, E. R., Barbot, A., Carrasco, M., & Winawer, J. (2021). Cortical magnification in human visual cortex parallels task performance around the visual field. eLife, 10, e67685. https://doi.org/10.7554/eLife.67685

Bergmann, T. O., Varatheeswaran, R., Hanlon, C. A., Madsen, K. H., Thielscher, A., & Siebner, H. R. (2021). Concurrent TMS-fMRI for causal network perturbation and proof of target engagement. NeuroImage, 237, 118093. https://doi.org/10.1016/j.neuroimage.2021.118093

Berman, R. A., & Wurtz, R. H. (2010). Functional identification of a pulvinar path from superior colliculus to cortical area MT. The Journal of neuroscience: the official journal of the Society for Neuroscience, 30(18), 6342–6354. https://doi.org/10.1523/JNEUROSCI.6176-09.2010

Berman, R. A., & Wurtz, R. H. (2011). Signals conveyed in the pulvinar pathway from superior colliculus to cortical area MT. The Journal of neuroscience: the official journal of the Society for Neuroscience, 31(2), 373–384. https://doi.org/10.1523/JNEUROSCI.4738-10.2011

Bordier, C., Hupé, J. M., & Dojat, M. (2015). Quantitative evaluation of fMRI retinotopic maps, from V1 to V4, for cognitive experiments. *Frontiers in human neuroscience*, *9*, 277. https://doi.org/10.3389/fnhum.2015.00277.

Born, R. T., & Bradley, D. C. (2005). Structure and function of visual area MT. Annual review of neuroscience, 28, 157–189. https://doi.org/10.1146/annurev.neuro.26.041002.131052

Born, R. T., & Tootell, R. B. (1992). Segregation of global and local motion processing in primate middle temporal visual area. Nature, 357(6378), 497–499. https://doi.org/10.1038/357497a0

Bosco, G., Monache, S. D., Gravano, S., Indovina, I., La Scaleia, B., Maffei, V., Zago, M., & Lacquaniti, F. (2015). Filling gaps in visual motion for target capture. *Frontiers in integrative neuroscience*, *9*, 13. https://doi.org/10.3389/fnint.2015.00013

Boulinguez, P., Savazzi, S., & Marzi, C. A. (2009). Visual trajectory perception in humans: is it lateralized? Clues from online rTMS of the middle-temporal complex (MT/V5). *Behavioural brain research*, *197*(2), 481–486. https://doi.org/10.1016/j.bbr.2008.10.014

Brainard D. H. (1997). The Psychophysics Toolbox. *Spatial vision*, *10*(4), 433–436.

Brett, M., Anton, J.C., Valabregue, R., Poline, J.B. (2002). Region of interest analysis using an SPM toolbox. (abstract). Presented at the 8th International Conference on Functional Mapping of the Human Brain, June 2-6, 2002, Sendai, Japan. Available on CD-ROM in *NeuroImage*, Vol 16, No 2.

Brindley, G. S., & Lewin, W. S. (1968). The sensations produced by electrical stimulation of the visual cortex. The Journal of physiology, 196(2), 479–493. https://doi.org/10.1113/jphysiol.1968.sp008519

Bubic, A., von Cramon, D. Y., & Schubotz, R. I. (2010). Prediction, cognition and the brain. *Frontiers in human neuroscience*, *4*, 25. https://doi.org/10.3389/fnhum.2010.00025

Buchner, H., Gobbelé, R., Wagner, M., Fuchs, M., Waberski, T. D., & Beckmann, R. (1997). Fast visual evoked potential input into human area V5. Neuroreport, 8(11), 2419–2422. https://doi.org/10.1097/00001756-199707280-00002

Bullier J. (2001). Integrated model of visual processing. *Brain research. Brain research reviews*, *36*(2-3), 96–107. https://doi.org/10.1016/s0165-0173(01)00085-6

Burke, L. (1952). On the tunnel effect. *Quarterly Journal of Experimental Psychology*, *4*(3), 121-138. https://doi.org/10.1080/17470215208416611

Carrasco, M., Giordano, A. M., & McElree, B. (2004). Temporal performance fields: visual and attentional factors. *Vision research*, *44*(12), 1351–1365. https://doi.org/10.1016/j.visres.2003.11.026

Carrasco, M., Talgar, C. P., & Cameron, E. L. (2001). Characterizing visual performance fields: effects of transient covert attention, spatial frequency, eccentricity, task and set size. *Spatial vision*, 15(1), 61–75. https://doi.org/10.1163/15685680152692015.

Caudek, C., Ceccarini, F., & Sica, C. (2015). Posterror speeding after threat-detection failure. Journal of experimental psychology. Human perception and performance, 41(2), 324–341. https://doi.org/10.1037/a0038753

Conway C. M. (2020). How does the brain learn environmental structure? Ten core principles for understanding the neurocognitive mechanisms of statistical learning. *Neuroscience and biobehavioral reviews*, *112*, 279–299. https://doi.org/10.1016/j.neubiorev.2020.01.032

Coull, J. T., Vidal, F., Goulon, C., Nazarian, B., & Craig, C. (2008). Using time-to-contact information to assess potential collision modulates both visual and temporal prediction networks. Frontiers in human neuroscience, 2, 10. https://doi.org/10.3389/neuro.09.010.2008

Cowey A. (2010). The blindsight saga. Experimental brain research, 200(1), 3–24. https://doi.org/10.1007/s00221-009-1914-2

Cox, D. D., & Savoy, R. L. (2003). Functional magnetic resonance imaging (fMRI) "brain reading": detecting and classifying distributed patterns of fMRI activity in human visual cortex. NeuroImage, 19(2 Pt 1), 261–270. https://doi.org/10.1016/s1053-8119(03)00049-1

Danckert, J., & Goodale, M. A. (2001). Superior performance for visually guided pointing in the lower visual field. *Experimental brain research*, *137*(3-4), 303–308. https://doi.org/10.1007/s002210000653.

Danielmeier, C., & Ullsperger, M. (2011). Post-error adjustments. Frontiers in psychology, 2, 233. https://doi.org/10.3389/fpsyg.2011.00233

de Goede, A. A., Ter Braack, E. M., & van Putten, M. (2018). Accurate Coil Positioning is Important for Single and Paired Pulse TMS on the Subject Level. *Brain topography*, *31*(6), 917–930. https://doi.org/10.1007/s10548-018-0655-6

de Hollander, G., van der Zwaag, W., Qian, C., Zhang, P., & Knapen, T. (2021). Ultra-high field fMRI reveals origins of feedforward and feedback activity within laminae of human ocular dominance columns. *NeuroImage*, *228*, 117683. https://doi.org/10.1016/j.neuroimage.2020.117683.

De Lestrange-Anginieur, E., & Kee, C. S. (2020). Investigation of the impact of blur under mobile attentional orientation using a vision simulator. PLoS One, 15(6), e0234380, https://doi.org/10.1371/journal.pone.0234380.

DeLucia, P. R., & Liddell, G. W. (1998). Cognitive motion extrapolation and cognitive clocking in prediction motion task. *Journal of experimental psychology. Human perception and performance*, *24*(3), 901–914. https://doi.org/10.1037//0096-1523.24.3.901.

Dercksen, T. T., Widmann, A., Noesselt, t., & Wetzel, N. (2022). Somatosensory omissions reveal action-related predictive processing. https://doi.org/10.31234/osf.io/8aze5

de'Sperati, C., & Deubel, H. (2006). Mental extrapolation of motion modulates responsiveness to visual stimuli. *Vision research*, *46*(16), 2593–2601. https://doi.org/10.1016/j.visres.2005.12.019.

DeYoe, E. A., Bandettini, P., Neitz, J., Miller, D., & Winans, P. (1994). Functional magnetic resonance imaging (FMRI) of the human brain. *Journal of neuroscience methods*, *54*(2), 171–187. https://doi.org/10.1016/0165-0270(94)90191-0

Di Russo, F., Martínez, A., Sereno, M. I., Pitzalis, S., & Hillyard, S. A. (2002). Cortical sources of the early components of the visual evoked potential. Human brain mapping, 15(2), 95–111. https://doi.org/10.1002/hbm.10010

Dittrich, S., & Noesselt, T. (2018). Temporal Audiovisual Motion Prediction in 2D- vs. 3D-Environments. Frontiers in psychology, 9, 368. https://doi.org/10.3389/fpsyg.2018.00368x

Doherty, J. R., Rao, A., Mesulam, M. M., & Nobre, A. C. (2005). Synergistic effect of combined temporal and spatial expectations on visual attention. The Journal of neuroscience: the official journal of the Society for Neuroscience, 25(36), 8259–8266. https://doi.org/10.1523/JNEUROSCI.1821-05.2005

Duncan, R. O., & Boynton, G. M. (2003). Cortical magnification within human primary visual cortex correlates with acuity thresholds. *Neuron*, *38*(4), 659–671. https://doi.org/10.1016/s0896-6273(03)00265-4

Edwards G, Vetter P, McGruer F, Petro LS, Muckli L. (2017). Predictive feedback to V1 dynamically updates with sensory input. *Sci Rep*, 28, 7(1):16538. doi: 10.1038/s41598-017-16093-y

Ekman, M., Kok, P., & de Lange, F. P. (2017). Time-compressed preplay of anticipated events in human primary visual cortex. *Nature communications*, 8, 15276. https://doi.org/10.1038/ncomms15276.

Emmerling, T. C., Zimmermann, J., Sorger, B., Frost, M. A., & Goebel, R. (2016). Decoding the direction of imagined visual motion using 7T ultra-high field fMRI. *NeuroImage*, 125, 61–73. https://doi.org/10.1016/j.neuroimage.2015.10.022.

Engel, S. A., Rumelhart, D. E., Wandell, B. A., Lee, A. T., Glover, G. H., Chichilnisky, E.-J., & Shadlen, M. N. (1994). fMRI of human visual cortex. *Nature, 369*(6481), 525. https://doi.org/10.1038/369525a0

Erlikhman, G., & Caplovitz, G. P. (2017). Decoding information about dynamically occluded objects in visual cortex. *NeuroImage*, 146, 778–788. https://doi.org/10.1016/j.neuroimage.2016.09.024.

Eskandar, E. N., & Assad, J. A. (1999). Dissociation of visual, motor and predictive signals in parietal cortex during visual guidance. *Nature neuroscience*, *2*(1), 88–93. https://doi.org/10.1038/4594

Etzel, J. A. (2017). MVPA significance testing when just above chance, and related properties of permutation tests. In 2017 International Workshop on Pattern Recognition in Neuroimaging (PRNI) (pp. 1-4). IEEE. DOI: 10.1109/PRNI.2017.7981498

Etzel, J. A. and Braver, T. S. (2013)."MVPA Permutation Schemes: Permutation Testing in the Land of Cross-Validation". International Workshop on Pattern Recognition in Neuroimaging, 2013, pp. 140-143, doi: 10.1109/PRNI.2013.44.

Feldman, H., & Friston, K. J. (2010). Attention, uncertainty, and free-energy. *Frontiers in human neuroscience*, *4*, 215. https://doi.org/10.3389/fnhum.2010.00215

Felleman, D. J., & Van Essen, D. C. (1991). Distributed hierarchical processing in the primate cerebral cortex. Cerebral cortex (New York, N.Y.: 1991), 1(1), 1–47. https://doi.org/10.1093/cercor/1.1.1-a

Ffytche, D. H., Guy, C. N., & Zeki, S. (1995). The parallel visual motion inputs into areas V1 and V5 of human cerebral cortex. Brain: a journal of neurology, 118, 1375–1394. https://doi.org/10.1093/brain/118.6.1375

Ffytche, D. H., Guy, C. N., & Zeki, S. (1996). Motion specific responses from a blind hemifield. Brain : a journal of neurology, 119 (Pt 6), 1971–1982. https://doi.org/10.1093/brain/119.6.1971

Fischer, R., Plessow, F., & Ruge, H. (2013). Priming of visual cortex by temporal attention? The effects of temporal predictability on stimulus(-specific) processing in early visual cortical areas. NeuroImage, 66, 261–269. https://doi.org/10.1016/j.neuroimage.2012.10.091

Fiser, J., & Aslin, R. N. (2002). Statistical learning of higher-order temporal structure from visual shape sequences. *Journal of experimental psychology. Learning, memory, and cognition*, *28*(3), 458–467. https://doi.org/10.1037//0278-7393.28.3.458

Flombaum, J. I., Scholl, B. J., & Pylyshyn, Z. W. (2008). Attentional resources in visual tracking through occlusion: the high-beams effect. *Cognition*, 107(3), 904–931. https://doi.org/10.1016/j.cognition.2007.12.015.

Foxe, J. J., Murray, M. M., & Javitt, D. C. (2005). Filling-in in schizophrenia: a high-density electrical mapping and source-analysis investigation of illusory contour processing. Cerebral cortex (New York, N.Y. : 1991), 15(12), 1914–1927. https://doi.org/10.1093/cercor/bhi069

Fregni, F., Simon, D. K., Wu, A., & Pascual-Leone, A. (2005). Non-invasive brain stimulation for Parkinson's disease: a systematic review and meta-analysis of the literature. *Journal of neurology, neurosurgery, and psychiatry*, *76*(12), 1614–1623. https://doi.org/10.1136/jnnp.2005.069849

Frielink-Loing, A. F., Koning, A., & van Lier, R. (2017). Distinguishing influences of overt and covert attention in anticipatory attentional target tracking. *Journal of vision*, *17*(4), 3. https://doi.org/10.1167/17.4.3

Friston K. (2003). Learning and inference in the brain. Neural networks: the official journal of the International Neural Network Society, 16(9), 1325–1352. https://doi.org/10.1016/j.neunet.2003.06.005

Friston, K. J., & Stephan, K. E. (2007). Free-energy and the brain. *Synthese*, *159*(3), 417–458. https://doi.org/10.1007/s11229-007-9237-y

Friston, K. J., Buechel, C., Fink, G. R., Morris, J., Rolls, E., & Dolan, R. J. (1997). Psychophysiological and modulatory interactions in neuroimaging. *NeuroImage*, *6*(3), 218–229. https://doi.org/10.1006/nimg.1997.0291

Friston, K. J., Fletcher, P., Josephs, O., Holmes, A., Rugg, M. D., & Turner, R. (1998). Event-related fMRI: characterizing differential responses. *NeuroImage*, *7*(1), 30–40. https://doi.org/10.1006/nimg.1997.0306

Friston, K. J., Harrison, L., & Penny, W. (2003). Dynamic causal modelling. NeuroImage, 19(4), 1273–1302. https://doi.org/10.1016/s1053-8119(03)00202-7

Friston, K. J., Holmes, A. P., Poline, J. B., Grasby, P. J., Williams, S. C., Frackowiak, R. S., & Turner, R. (1995). Analysis of fMRI time-series revisited. *NeuroImage*, *2*(1), 45–53. https://doi.org/10.1006/nimg.1995.1007

Friston, K., & Kiebel, S. (2009). Predictive coding under the free-energy principle. *Philosophical transactions of the Royal Society of London. Series B, Biological sciences*, *364*(1521), 1211–1221. https://doi.org/10.1098/rstb.2008.0300

Friston, K., Kilner, J., & Harrison, L. (2006). A free energy principle for the brain. *Journal of physiology, Paris*, *100*(1-3), 70–87. https://doi.org/10.1016/j.jphysparis.2006.10.001

George, M. S., Nahas, Z., Borckardt, J. J., Anderson, B., Foust, M. J., Burns, C., Kose, S., & Short, E. B. (2007). Brain stimulation for the treatment of psychiatric disorders. *Current opinion in psychiatry*, *20*(3), 250–249. https://doi.org/10.1097/YCO.0b013e3280ad4698

Georgieva, S., Peeters, R., Kolster, H., Todd, J. T., & Orban, G. A. (2009). The processing of three-dimensional shape from disparity in the human brain. *The Journal of neuroscience : the official journal of the Society for Neuroscience*, *29*(3), 727–742. https://doi.org/10.1523/JNEUROSCI.4753-08.2009.

Gibson, J. J. (1968). What gives rise to the perception of motion? *Psychological Review, 75*(4), 335–346. https://doi.org/10.1037/h0025893

Gießing, C., Alavash, M., Herrmann, C. S., Hilgetag, C. C., & Thiel, C. M. (2020). Individual differences in local functional brain connectivity affect TMS effects on behavior. Scientific reports, 10(1), 10422. https://doi.org/10.1038/s41598-020-67162-8

Gilden, D., Blake, R., & Hurst, G. (1995). Neural adaptation of imaginary visual motion. Cognitive psychology, 28(1), 1–16. https://doi.org/10.1006/cogp.1995.1001

Goebel, R., Khorram-Sefat, D., Muckli, L., Hacker, H., & Singer, W. (1998). The constructive nature of vision: direct evidence from functional magnetic resonance imaging studies of apparent motion and motion imagery. The European journal of neuroscience, 10(5), 1563–1573. https://doi.org/10.1046/j.1460-9568.1998.00181.x

Gomez-Tames, J., Hamasaka, A., Laakso, I., Hirata, A., & Ugawa, Y. (2018). Atlas of optimal coil orientation and position for TMS: A computational study. Brain stimulation, 11(4), 839–848. https://doi.org/10.1016/j.brs.2018.04.011

Gottsdanker, R. M. (1952). The accuracy of prediction motion. *Journal of Experimental Psychology, 43*(1), 26–36. https://doi.org/10.1037/h0062840

Gottsdanker, R. M. (1956). The ability of human operators to detect acceleration of target motion. *Psychological Bulletin, 53*(6), 477–487. https://doi.org/10.1037/h0045160

Grasso, P. A., Làdavas, E., Bertini, C., Caltabiano, S., Thut, G., & Morand, S. (2018). Decoupling of Early V5 Motion Processing from Visual Awareness: A Matter of Velocity as Revealed by Transcranial Magnetic Stimulation. *Journal of cognitive neuroscience*, *30*(10), 1517–1531. https://doi.org/10.1162/jocn_a_01298

Greenlee M. W. (2000). Human cortical areas underlying the perception of optic flow: brain imaging studies. International review of neurobiology, 44, 269–292. https://doi.org/10.1016/s0074-7742(08)60746-1

Greenwood, J. A., Szinte, M., Sayim, B., & Cavanagh, P. (2017). Variations in crowding, saccadic precision, and spatial localization reveal the shared topology of spatial vision. Proceedings of the

National Academy of Sciences of the United States of America, 114(17), E3573–E3582, https://doi.org/10.1073/pnas.1615504114.

Hallett, M. Transcranial magnetic stimulation and the human brain. Nature 406, 147–150 (2000). https://doi.org/10.1038/35018000

Hampson, M., Olson, I. R., Leung, H. C., Skudlarski, P., & Gore, J. C. (2004). Changes in functional connectivity of human MT/V5 with visual motion input. Neuroreport, 15(8), 1315–1319. https://doi.org/10.1097/01.wnr.0000129997.95055.15

Hanning, N. M., Himmelberg, M. M., & Carrasco, M. (2022). Presaccadic attention enhances contrast sensitivity, but not at the upper vertical meridian. *iScience*, *25*(2), 103851. https://doi.org/10.1016/j.isci.2022.103851

Hanson, S. J., Matsuka, T., & Haxby, J. V. (2004). Combinatorial codes in ventral temporal lobe for object recognition: Haxby (2001) revisited: is there a "face" area?. NeuroImage, 23(1), 156–166. https://doi.org/10.1016/j.neuroimage.2004.05.020

Haxby J. V. (2012). Multivariate pattern analysis of fMRI: the early beginnings. *NeuroImage*, *62*(2), 852–855. https://doi.org/10.1016/j.neuroimage.2012.03.016

Haxby, J. V., Connolly, A. C., & Guntupalli, J. S. (2014). Decoding neural representational spaces using multivariate pattern analysis. *Annual review of neuroscience*, *37*, 435–456. https://doi.org/10.1146/annurev-neuro-062012-170325

He, S., Cavanagh, P., & Intriligator, J. (1996). Attentional resolution and the locus of visual awareness. *Nature*, *383*(6598), 334–337. https://doi.org/10.1038/383334a0.

Hecht, H., & Savelsbergh, G. J. P. (Eds.). (2004). *Advances in psychology*, Vol. 135. Time-to-contact. Elsevier Science Publishers B.V.

Heilbron, M., & Chait, M. (2018). Great Expectations: Is there Evidence for Predictive Coding in Auditory Cortex?. *Neuroscience*, *389*, 54–73. https://doi.org/10.1016/j.neuroscience.2017.07.061

Helmholtz, H. (1866/1962). Concerning the perceptions in general. In J. Southall (Ed.) Treatise on physiological optics (3rd ed., Vol. III). New York: Dover, (Translation).

Himmelberg, M. M., Kurzawski, J. W., Benson, N. C., Pelli, D. G., Carrasco, M., & Winawer, J. (2021). Cross-dataset reproducibility of human retinotopic maps. NeuroImage, 244, 118609. https://doi.org/10.1016/j.neuroimage.2021.118609

Himmelberg, M. M., Winawer, J., & Carrasco, M. (2022). Linking individual differences in human primary visual cortex to contrast sensitivity around the visual field. Nature communications, 13(1), 3309. https://doi.org/10.1038/s41467-022-31041-9

Himmelberg, M. M., Winawer, J., & Carrasco, M. (2020). Stimulus-dependent contrast sensitivity asymmetries around the visual field. Journal of vision, 20(9), 18. https://doi.org/10.1167/jov.20.9.18

Hubbard T. L. (1995). Environmental invariants in the representation of motion: Implied dynamics and representational momentum, gravity, friction, and centripetal force. Psychonomic bulletin & review, 2(3), 322–338. https://doi.org/10.3758/BF03210971

Huber, S., & Krist, H. (2004). When Is the Ball Going to Hit the Ground? Duration Estimates, Eye Movements, and Mental Imagery of Object Motion. *Journal of Experimental Psychology: Human Perception and Performance, 30*(3), 431–444. https://doi.org/10.1037/0096-1523.30.3.431

Hulme, O. J., & Zeki, S. (2007). The sightless view: neural correlates of occluded objects. *Cerebral cortex (New York, N.Y. : 1991)*, *17*(5), 1197–1205. https://doi.org/10.1093/cercor/bhl031

Hurme, M., Koivisto, M., Revonsuo, A., & Railo, H. (2017). Early processing in primary visual cortex is necessary for conscious and unconscious vision while late processing is necessary only for conscious vision in neurologically healthy humans. *NeuroImage*, *150*, 230–238. https://doi.org/10.1016/j.neuroimage.2017.02.060

Hurme, M., Koivisto, M., Revonsuo, A., & Railo, H. (2019). V1 activity during feedforward and early feedback processing is necessary for both conscious and unconscious motion perception. *NeuroImage*, *185*, 313–321. https://doi.org/10.1016/j.neuroimage.2018.10.058

Intriligator, J., & Cavanagh, P. (2001). The spatial resolution of visual attention. *Cognitive psychology*, *43*(3), 171–216. https://doi.org/10.1006/cogp.2001.0755.

Janssen, A. M., Oostendorp, T. F., & Stegeman, D. F. (2015). The coil orientation dependency of the electric field induced by TMS for M1 and other brain areas. *Journal of neuroengineering and rehabilitation*, *12*, 47. https://doi.org/10.1186/s12984-015-0036-2

Kaas, A., Weigelt, S., Roebroeck, A., Kohler, A., & Muckli, L. (2010). Imagery of a moving object: the role of occipital cortex and human MT/V5+. *NeuroImage*, *49*(1), 794–804. https://doi.org/10.1016/j.neuroimage.2009.07.055

Kahneman, D., & Tversky, A. (1972). Subjective probability: A judgment of representativeness. Cognitive Psychology, 3(3), 430–454. https://doi.org/10.1016/0010-0285(72)90016-3

Kammer T. (1999). Phosphenes and transient scotomas induced by magnetic stimulation of the occipital lobe: their topographic relationship. *Neuropsychologia*, *37*(2), 191–198. https://doi.org/10.1016/s0028-3932(98)00093-1

Kammer, T., & Baumann, L. W. (2010). Phosphene thresholds evoked with single and double TMS pulses. *Clinical neurophysiology : official journal of the International Federation of Clinical Neurophysiology*, *121*(3), 376–379. https://doi.org/10.1016/j.clinph.2009.12.002

Kanizsa, G. (1976). Subjective Contours. *Scientific American*, *234*(4), 48–53. http://www.jstor.org/stable/24950327

Kanizsa, G. (1985). Seeing and thinking. *Acta psychologica*, *59*(1), 23-33. https://doi.org/10.1016/0001-6918(85)90040-X

Karim, A. K., & Kojima, H. (2010). The what and why of perceptual asymmetries in the visual domain. *Advances in cognitive psychology*, *6*, 103–115. https://doi.org/10.2478/v10053-008-0080-6.

Keane, B. P., & Pylyshyn, Z. W. (2006). Is motion extrapolation employed in multiple object tracking? Tracking as a low-level, non-predictive function. *Cognitive psychology*, 52(4), 346–368. https://doi.org/10.1016/j.cogpsych.2005.12.001.

Kerzel D. (2003). Attention maintains mental extrapolation of target position: irrelevant distractors eliminate forward displacement after implied motion. *Cognition*, *88*(1), 109–131. https://doi.org/10.1016/s0010-0277(03)00018-0

Khoei, M. A., Masson, G. S., & Perrinet, L. U. (2013). Motion-based prediction explains the role of tracking in motion extrapolation. *Journal of physiology*, Paris, 107(5), 409–420. https://doi.org/10.1016/j.jphysparis.2013.08.001.

King, J. A., Korb, F. M., von Cramon, D. Y., & Ullsperger, M. (2010). Post-error behavioral adjustments are facilitated by activation and suppression of task-relevant and task-irrelevant information processing. The Journal of neuroscience: the official journal of the Society for Neuroscience, 30(38), 12759–12769. https://doi.org/10.1523/JNEUROSCI.3274-10.2010

Klein, B. P., Fracasso, A., van Dijk, J. A., Paffen, C., Te Pas, S. F., & Dumoulin, S. O. (2018). Cortical depth dependent population receptive field attraction by spatial attention in human V1. *NeuroImage*, *176*, 301–312. https://doi.org/10.1016/j.neuroimage.2018.04.055.

Klein, B. P., Harvey, B. M., & Dumoulin, S. O. (2014). Attraction of position preference by spatial attention throughout human visual cortex. *Neuron*, *84*(1), 227–237. https://doi.org/10.1016/j.neuron.2014.08.047.

Koivisto, M., Harjuniemi, I., Railo, H., Salminen-Vaparanta, N., & Revonsuo, A. (2017). Transcranial magnetic stimulation of early visual cortex suppresses conscious representations in a dichotomous manner without gradually decreasing their precision. *NeuroImage*, *158*, 308–318. https://doi.org/10.1016/j.neuroimage.2017.07.011

Koivisto, M., Mäntylä, T., & Silvanto, J. (2010). The role of early visual cortex (V1/V2) in conscious and unconscious visual perception. NeuroImage, 51(2), 828–834. https://doi.org/10.1016/j.neuroimage.2010.02.042

Kok, P., Rahnev, D., Jehee, J. F., Lau, H. C., & de Lange, F. P. (2012). Attention reverses the effect of prediction in silencing sensory signals. Cerebral cortex (New York, N.Y. : 1991), 22(9), 2197–2206. https://doi.org/10.1093/cercor/bhr310

Kolster, H., Peeters, R., & Orban, G. A. (2010). The retinotopic organization of the human middle temporal area MT/V5 and its cortical neighbors. The Journal of neuroscience : the official journal of the Society for Neuroscience, 30(29), 9801–9820. https://doi.org/10.1523/JNEUROSCI.2069-10.2010

Kosslyn, S. M., Pascual-Leone, A., Felician, O., Camposano, S., Keenan, J. P., Thompson, W. L., Ganis, G., Sukel, K. E., & Alpert, N. M. (1999). The role of area 17 in visual imagery: convergent evidence from PET and rTMS. *Science (New York, N.Y.), 284*(5411), 167–170. https://doi.org/10.1126/science.284.5411.167

Krala, M., van Kemenade, B., Straube, B., Kircher, T., & Bremmer, F. (2019). Predictive coding in a multisensory path integration task: An fMRI study. Journal of vision, 19(11), 13. https://doi.org/10.1167/19.11.13

Kriegeskorte, N., Goebel, R., & Bandettini, P. (2006). Information-based functional brain mapping. Proceedings of the National Academy of Sciences of the United States of America, 103(10), 3863–3868. https://doi.org/10.1073/pnas.0600244103

Lakha, L., & Humphreys, G. (2005). Lower visual field advantage for motion segmentation during high competition for selection. *Spatial vision*, *18*(4), 447–460. https://doi.org/10.1163/1568568054389570.

Lambrechts, A., Walsh, V., & van Wassenhove, V. (2013). Evidence accumulation in the magnitude system. PloS one, 8(12), e82122. https://doi.org/10.1371/journal.pone.0082122

Lamme, V. A., & Roelfsema, P. R. (2000). The distinct modes of vision offered by feedforward and recurrent processing. Trends in neurosciences, 23(11), 571–579. https://doi.org/10.1016/s0166-2236(00)01657-x

Laycock, R., Crewther, D. P., Fitzgerald, P. B., & Crewther, S. G. (2007). Evidence for fast signals and later processing in human V1/V2 and V5/MT+: A TMS study of motion perception. Journal of neurophysiology, 98(3), 1253–1262. https://doi.org/10.1152/jn.00416.2007

Lee, D. N. (1974). Visual information during locomotion. In R. B. MacLeod & H. L. Pick (Eds.), *Perception: Essays in honor of James J. Gibson.* Cornell University Press.

Lencer, R., Nagel, M., Sprenger, A., Zapf, S., Erdmann, C., Heide, W., & Binkofski, F. (2004). Cortical mechanisms of smooth pursuit eye movements with target blanking. An fMRI study. *The European journal of neuroscience*, *19*(5), 1430–1436. https://doi.org/10.1111/j.1460-9568.2004.03229.x

Levine, M. W., & McAnany, J. J. (2005). The relative capabilities of the upper and lower visual hemifields. *Vision research*, 45(21), 2820–2830. https://doi.org/10.1016/j.visres.2005.04.001.

Lyon, D. C., Nassi, J. J., & Callaway, E. M. (2010). A disynaptic relay from superior colliculus to dorsal stream visual cortex in macaque monkey. Neuron, 65(2), 270–279. https://doi.org/10.1016/j.neuron.2010.01.003

Lyon, D. R., & Waag, W. L. (1995). Time course of visual extrapolation accuracy. *Acta psychologica*, *89*(3), 239–260. https://doi.org/10.1016/0001-6918(95)98945-z

Makin A. (2018). The common rate control account of prediction motion. *Psychonomic bulletin & review*, *25*(5), 1784–1797. https://doi.org/10.3758/s13423-017-1403-8

Makin, A. D., & Bertamini, M. (2014). Do different types of dynamic extrapolation rely on the same mechanism? *Journal of experimental psychology. Human perception and performance*, 40(4), 1566–1579. https://doi.org/10.1037/a0036680.

Makin, A. D., & Chauhan, T. (2014). Memory-guided tracking through physical space and feature space. *Journal of vision*, *14*(13), 10. https://doi.org/10.1167/14.13.10

Makin, A. D., & Poliakoff, E. (2011). Do common systems control eye movements and motion extrapolation? *Quarterly journal of experimental psychology (2006)*, *64*(7), 1327–1343. https://doi.org/10.1080/17470218.2010.548562.

Makin, A. D., Poliakoff, E., Chen, J., & Stewart, A. J. (2008). The effect of previously viewed velocities on motion extrapolation. *Vision research*, *48*(18), 1884–1893. https://doi.org/10.1016/j.visres.2008.05.023.

Marg, E., & Rudiak, D. (1994). Phosphenes induced by magnetic stimulation over the occipital brain: description and probable site of stimulation. *Optometry and vision science : official publication of*

the American Academy of Optometry, *71*(5), 301–311. https://doi.org/10.1097/00006324-199405000-00001

McConnell, K. A., Nahas, Z., Shastri, A., Lorberbaum, J. P., Kozel, F. A., Bohning, D. E., & George, M. S. (2001). The transcranial magnetic stimulation motor threshold depends on the distance from coil to underlying cortex: a replication in healthy adults comparing two methods of assessing the distance to cortex. Biological psychiatry, 49(5), 454–459. https://doi.org/10.1016/s0006-3223(00)01039-8

McGee, T., Kraus, N., Comperatore, C., & Nicol, T. (1991). Subcortical and cortical components of the MLR generating system. Brain research, 544(2), 211–220. https://doi.org/10.1016/0006-8993(91)90056-2

Merabet, L. B., Theoret, H., & Pascual-Leone, A. (2003). Transcranial magnetic stimulation as an investigative tool in the study of visual function. Optometry and vision science : official publication of the American Academy of Optometry, 80(5), 356–368. https://doi.org/10.1097/00006324-200305000-00010

Merkel, C., Hopf, J.-M., Schoenfeld, M.A. (2020). Modulating the global orientation bias of the visual system changes population receptive field elongations. *Human Brain Mapping*. 41(7):1765-1774. doi: 10.1002/hbm.24909.

Michotte, A. (1946). The perception of causality, trans. *R. Miles and E. Miles (London: Methuen & Co., Ltd., 1963)*.

Michotte, A. (1950). Concerning The Phenomenal Permanence, Facts And Theories. *Acta Psychologica*, *7*, 298-322.

Mitchell, T.M., Hutchinson, R., Niculescu, R.S. et al. (2004). Learning to Decode Cognitive States from Brain Images. Machine Learning 57, 145–175 https://doi.org/10.1023/B:MACH.0000035475.85309.1b

Moliadze, V., Giannikopoulos, D., Eysel, U. T., & Funke, K. (2005). Paired-pulse transcranial magnetic stimulation protocol applied to visual cortex of anaesthetized cat: effects on visually evoked single-unit activity. *The Journal of physiology*, *566*(Pt 3), 955–965. https://doi.org/10.1113/jphysiol.2005.086090

Mourão-Miranda, J., Bokde, A. L., Born, C., Hampel, H., & Stetter, M. (2005). Classifying brain states and determining the discriminating activation patterns: Support Vector Machine on functional MRI data. NeuroImage, 28(4), 980–995. https://doi.org/10.1016/j.neuroimage.2005.06.070

Muckli L, Kohler A, Kriegeskorte N, Singer W. (2005). Primary visual cortex activity along the apparent-motion trace reflects illusory perception. *PLoS Biol*, 3(8):e265. doi: 10.1371/journal.pbio.0030265.

Muckli, L., Kriegeskorte, N., Lanfermann, H., Zanella, F. E., Singer, W., & Goebel, R. (2002). Apparent motion: event-related functional magnetic resonance imaging of perceptual switches and States. The Journal of neuroscience: the official journal of the Society for Neuroscience, 22(9), RC219. https://doi.org/10.1523/JNEUROSCI.22-09-j0003.2002

Mumford D. (1992). On the computational architecture of the neocortex. II. The role of cortico-cortical loops. Biological cybernetics, 66(3), 241–251. https://doi.org/10.1007/BF00198477

Mumford, J. A., Turner, B. O., Ashby, F. G., & Poldrack, R. A. (2012). Deconvolving BOLD activation in event-related designs for multivoxel pattern classification analyses. NeuroImage, 59(3), 2636–2643. https://doi.org/10.1016/j.neuroimage.2011.08.076

Müsseler, J., & Aschersleben, G. (1998). Localizing the first position of a moving stimulus: the Fröhlich effect and an attention-shifting explanation. *Perception & psychophysics*, *60*(4), 683–695. https://doi.org/10.3758/bf03206055

Nasr, S., & Tootell, R. (2018). Visual field biases for near and far stimuli in disparity selective columns in human visual cortex. *NeuroImage*, 168, 358–365. https://doi.org/10.1016/j.neuroimage.2016.09.012.

Nasr, S., & Tootell, R. (2020). Asymmetries in Global Perception Are Represented in Near- versus Far-Preferring Clusters in Human Visual Cortex. *The Journal of neuroscience : the official journal of the Society for Neuroscience,* 40(2), 355–368. https://doi.org/10.1523/JNEUROSCI.2124-19.2019.

Nasr, S., & Tootell, R. B. (2012). Role of fusiform and anterior temporal cortical areas in facial recognition. NeuroImage, 63(3), 1743–1753. https://doi.org/10.1016/j.neuroimage.2012.08.031

Nicolo, P., Ptak, R., & Guggisberg, A. G. (2015). Variability of behavioural responses to transcranial magnetic stimulation: Origins and predictors. Neuropsychologia, 74, 137–144. https://doi.org/10.1016/j.neuropsychologia.2015.01.033

Noesselt, T., Hillyard, S. A., Woldorff, M. G., Schoenfeld, A., Hagner, T., Jäncke, L., Tempelmann, C., Hinrichs, H., & Heinze, H. J. (2002). Delayed striate cortical activation during spatial attention. *Neuron*, *35*(3), 575–587. https://doi.org/10.1016/s0896-6273(02)00781-x

Norman, K. A., Polyn, S. M., Detre, G. J., & Haxby, J. V. (2006). Beyond mind-reading: multi-voxel pattern analysis of fMRI data. *Trends in cognitive sciences*, *10*(9), 424–430. https://doi.org/10.1016/j.tics.2006.07.005

Olson, I. R., Gatenby, J. C., Leung, H. C., Skudlarski, P., & Gore, J. C. (2004). Neuronal representation of occluded objects in the human brain. *Neuropsychologia*, 42(1), 95–104. https://doi.org/10.1016/s0028-3932(03)00151-9.

Oosterhof, N. N., Connolly, A. C., and Haxby, J. V. (2016). CoSMoMVPA: multi-modal multivariate pattern analysis of neuroimaging data in Matlab / GNU Octave. *Frontiers in Neuroinformatics*, doi:10.3389/fninf.2016.00027.

O'Reilly, J. X., Mesulam, M. M., & Nobre, A. C. (2008). The cerebellum predicts the timing of perceptual events. *The Journal of neuroscience : the official journal of the Society for Neuroscience*, *28*(9), 2252–2260. https://doi.org/10.1523/JNEUROSCI.2742-07.2008.

Pascual-Leone, A., & Walsh, V. (2001). Fast backprojections from the motion to the primary visual area necessary for visual awareness. *Science (New York, N.Y.)*, *292*(5516), 510–512. https://doi.org/10.1126/science.1057099

Pascual-Leone, A., Valls-Solé, J., Brasil-Neto, J. P., Cohen, L. G., & Hallett, M. (1992). Seizure induction and transcranial magnetic stimulation. Lancet (London, England), 339(8799), 997. https://doi.org/10.1016/0140-6736(92)91582-s

Pasternak, T., & Greenlee, M. W. (2005). Working memory in primate sensory systems. Nature reviews. Neuroscience, 6(2), 97–107. https://doi.org/10.1038/nrn1603

Patton, Lydia, "Hermann von Helmholtz", The Stanford Encyclopedia of Philosophy (Winter 2018 Edition), Edward N. Zalta (ed.), URL = <https://plato.stanford.edu/archives/win2018/entries/hermann-helmholtz/>

Poldrack, R. A., Mumford, J. A., & Nichols, T. E. (2011). *Handbook of functional MRI data analysis*. Cambridge University Press.

Poppel, E., Held, R., & Frost, D. (1973). Leter: Residual visual function after brain wounds involving the central visual pathways in man. Nature, 243(5405), 295–296. https://doi.org/10.1038/243295a0

Previc, F. (1990). Functional specialization in the lower and upper visual fields in humans: Its ecological origins and neurophysiological implications. Behavioral and Brain Sciences, 13(3), 519-542. doi:10.1017/S0140525X00080018

Raffin, E., Salamanca-Giron, R. F., Huxlin, K. R., Reynaud, O., Mattera, L., Martuzzi, R., & Hummel, F. C. (2022). Concurrent TMS-fMRI to determine adaptive brain changes to virtual lesions interfering with visual processing. *bioRxiv*.

Railo, H., & Hurme, M. (2021). Is the primary visual cortex necessary for blindsight-like behavior? Review of transcranial magnetic stimulation studies in neurologically healthy individuals. *Neuroscience and biobehavioral reviews*, *127*, 353–364. https://doi.org/10.1016/j.neubiorev.2021.04.038

Rao R. P. (2005). Bayesian inference and attentional modulation in the visual cortex. Neuroreport, 16(16), 1843–1848. https://doi.org/10.1097/01.wnr.0000183900.92901.fc

Rao, R. P., & Ballard, D. H. (1999). Predictive coding in the visual cortex: a functional interpretation of some extra-classical receptive-field effects. *Nature neuroscience*, 2(1), 79–87. https://doi.org/10.1038/4580

Riddoch, G. (1917). Dissociation of visual perceptions due to occipital injuries, with especial reference to appreciation of movement. Brain, 40(1), 15-57.

Rijsdijk, J. P., Kroon, J. N., & van der Wildt, G. J. (1980). Contrast sensitivity as a function of position on the retina. Vision research, 20(3), 235–241. https://doi.org/10.1016/0042-6989(80)90108-x

Rinaldi, L., Di Luca, S., Henik, A., & Girelli, L. (2014). Reading direction shifts visuospatial attention: an Interactive Account of attentional biases. *Acta psychologica*, *151*, 98–105. https://doi.org/10.1016/j.actpsy.2014.05.018.

Rizzolatti, G., Riggio, L., Dascola, I., & Umiltá, C. (1987). Reorienting attention across the horizontal and vertical meridians: evidence in favor of a premotor theory of attention. *Neuropsychologia*, *25*(1A), 31–40. https://doi.org/10.1016/0028-3932(87)90041-8

Rosander, K., & von Hofsten, C. (2004). Infants' emerging ability to represent occluded object motion. *Cognition*, *91*(1), 1–22. https://doi.org/10.1016/s0010-0277(03)00166-5

Rossi, S., Hallett, M., Rossini, P. M., Pascual-Leone, A., & Safety of TMS Consensus Group (2009). Safety, ethical considerations, and application guidelines for the use of transcranial magnetic stimulation in clinical practice and research. *Clinical neurophysiology: official journal of the International Federation of Clinical Neurophysiology*, *120*(12), 2008–2039. https://doi.org/10.1016/j.clinph.2009.08.016

Sack, A. T., Kohler, A., Linden, D. E., Goebel, R., & Muckli, L. (2006). The temporal characteristics of motion processing in hMT/V5+: combining fMRI and neuronavigated TMS. NeuroImage, 29(4), 1326–1335. https://doi.org/10.1016/j.neuroimage.2005.08.027

Saffran, J. R., Aslin, R. N., & Newport, E. L. (1996). Statistical learning by 8-month-old infants. *Science (New York, N.Y.)*, *274*(5294), 1926–1928. https://doi.org/10.1126/science.274.5294.1926

Sanders, M. D., Warrington, E. K., Marshall, J., & Wieskrantz, L. (1974). "Blindsight": Vision in a field defect. Lancet (London, England), 1(7860), 707–708. https://doi.org/10.1016/s0140-6736(74)92907-9

Schapiro, A., & Turk-Browne, N. (2015). Statistical Learning. In *Social Cognitive Neuroscience, Cognitive Neuroscience, Clinical Brain Mapping* (Vol. 3, pp. 501-506). Elsevier Inc.. https://doi.org/10.1016/B978-0-12-397025-1.00276-1

Schellekens, W., van Wezel, R. J., Petridou, N., Ramsey, N. F., & Raemaekers, M. (2016). Predictive coding for motion stimuli in human early visual cortex. *Brain structure & function*, 221(2), 879–890. https://doi.org/10.1007/s00429-014-0942-2

Schoenfeld, M. A., Heinze, H. J., & Woldorff, M. G. (2002a). Unmasking motion-processing activity in human brain area V5/MT+ mediated by pathways that bypass primary visual cortex. *NeuroImage*, *17*(2), 769–779.

Schoenfeld, M. A., Noesselt, T., Poggel, D., Tempelmann, C., Hopf, J. M., Woldorff, M. G., Heinze, H. J., & Hillyard, S. A. (2002b). Analysis of pathways mediating preserved vision after striate cortex lesions. *Annals of neurology*, *52*(6), 814–824. https://doi.org/10.1002/ana.10394

Scholl, B. J., & Pylyshyn, Z. W. (1999). Tracking multiple items through occlusion: Clues to visual objecthood. *Cognitive psychology*, 38(2), 259-290.

Sengupta, P., Burgaleta, M., Zamora-López, G., Basora, A., Sanjuán, A., Deco, G., & Sebastian-Galles, N. (2019). Traces of statistical learning in the brain's functional connectivity after artificial language exposure. *Neuropsychologia*, *124*, 246–253. https://doi.org/10.1016/j.neuropsychologia.2018.12.001

Shipp, S., Adams, R. A., & Friston, K. J. (2013). Reflections on agranular architecture: predictive coding in the motor cortex. Trends in neurosciences, 36(12), 706–716. https://doi.org/10.1016/j.tins.2013.09.004

Shuwairi, S. M., Curtis, C. E., & Johnson, S. P. (2007). Neural substrates of dynamic object occlusion. *Journal of cognitive neuroscience*, 19(8), 1275–1285. https://doi.org/10.1162/jocn.2007.19.8.1275.

Silvanto, J., & Muggleton, N. G. (2008). Testing the validity of the TMS state-dependency approach: targeting functionally distinct motion-selective neural populations in visual areas V1/V2 and V5/MT+. *NeuroImage*, *40*(4), 1841–1848. https://doi.org/10.1016/j.neuroimage.2008.02.002

Silvanto, J., Lavie, N., & Walsh, V. (2005). Double dissociation of V1 and V5/MT activity in visual awareness. Cerebral cortex (New York, N.Y.: 1991), 15(11), 1736–1741. https://doi.org/10.1093/cercor/bhi050

Skrandies, W. (1987). The Upper and Lower Visual Field of Man: Electrophysiological and Functional Differences. In: Autrum, H., Ottoson, D., Perl, E.R., Schmidt, R.F., Shimazu, H., Willis, W.D. (eds) Progress in Sensory Physiology. Progress in Sensory Physiology, vol 8. Springer, Berlin, Heidelberg. https://doi.org/10.1007/978-3-642-71060-5_1

Slotnick, S. D., Thompson, W. L., & Kosslyn, S. M. (2005). Visual mental imagery induces retinotopically organized activation of early visual areas. *Cerebral cortex (New York, N.Y. : 1991)*, *15*(10), 1570–1583. https://doi.org/10.1093/cercor/bhi035

Song, C., Schwarzkopf, D. S., Kanai, R., & Rees, G. (2015). Neural population tuning links visual cortical anatomy to human visual perception. *Neuron*, *85*(3), 641–656. https://doi.org/10.1016/j.neuron.2014.12.041

Spratling M. W. (2017). A review of predictive coding algorithms. *Brain and cognition*, 112, 92–97. https://doi.org/10.1016/j.bandc.2015.11.003

Sterzer P, Haynes JD, Rees G. (2006). Primary visual cortex activation on the path of apparent motion is mediated by feedback from hMT+/V5. *Neuroimage,* 32(3):1308-16. doi: 10.1016/j.neuroimage.2006.05.029.

Summerfield, C., Egner, T., Greene, M., Koechlin, E., Mangels, J., & Hirsch, J. (2006). Predictive codes for forthcoming perception in the frontal cortex. Science (New York, N.Y.), 314(5803), 1311–1314. https://doi.org/10.1126/science.1132028

Talgar, C. P., & Carrasco, M. (2002). Vertical meridian asymmetry in spatial resolution: visual and attentional factors. Psychonomic bulletin & review, 9(4), 714–722. https://doi.org/10.3758/bf03196326

Thielen, J., Bosch, S. E., van Leeuwen, T. M., van Gerven, M., & van Lier, R. (2019). Neuroimaging Findings on Amodal Completion: A Review. *i-Perception*, *10*(2), 2041669519840047. https://doi.org/10.1177/2041669519840047.

Thompson, B., & Liu, Z. (2006). Learning motion discrimination with suppressed and un-suppressed MT. *Vision research*, *46*(13), 2110–2121. https://doi.org/10.1016/j.visres.2006.01.005

Thompson, B., Deblieck, C., Wu, A., Iacoboni, M., & Liu, Z. (2016). Psychophysical and rTMS Evidence for the Presence of Motion Opponency in Human V5. *Brain stimulation*, *9*(6), 876–881. https://doi.org/10.1016/j.brs.2016.05.012

Todorovic, A., & Auksztulewicz, R. (2021). Dissociable neural effects of temporal expectations due to passage of time and contextual probability. Hearing research, 399, 107871. https://doi.org/10.1016/j.heares.2019.107871

Tresilian J. R. (1995). Perceptual and cognitive processes in time-to-contact estimation: analysis of prediction-motion and relative judgment tasks. *Perception & psychophysics*, *57*(2), 231–245. https://doi.org/10.3758/bf03206510

Tresilian J. R. (1999). Visually timed action: time-out for 'tau'?. *Trends in cognitive sciences*, *3*(8), 301–310. https://doi.org/10.1016/s1364-6613(99)01352-2

Turk-Browne N. B. (2012). Statistical learning and its consequences. *Nebraska Symposium on Motivation. Nebraska Symposium on Motivation*, *59*, 117–146. https://doi.org/10.1007/978-1-4614-4794-8_6

Tversky, A., & Kahneman, D. (1971). Belief in the law of small numbers. *Psychological Bulletin, 76*(2), 105–110. https://doi.org/10.1037/h0031322

Tversky, A., & Kahneman, D. (1973). Availability: A heuristic for judging frequency and probability. Cognitive psychology, 5(2), 207-232. https://doi.org/10.1016/0010-0285(73)90033-9

Tyll, S., Bonath, B., Schoenfeld, M. A., Heinze, H.-J., Ohl, F. W., & Noesselt, T. (2013). Neural basis of multisensory looming signals. *NeuroImage*, 65, 13–22. https://doi.org/10.1016/j.neuroimage.2012.09.056.

van Heusden, E., Harris, A. M., Garrido, M. I., & Hogendoorn, H. (2019). Predictive coding of visual motion in both monocular and binocular human visual processing. *Journal of vision*, 19(1), 3. https://doi.org/10.1167/19.1.3.

van Kemenade, B. M., Wilbertz, G., Müller, A., & Sterzer, P. (2022). Non-stimulated regions in early visual cortex encode the contents of conscious visual perception. *Human brain mapping*, *43*(4), 1394–1402. https://doi.org/10.1002/hbm.25731.

van Lier, R. J., & Gerbino, W. (2015). Perceptual completions in Oxford Handbook of Perceptual Organization (ed. Wagemans, J.) 294–320.

Verghese, P., & McKee, S. P. (2002). Predicting future motion. *Journal of vision*, 2(5), 413–423. https://doi.org/10.1167/2.5.5.

Vetter, P., Grosbras, M. H., & Muckli, L. (2015). TMS over V5 disrupts motion prediction. Cerebral cortex (New York, N.Y. : 1991), 25(4), 1052–1059. https://doi.org/10.1093/cercor/bht297

Vicovaro, M., Noventa, S., & Battaglini, L. (2019). Intuitive physics of gravitational motion as shown by perceptual judgment and prediction-motion tasks. *Acta psychologica*, 194, 51–62. https://doi.org/10.1016/j.actpsy.2019.02.001.

von Hofsten, C., Kochukhova, O., & Rosander, K. (2007). Predictive tracking over occlusions by 4-month-old infants. *Developmental science*, *10*(5), 625–640. https://doi.org/10.1111/j.1467-7687.2007.00604.x

Vul, E., Alvarez, G., Tenenbaum, J., & Black, M. (2009). Explaining human multiple object tracking as resource-constrained approximate inference in a dynamic probabilistic model. *Advances in neural information processing systems*, 22.

Wang, H. X., Merriam, E. P., Freeman, J., & Heeger, D. J. (2014). Motion direction biases and decoding in human visual cortex. *The Journal of neuroscience : the official journal of the Society for Neuroscience*, 34(37), 12601–12615. https://doi.org/10.1523/JNEUROSCI.1034-14.2014.

Wang, P., & Nikolić, D. (2011). An LCD Monitor with Sufficiently Precise Timing for Research in Vision. *Frontiers in human neuroscience*, *5*, 85. https://doi.org/10.3389/fnhum.2011.00085

Wang, R., Shen, Y., Tino, P., Welchman, A. E., & Kourtzi, Z. (2017). Learning Predictive Statistics: Strategies and Brain Mechanisms. *The Journal of neuroscience : the official journal of the Society for Neuroscience*, *37*(35), 8412–8427. https://doi.org/10.1523/JNEUROSCI.0144-17.2017

Warnking, J., Dojat, M., Guérin-Dugué, A., Delon-Martin, C., Olympieff, S., Richard, N., Chéhikian, A., & Segebarth, C. (2002). fMRI retinotopic mapping--step by step. *NeuroImage*, *17*(4), 1665–1683. https://doi.org/10.1006/nimg.2002.1304.

Welch, R.B. & Warren, D.H. (1986). Intersensory interactions. In K. Boff, L. Kaufmann, J. Thomas (Eds.), *Handbook of Perception and Human Performance: Sensory Processes and Perception* (pp. 1-36). New York: Wiley-Interscience.

Yildirim, F. Z., Coates, D. R., & Sayim, B. (2022). Atypical visual field asymmetries in redundancy masking. *Journal of vision*, *22*(5), 4. https://doi.org/10.1167/jov.22.5.4

Zeki, S., & Ffytche, D. H. (1998). The Riddoch syndrome: insights into the neurobiology of conscious vision. Brain : a journal of neurology, 121 (Pt 1), 25–45. https://doi.org/10.1093/brain/121.1.25

Zeki, S., & Shipp, S. (1988). The functional logic of cortical connections. *Nature*, *335*(6188), 311–317. https://doi.org/10.1038/335311a0

Zhong, S. H., Ma, Z., Wilson, C., Liu, Y., & Flombaum, J. I. (2014). Why do people appear not to extrapolate trajectories during multiple object tracking? A computational investigation. *Journal of vision*, 14(12), 12. https://doi.org/10.1167/14.12.12.

Zuanazzi, A., & Noppeney, U. (2019). Distinct Neural Mechanisms of Spatial Attention and Expectation Guide Perceptual Inference in a Multisensory World. The Journal of neuroscience: the official journal of the Society for Neuroscience, 39(12), 2301–2312. https://doi.org/10.1523/JNEUROSCI.2873-18.2019

Zuanazzi, A., & Noppeney, U. (2020). Modality-specific and multisensory mechanisms of spatial attention and expectation. *Journal of vision*, 20(8), 1. https://doi.org/10.1167/jov.20.8.1.

Zylberberg, A., Fetsch, C. R., & Shadlen, M. N. (2016). The influence of evidence volatility on choice, reaction time and confidence in a perceptual decision. *eLife*, *5*, e17688. https://doi.org/10.7554/eLife.17688

Appendix A – Chapter 2

Univariate Analysis

Subject-specific results

Figure 1 depicts modulations in fMRI signals during Visible (left maps) and Occluded (right maps) phases. Trajectory comparisons (upward vs. downward) revealed increased pattern of activity in regions representing upper and lower visual quadrants opposite to the stimulated visual field, as expected.
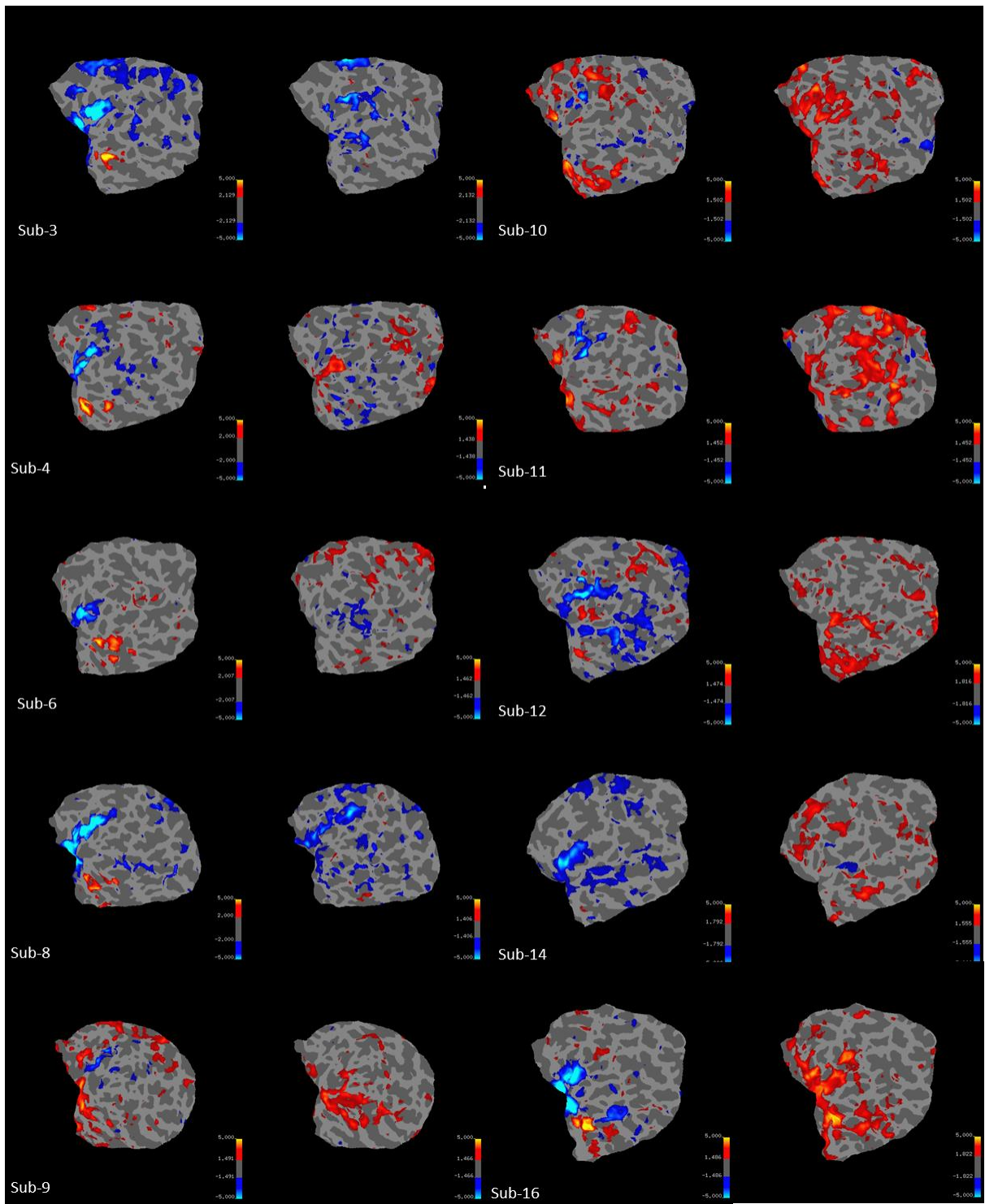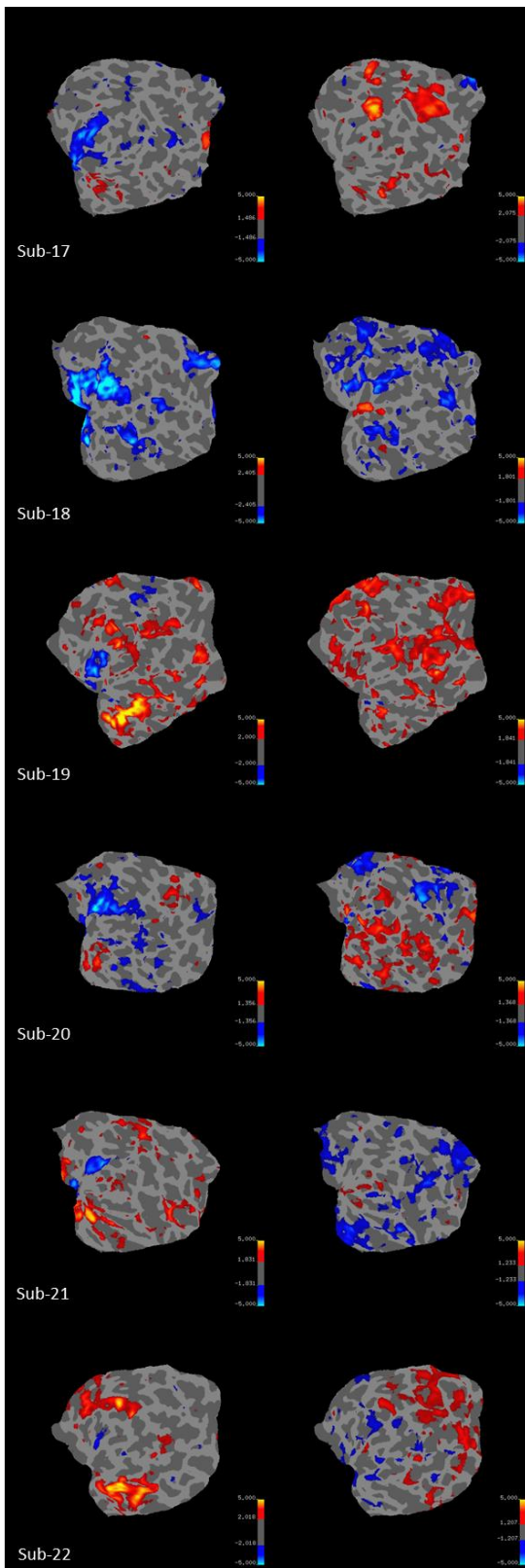
Appendix A. Figure 1 ˗ Univariate results of all participants, during (A) Visible Phase and (B) Occluded Phase, for the contrast upward (warm colours) vs. downward (cold colours) motion projected on the individual flat map. Visual flat maps were created by cutting V1 along the fundus of the calcarine figure. However, this fundus was not the border between lower and upper field representations in all subjects (see, for instance subject 10, whose upper visual field representations reach into the upper lip of the calcarine sulcus). Therefore, activations corresponding to upper and lower field representations are not always restricted to the upper and lower anatomical part of low-level visual areas, but appear to spread into the other quadrant as well.

129

Post-hoc tests indicated that significant differences from the interaction between velocity and visual fields (VFs) resulted from fast motion in V1 compared to V2 (MD=6.349, SE=1.386, t=4.581, p_{bonf} <.001) and V1 compared to V3 (MD=8.681, SE=1.386, t=6.264, p_{bonf}<.001). Comparison from the triple interaction (velocity*VFs*direction) showed significant differences, mainly in V1 (see suppl. Fig. 2). Fast motion in upward direction was more prominent compared to fast motion in downward direction (MD=5.912, SE=0.837, t=7.061, p_{bonf} <.001) and to slow motion in upward direction (MD=8.549, SE=1.419, t=6.025, p_{bonf} <.001). Fast motion in upward direction also modulated higher fMRI-signals in V1 compared to V2 (MD=7.665, SE=1.418, t=5.405, p_{bonf} <.001) and V3 (MD=10.356, SE=1.418, t=7.303, p_{bonf} <.001). In contrast, differences in fast motion was also observed in downward direction in V1 compared to V3 (MD=7.006, SE=1.418, t=4.940, p_{bonf} <.001).
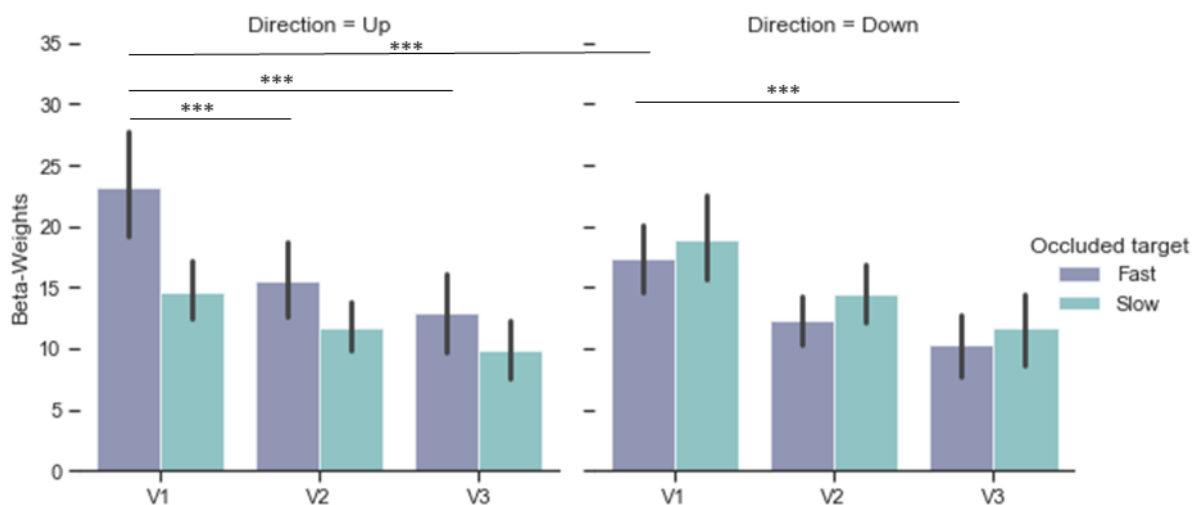
Appendix A. Figure 2 - Univariate beta weights (proportional to percent signal change) occluded phase. Purple bars (from left to right) depict average beta weights for fast motion, while green bars, the average beta weights for slow motion. Stars indicate significance between conditions inside each region on interest

Multivariate Pattern Analysis - *Complementary Analysis*

In addition to the low-level visual ROIs V1-V3, we also performed classification analyses with LO1, LO2 and hMT/V5+, for easy comparison with previous results.

Classifying additional ROIs: We trained a classifier on the distinction of up vs. downward condition during the visible phase and tested on the occluded up- vs. downward trajectories. Accuracy levels above chance were found in right LO1 (Accuracy (Acc)=0.589, SE=0.007, permutation p (p_{perm})<.001), right LO2(Acc=0.597, SE=0.007, p_{perm} <.001), right hMT/V5+ (Acc=0.597, SE=0.006, p_{perm}<.001) and left (Acc=0.588, SE=0.005, p_{perm}<.001). Results suggested that these regions also carried a similar pattern of information found in low-level visual areas.

Classifying Velocity Patterns of Visible from Occluded Phase: Here we carried out a classification analysis training in visible and testing in occluded phases (same procedure used in the first described analysis), but setting fast and slow as targets. Results indicated accuracies significantly above chance in lower V1 (Acc=0.607, SE=0.005, p_{perm}<.001), upper V1 (Acc=0.597, SE=0.006, p_{perm}<.001) and bilateral hMT/V5 (rh: Acc=0.608, SE=0.004, p_{perm}<.001, lh: Acc=0.605, SE=0.006, p_{perm}<.001).

Appendix B – Chapter 3

Behavioural Analysis

Low Predictability
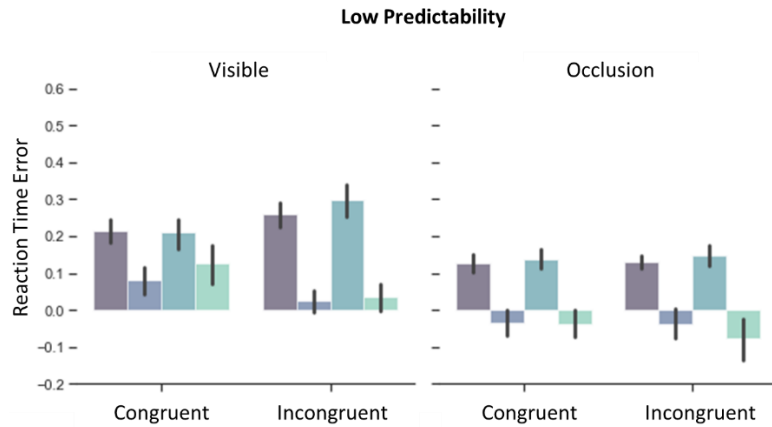
Appendix B. Figure 1 – Reaction time error of visible and occlusion phases in low predictability context. Differently from what was showed in the main text, for the sake of comparison, reaction time error here was calculated based on the expected velocity subtracted from participants' response. Interestingly, we observed the same pattern of response seen in congruent condition during occlusion in the LP context, suggesting that participants were not estimating according to the feedback, rather they were responding according to the learning velocity-direction association.

Univariate Analysis

Below we presented the results of the full 2x2x2x2x2 repeated measures ANOVA (direction: up vs down, velocity: fast vs. slow, predictability: low vs high, V1 quadrant: upper vs. lower, task order: 70 vs 100).

Reapeated Measures ANOVA

Cases	Sum of Squares	df	Mean Square	F	p	η²ₚ
Predictability - 100 x70	7.306	1	7.306	0.064	0.804	0.005
Predictability * TaskOrder	30.677	1	30.677	0.269	0.612	0.019
Residuals	1.599.500	14	114.250			
Visibility Vis x Occ	34.365	1	34.365	0.768	0.396	0.052
Visibility * TaskOrder	35.327	1	35.327	0.790	0.389	0.053
Residuals	626.115	14	44.723			
V1 Quad	30.593	1	30.593	0.495	0.493	0.034
V1 Quad * TaskOrder	24.130	1	24.130	0.390	0.542	0.027
Residuals	865.477	14	61.820			
direction	49.014	1	49.014	5.284	0.037	0.274
direction * TaskOrder	2.245	1	2.245	0.242	0.630	0.017
Residuals	129.851	14	9.275			
Velocity	1.989.599	1	1.989.599	67.525	< .001	0.828
Velocity * TaskOrder	82.857	1	82.857	2.812	0.116	0.167
Residuals	412.503	14	29.465			
Predictability * Visibility	5.113	1	5.113	0.135	0.719	0.010
Predictability * Visibility * TaskOrder	2.046	1	2.046	0.054	0.820	0.004
Residuals	531.837	14	37.988			
Predictability * V1 Quad	12.977	1	12.977	1.469	0.246	0.095
Predictability * V1 Quad * TaskOrder	18.794	1	18.794	2.127	0.167	0.132
Residuals	123.674	14	8.834			
Visibility * V1 Quad	0.548	1	0.548	0.043	0.838	0.003
Visibility * V1 Quad * TaskOrder	9.968	1	9.968	0.788	0.390	0.053
Residuals	176.994	14	12.642			
Predictability * direction	17.069	1	17.069	9.625	0.008	0.407
Predictability * direction * TaskOrder	0.446	1	0.446	0.251	0.624	0.018
Residuals	24.827	14	1.773			
Visibility * direction	0.007	1	0.007	0.003	0.961	1.808e -4
Visibility * direction * TaskOrder	4.185	1	4.185	1.459	0.247	0.094
Residuals	40.166	14	2.869			
V1 Quad * direction	241.385	1	241.385	51.409	< .001	0.786
V1 Quad * direction * TaskOrder	21.285	1	21.285	4.533	0.051	0.245
Residuals	65.736	14	4.695			
Predictability * Velocity	1.891	1	1.891	0.201	0.661	0.014
Predictability * Velocity * TaskOrder	0.479	1	0.479	0.051	0.825	0.004
Residuals	131.636	14	9.403			
Visibility * Velocity	0.010	1	0.010	0.003	0.957	2.182e -4
Visibility * Velocity * TaskOrder	0.238	1	0.238	0.069	0.796	0.005
Residuals	48.018	14	3.430			
V1 Quad * Velocity	0.104	1	0.104	0.026	0.875	0.002
V1 Quad * Velocity * TaskOrder	3.228	1	3.228	0.805	0.385	0.054
Residuals	56.156	14	4.011			
direction * Velocity	169.216	1	169.216	3.474	0.083	0.199
direction * Velocity * TaskOrder	2.880	1	2.880	0.059	0.811	0.004
Residuals	681.991	14	48.714			
Predictability * Visibility * V1 Quad	11.182	1	11.182	5.109	0.040	0.267
Predictability * Visibility * V1 Quad * TaskOrder	1.288	1	1.288	0.588	0.456	0.040
Residuals	30.642	14	2.189			
Predictability * Visibility * direction	2.310	1	2.310	0.664	0.429	0.045
Predictability * Visibility * direction * TaskOrder	9.200	1	9.200	2.645	0.126	0.159
Residuals	48.691	14	3.478			
Predictability * V1 Quad * direction	0.714	1	0.714	0.719	0.411	0.049
Predictability * V1 Quad * direction * TaskOrder	1.183	1	1.183	1.192	0.293	0.078
Residuals	13.900	14	0.993			
Visibility * V1 Quad * direction	73.152	1	73.152	36.961	< .001	0.725
Visibility * V1 Quad * direction * TaskOrder	6.141	1	6.141	3.103	0.100	0.181
Residuals	27.708	14	1.979			
Predictability * Visibility * Velocity	2.931	1	2.931	0.843	0.374	0.057
Predictability * Visibility * Velocity * TaskOrder	2.118	1	2.118	0.609	0.448	0.042
Residuals	48.666	14	3.476			
Predictability * V1 Quad * Velocity	1.713	1	1.713	1.556	0.233	0.100
Predictability * V1 Quad * Velocity * TaskOrder	0.415	1	0.415	0.376	0.549	0.026
Residuals	15.417	14	1.101			
Visibility * V1 Quad * Velocity	0.064	1	0.064	0.035	0.854	0.003
Visibility * V1 Quad * Velocity * TaskOrder	2.099	1	2.099	1.157	0.300	0.076
Residuals	25.396	14	1.814			
Predictability * direction * Velocity	162.415	1	162.415	4.929	0.043	0.260
Predictability * direction * Velocity * TaskOrder	20.612	1	20.612	0.626	0.442	0.043
Residuals	461.298	14	32.950			
Visibility * direction * Velocity	1.916	1	1.916	0.047	0.831	0.003
Visibility * direction * Velocity * TaskOrder	1.366	1	1.366	0.034	0.857	0.002

	Sum of Squares	df	Mean Square	F	p	η^2_p
Residuals	565.816	14	40.415			
V1 Quad ∗ direction ∗ Velocity	51.035	1	51.035	5.421	0.035	0.279
V1 Quad ∗ direction ∗ Velocity ∗ TaskOrder	7.121	1	7.121	0.756	0.399	0.051
Residuals	131.798	14	9.414			
Predictability ∗ Visibility ∗ V1 Quad ∗ direction	2.332	1	2.332	2.020	0.177	0.126
Predictability ∗ Visibility ∗ V1 Quad ∗ direction ∗ TaskOrder	2.684	1	2.684	2.325	0.150	0.142
Residuals	16.164	14	1.155			
Predictability ∗ Visibility ∗ V1 Quad ∗ Velocity	0.838	1	0.838	2.741	0.120	0.164
Predictability ∗ Visibility ∗ V1 Quad ∗ Velocity ∗ TaskOrder	0.227	1	0.227	0.744	0.403	0.050
Residuals	4.279	14	0.306			
Predictability ∗ Visibility ∗ direction ∗ Velocity	6.157	1	6.157	0.197	0.664	0.014
Predictability ∗ Visibility ∗ direction ∗ Velocity ∗ TaskOrder	15.970	1	15.970	0.510	0.487	0.035
Residuals	438.178	14	31.298			
Predictability ∗ V1 Quad ∗ direction ∗ Velocity	1.781	1	1.781	0.469	0.505	0.032
Predictability ∗ V1 Quad ∗ direction ∗ Velocity ∗ TaskOrder	1.722	1	1.722	0.453	0.512	0.031
Residuals	53.178	14	3.798			
Visibility ∗ V1 Quad ∗ direction ∗ Velocity	33.505	1	33.505	14.998	0.002	0.517
Visibility ∗ V1 Quad ∗ direction ∗ Velocity ∗ TaskOrder	0.172	1	0.172	0.077	0.785	0.005
Residuals	31.276	14	2.234			
Predictability ∗ Visibility ∗ V1 Quad ∗ direction ∗ Velocity	3.868	1	3.868	0.530	0.479	0.036
Predictability ∗ Visibility ∗ V1 Quad ∗ direction ∗ Velocity ∗ TaskOrder	1.696	1	1.696	0.232	0.637	0.016
Residuals	102.198	14	7.300			

Note. Type III Sum of Squares

Between Subjects Effects

Cases	Sum of Squares	df	Mean Square	F	p	η^2_p
TaskOrder	1.266.029	1	1.266.029	3.251	0.093	0.188
Residuals	5.452.338	14	389.453			

Note. Type III Sum of Squares

Post Hoc Tests

Post Hoc Comparisons - direction

		Mean Difference	SE	t	P bonf
up	down	-0.624	0.271	-2.299	0.037

* p < .05

Note. Results are averaged over the levels of: TaskOrder, Predictability, Visibility, V1 Quad , Velocity

Post Hoc Comparisons - Velocity

		Mean Difference	SE	t	P bonf
Fast	Slow	3.974	0.484	8.217	< .001

*** p < .001

Note. Results are averaged over the levels of: TaskOrder, Predictability, Visibility, V1 Quad , direction

Post Hoc Comparisons - Predictability ∗ direction

		Mean Difference	SE	t	P bonf
100, up	70, up	0.127	0.960	0.133	1.000
	100, down	-0.256	0.296	-0.863	1.000
	70, down	-0.865	0.990	-0.873	1.000
70, up	100, down	-0.383	0.990	-0.387	1.000
	70, down	-0.992	0.296	-3.349	0.020
100, down	70, down	-0.609	0.960	-0.635	1.000

* p < .05

Note. P-value adjusted for comparing a family of 6

Note. Results are averaged over the levels of: TaskOrder, Visibility, V1 Quad , Velocity

Post Hoc Comparisons - V1 Quad ∗ direction

		Mean Difference	SE	t	P bonf
Lower, up	Upper, up	1.877	0.727	2.583	0.120
	Lower, down	0.760	0.333	2.284	0.186

		Mean Difference	SE	t	P bonf
	Upper, down	-0.131	0.751	-0.174	1.000
Upper, up	Lower, down	-1.116	0.751	-1.486	0.926
	Upper, down	-2.008	0.333	-6.030	<.001
Lower, down	Upper, down	-0.891	0.727	-1.227	1.000

*** p < .001
Note. P-value adjusted for comparing a family of 6
Note. Results are averaged over the levels of: TaskOrder, Predictability, Visibility, Velocity

Post Hoc Comparisons - direction ✳ Velocity

		Mean Difference	SE	t	P bonf
up, Fast	down, Fast	-1.783	0.678	-2.628	0.099
	up, Slow	2.815	0.788	3.574	0.008
	down, Slow	3.350	0.554	6.042	<.001
down, Fast	up, Slow	4.597	0.554	8.291	<.001
	down, Slow	5.133	0.788	6.516	<.001
up, Slow	down, Slow	0.535	0.678	0.789	1.000

* p < .05, ** p < .01, *** p < .001
Note. P-value adjusted for comparing a family of 6
Note. Results are averaged over the levels of: TaskOrder, Predictability, Visibility, V1 Quad

Post Hoc Comparisons - Visibility ✳ V1 Quad ✳ direction

		Mean Difference	SE	t	P bonf
Visible, Lower, up	Occluded, Lower, up	1.211	0.703	1.723	1.000
	Visible, Upper, up	2.573	0.802	3.206	0.110
	Occluded, Upper, up	2.392	0.952	2.513	0.486
	Visible, Lower, down	1.515	0.386	3.920	0.009
	Occluded, Lower, down	1.217	0.752	1.617	1.000
	Visible, Upper, down	-0.204	0.829	-0.247	1.000
	Occluded, Upper, down	1.153	0.967	1.193	1.000
Occluded, Lower, up	Visible, Upper, up	1.362	0.952	1.431	1.000
	Occluded, Upper, up	1.181	0.802	1.472	1.000
	Visible, Lower, down	0.304	0.752	0.404	1.000
	Occluded, Lower, down	0.006	0.386	0.016	1.000
	Visible, Upper, down	-1.415	0.967	-1.464	1.000
	Occluded, Upper, down	-0.057	0.829	-0.069	1.000
Visible, Upper, up	Occluded, Upper, up	-0.181	0.703	-0.258	1.000
	Visible, Lower, down	-1.058	0.829	-1.276	1.000
	Occluded, Lower, down	-1.356	0.967	-1.403	1.000
	Visible, Upper, down	-2.777	0.386	-7.187	<.001
	Occluded, Upper, down	-1.420	0.752	-1.887	1.000
Occluded, Upper, up	Visible, Lower, down	-0.877	0.967	-0.907	1.000
	Occluded, Lower, down	-1.175	0.829	-1.417	1.000
	Visible, Upper, down	-2.596	0.752	-3.450	0.045
	Occluded, Upper, down	-1.238	0.386	-3.204	0.073
Visible, Lower, down	Occluded, Lower, down	-0.298	0.703	-0.424	1.000
	Visible, Upper, down	-1.719	0.802	-2.142	1.000
	Occluded, Upper, down	-0.362	0.952	-0.380	1.000
Occluded, Lower, down	Visible, Upper, down	-1.421	0.952	-1.493	1.000
	Occluded, Upper, down	-0.063	0.802	-0.079	1.000
Visible, Upper, down	Occluded, Upper, down	1.358	0.703	1.932	1.000

* p < .05, ** p < .01, *** p < .001
Note. P-value adjusted for comparing a family of 28
Note. Results are averaged over the levels of: TaskOrder, Predictability, Velocity

Post Hoc Comparisons - Predictability ✳ direction ✳ Velocity

		Mean Difference	SE	t	P bonf
100, up, Fast	70, up, Fast	1.140	1.121	1.017	1.000
	100, down, Fast	-0.279	0.858	-0.325	1.000
	70, down, Fast	-2.146	1.201	-1.787	1.000
	100, up, Slow	3.828	0.978	3.914	0.008
	70, up, Slow	2.942	1.241	2.370	0.670
	100, down, Slow	3.596	0.629	5.713	<.001
	70, down, Slow	4.245	1.215	3.494	0.040
70, up, Fast	100, down, Fast	-1.419	1.201	-1.182	1.000
	70, down, Fast	-3.286	0.858	-3.831	0.015
	100, up, Slow	2.688	1.241	2.165	1.000
	70, up, Slow	1.802	0.978	1.842	1.000
	100, down, Slow	2.455	1.215	2.021	1.000
	70, down, Slow	3.104	0.629	4.932	<.001
100, down, Fast	70, down, Fast	-1.867	1.121	-1.665	1.000
	100, up, Slow	4.107	0.629	6.525	<.001
	70, up, Slow	3.221	1.215	2.652	0.346

		Mean Difference	SE	t	P bonf
	100, down, Slow	3.875	0.978	3.962	0.007
	70, down, Slow	4.524	1.241	3.644	0.026
70, down, Fast	100, up, Slow	5.974	1.215	4.917	< .001
	70, up, Slow	5.088	0.629	8.084	< .001
	100, down, Slow	5.741	1.241	4.625	0.002
	70, down, Slow	6.390	0.978	6.534	< .001
100, up, Slow	70, up, Slow	-0.886	1.121	-0.790	1.000
	100, down, Slow	-0.232	0.858	-0.271	1.000
	70, down, Slow	0.417	1.201	0.347	1.000
70, up, Slow	100, down, Slow	0.653	1.201	0.544	1.000
	70, down, Slow	1.302	0.858	1.518	1.000
100, down, Slow	70, down, Slow	0.649	1.121	0.579	1.000

* p < .05, ** p < .01, *** p < .001

Note. P-value adjusted for comparing a family of 28

Note. Results are averaged over the levels of: TaskOrder, Visibility, V1 Quad

Post Hoc Comparisons - V1 Quad ✳ direction ✳ Velocity

		Mean Difference	SE	t	P bonf
Lower, up, Fast	Upper, up, Fast	2.485	0.797	3.119	0.137
	Lower, down, Fast	0.238	0.756	0.315	1.000
	Upper, down, Fast	-1.319	0.991	-1.330	1.000
	Lower, up, Slow	3.423	0.853	4.014	0.008
	Upper, up, Slow	4.692	1.072	4.378	0.002
	Lower, down, Slow	4.705	0.614	7.668	< .001
	Upper, down, Slow	4.479	0.934	4.794	< .001
Upper, up, Fast	Lower, down, Fast	-2.247	0.991	-2.266	0.837
	Upper, down, Fast	-3.803	0.756	-5.028	< .001
	Lower, up, Slow	0.938	1.072	0.875	1.000
	Upper, up, Slow	2.207	0.853	2.589	0.390
	Lower, down, Slow	2.221	0.934	2.377	0.646
	Upper, down, Slow	1.995	0.614	3.250	0.076
Lower, down, Fast	Upper, down, Fast	-1.556	0.797	-1.954	1.000
	Lower, up, Slow	3.185	0.614	5.190	< .001
	Upper, up, Slow	4.454	0.934	4.767	< .001
	Lower, down, Slow	4.467	0.853	5.240	< .001
	Upper, down, Slow	4.241	1.072	3.958	0.008
Upper, down, Fast	Lower, up, Slow	4.741	0.934	5.075	< .001
	Upper, up, Slow	6.010	0.614	9.794	< .001
	Lower, down, Slow	6.024	1.072	5.621	< .001
	Upper, down, Slow	5.798	0.853	6.800	< .001
Lower, up, Slow	Upper, up, Slow	1.269	0.797	1.593	1.000
	Lower, down, Slow	1.283	0.756	1.696	1.000
	Upper, down, Slow	1.057	0.991	1.066	1.000
Upper, up, Slow	Lower, down, Slow	0.014	0.991	0.014	1.000
	Upper, down, Slow	-0.213	0.756	-0.281	1.000
Lower, down, Slow	Upper, down, Slow	-0.226	0.797	-0.284	1.000

* p < .05, ** p < .01, *** p < .001

Note. P-value adjusted for comparing a family of 28

Note. Results are averaged over the levels of: TaskOrder, Predictability, Visibility

Post Hoc Comparisons - Visibility ✳ V1 Quad ✳ direction ✳ Velocity

		Mean Difference	SE	t	P bonf
Visible, Lower, up, Fast	Occluded, Lower, up, Fast	1.863	0.935	1.993	1.000
	Visible, Upper, up, Fast	3.719	0.885	4.204	0.023
	Occluded, Upper, up, Fast	3.113	1.166	2.670	1.000
	Visible, Lower, down, Fast	1.631	0.974	1.674	1.000
	Occluded, Lower, down, Fast	0.708	1.034	0.684	1.000
	Visible, Upper, down, Fast	-1.246	1.200	-1.038	1.000
	Occluded, Upper, down, Fast	0.472	1.182	0.399	1.000
	Visible, Lower, up, Slow	4.075	1.052	3.873	0.035
	Occluded, Lower, up, Slow	4.633	1.105	4.193	0.011
	Visible, Upper, up, Slow	5.502	1.270	4.333	0.006
	Occluded, Upper, up, Slow	5.745	1.248	4.602	0.003
	Visible, Lower, down, Slow	5.473	0.676	8.099	< .001
	Occluded, Lower, down, Slow	5.801	1.082	5.362	< .001
	Visible, Upper, down, Slow	4.912	1.020	4.815	0.002
	Occluded, Upper, down, Slow	5.909	1.256	4.703	0.002
Occluded, Lower, up, Fast	Visible, Upper, up, Fast	1.856	1.166	1.591	1.000
	Occluded, Upper, up, Fast	1.250	0.885	1.413	1.000
	Visible, Lower, down, Fast	-0.232	1.034	-0.224	1.000
	Occluded, Lower, down, Fast	-1.155	0.974	-1.186	1.000
	Visible, Upper, down, Fast	-3.109	1.182	-2.629	1.000

	Occluded, Upper, down, Fast	-1.391	1.200	-1.159	1.000
	Visible, Lower, up, Slow	2.212	1.105	2.002	1.000
	Occluded, Lower, up, Slow	2.770	1.052	2.633	1.000
	Visible, Upper, up, Slow	3.639	1.248	2.915	0.601
	Occluded, Upper, up, Slow	3.882	1.270	3.057	0.389
	Visible, Lower, down, Slow	3.610	1.082	3.337	0.170
	Occluded, Lower, down, Slow	3.938	0.676	5.827	< .001
	Visible, Upper, down, Slow	3.049	1.256	2.427	1.000
	Occluded, Upper, down, Slow	4.046	1.020	3.966	0.029
Visible, Upper, up, Fast	Occluded, Upper, up, Fast	-0.605	0.935	-0.648	1.000
	Visible, Lower, down, Fast	-2.088	1.200	-1.739	1.000
	Occluded, Lower, down, Fast	-3.011	1.182	-2.546	1.000
	Visible, Upper, down, Fast	-4.965	0.974	-5.096	< .001
	Occluded, Upper, down, Fast	-3.247	1.034	-3.140	0.330
	Visible, Lower, up, Slow	0.356	1.270	0.280	1.000
	Occluded, Lower, up, Slow	0.914	1.248	0.733	1.000
	Visible, Upper, up, Slow	1.783	1.052	1.695	1.000
	Occluded, Upper, up, Slow	2.026	1.105	1.833	1.000
	Visible, Lower, down, Slow	1.754	1.020	1.720	1.000
	Occluded, Lower, down, Slow	2.082	1.256	1.657	1.000
	Visible, Upper, down, Slow	1.193	0.676	1.766	1.000
	Occluded, Upper, down, Slow	2.190	1.082	2.025	1.000
Occluded, Upper, up, Fast	Visible, Lower, down, Fast	-1.482	1.182	-1.253	1.000
	Occluded, Lower, down, Fast	-2.406	1.200	-2.004	1.000
	Visible, Upper, down, Fast	-4.360	1.034	-4.216	0.012
	Occluded, Upper, down, Fast	-2.641	0.974	-2.711	1.000
	Visible, Lower, up, Slow	0.962	1.248	0.770	1.000
	Occluded, Lower, up, Slow	1.520	1.270	1.197	1.000
	Visible, Upper, up, Slow	2.388	1.105	2.162	1.000
	Occluded, Upper, up, Slow	2.631	1.052	2.501	1.000
	Visible, Lower, down, Slow	2.360	1.256	1.878	1.000
	Occluded, Lower, down, Slow	2.687	1.020	2.634	1.000
	Visible, Upper, down, Slow	1.799	1.082	1.663	1.000
	Occluded, Upper, down, Slow	2.796	0.676	4.137	0.018
Visible, Lower, down, Fast	Occluded, Lower, down, Fast	-0.924	0.935	-0.988	1.000
	Visible, Upper, down, Fast	-2.877	0.885	-3.253	0.316
	Occluded, Upper, down, Fast	-1.159	1.166	-0.994	1.000
	Visible, Lower, up, Slow	2.444	0.676	3.616	0.090
	Occluded, Lower, up, Slow	3.002	1.082	2.775	0.869
	Visible, Upper, up, Slow	3.871	1.020	3.794	0.050
	Occluded, Upper, up, Slow	4.113	1.256	3.274	0.204
	Visible, Lower, down, Slow	3.842	1.052	3.651	0.070
	Occluded, Lower, down, Slow	4.169	1.105	3.774	0.044
	Visible, Upper, down, Slow	3.281	1.270	2.584	1.000
	Occluded, Upper, down, Slow	4.278	1.248	3.427	0.134
Occluded, Lower, down, Fast	Visible, Upper, down, Fast	-1.954	1.166	-1.675	1.000
	Occluded, Upper, down, Fast	-0.235	0.885	-0.266	1.000
	Visible, Lower, up, Slow	3.367	1.082	3.113	0.333
	Occluded, Lower, up, Slow	3.926	0.676	5.809	< .001
	Visible, Upper, up, Slow	4.794	1.256	3.816	0.037
	Occluded, Upper, up, Slow	5.037	1.020	4.937	0.001
	Visible, Lower, down, Slow	4.766	1.105	4.313	0.007
	Occluded, Lower, down, Slow	5.093	1.052	4.840	0.001
	Visible, Upper, down, Slow	4.205	1.248	3.368	0.160
	Occluded, Upper, down, Slow	5.202	1.270	4.096	0.014
Visible, Upper, down, Fast	Occluded, Upper, down, Fast	1.718	0.935	1.838	1.000
	Visible, Lower, up, Slow	5.321	1.020	5.216	< .001
	Occluded, Lower, up, Slow	5.879	1.256	4.680	0.002
	Visible, Upper, up, Slow	6.748	0.676	9.986	< .001
	Occluded, Upper, up, Slow	6.991	1.082	6.462	< .001
	Visible, Lower, down, Slow	6.719	1.270	5.292	< .001
	Occluded, Lower, down, Slow	7.047	1.248	5.645	< .001
	Visible, Upper, down, Slow	6.158	1.052	5.853	< .001
	Occluded, Upper, down, Slow	7.155	1.105	6.476	< .001

Occluded, Upper, down, Fast	Visible, Lower, up, Slow	3.603	1.256	2.867	0.668
	Occluded, Lower, up, Slow	4.161	1.020	4.079	0.021
	Visible, Upper, up, Slow	5.030	1.082	4.649	0.002
	Occluded, Upper, up, Slow	5.272	0.676	7.802	< .001
	Visible, Lower, down, Slow	5.001	1.248	4.006	0.021
	Occluded, Lower, down, Slow	5.328	1.270	4.196	0.010
	Visible, Upper, down, Slow	4.440	1.105	4.019	0.020
	Occluded, Upper, down, Slow	5.437	1.052	5.167	< .001
Visible, Lower, up, Slow	Occluded, Lower, up, Slow	0.558	0.935	0.597	1.000
	Visible, Upper, up, Slow	1.427	0.885	1.613	1.000
	Occluded, Upper, up, Slow	1.670	1.166	1.432	1.000
	Visible, Lower, down, Slow	1.398	0.974	1.435	1.000
	Occluded, Lower, down, Slow	1.726	1.034	1.669	1.000
	Visible, Upper, down, Slow	0.837	1.200	0.697	1.000
	Occluded, Upper, down, Slow	1.834	1.182	1.551	1.000
Occluded, Lower, up, Slow	Visible, Upper, up, Slow	0.869	1.166	0.745	1.000
	Occluded, Upper, up, Slow	1.111	0.885	1.256	1.000
	Visible, Lower, down, Slow	0.840	1.034	0.812	1.000
	Occluded, Lower, down, Slow	1.167	0.974	1.198	1.000
	Visible, Upper, down, Slow	0.279	1.182	0.236	1.000
	Occluded, Upper, down, Slow	1.276	1.200	1.063	1.000
Visible, Upper, up, Slow	Occluded, Upper, up, Slow	0.243	0.935	0.260	1.000
	Visible, Lower, down, Slow	-0.029	1.200	-0.024	1.000
	Occluded, Lower, down, Slow	0.299	1.182	0.253	1.000
	Visible, Upper, down, Slow	-0.590	0.974	-0.605	1.000
	Occluded, Upper, down, Slow	0.407	1.034	0.394	1.000
Occluded, Upper, up, Slow	Visible, Lower, down, Slow	-0.271	1.182	-0.229	1.000
	Occluded, Lower, down, Slow	0.056	1.200	0.047	1.000
	Visible, Upper, down, Slow	-0.832	1.034	-0.805	1.000
	Occluded, Upper, down, Slow	0.165	0.974	0.169	1.000
Visible, Lower, down, Slow	Occluded, Lower, down, Slow	0.328	0.935	0.350	1.000
	Visible, Upper, down, Slow	-0.561	0.885	-0.634	1.000
	Occluded, Upper, down, Slow	0.436	1.166	0.374	1.000
Occluded, Lower, down, Slow	Visible, Upper, down, Slow	-0.888	1.166	-0.762	1.000
	Occluded, Upper, down, Slow	0.108	0.885	0.123	1.000
Visible, Upper, down, Slow	Occluded, Upper, down, Slow	0.997	0.935	1.067	1.000

* $p < .05$, ** $p < .01$, *** $p < .001$
Note. P-value adjusted for comparing a family of 120
Note. Results are averaged over the levels of: TaskOrder, Predictability

Appendix B. Table 1 – Full 2x2x2x2x2 repeated measures ANOVA (direction: up vs down, velocity: fast vs. slow, predictability: low vs high, V1 quadrant: upper vs. lower, task order: 70 vs 100).

Multivariate Analysis

Direction: Number of spheres
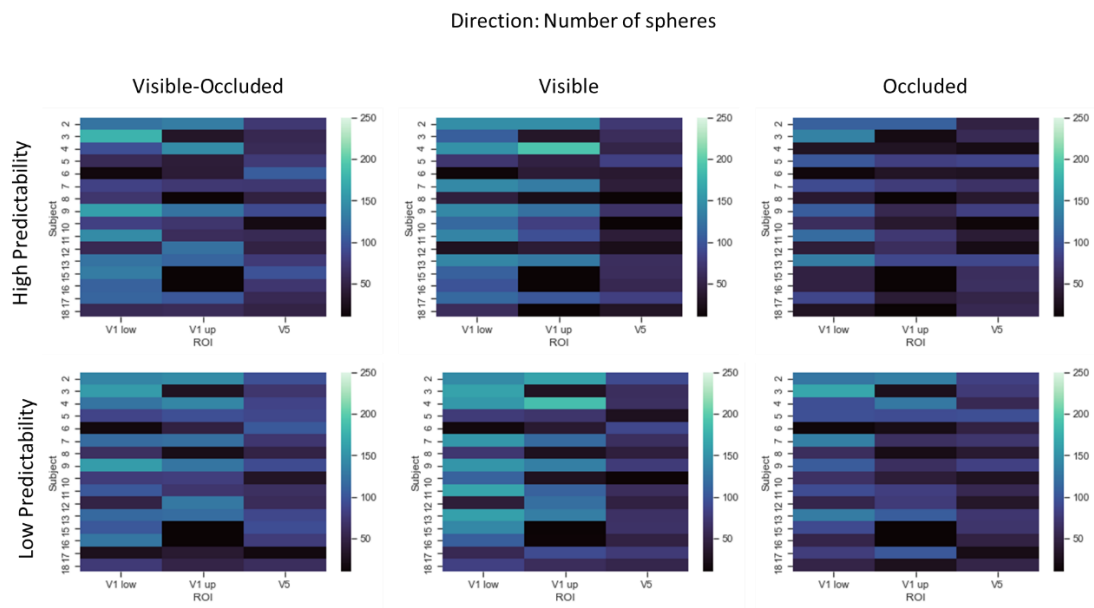
Appendix B. Figure 2 - Single-subject classification analysis of Direction. The upper row depicts the number of spheres included in the calculation of the 5% highest accuracy values, for each subject in each ROI, for classifications which used data from high predictable context and lower row, for classifications which used data from low predictable context. The left row represents number of spheres from classification analysis in which the classifier was trained in visible phase data and tested in occluded phase data; the middle row show results of analysis in which the classifier was trained and tested in visible phase data; and right row, train and test was carried out in occluded phase data.

Velocity: Number of spheres
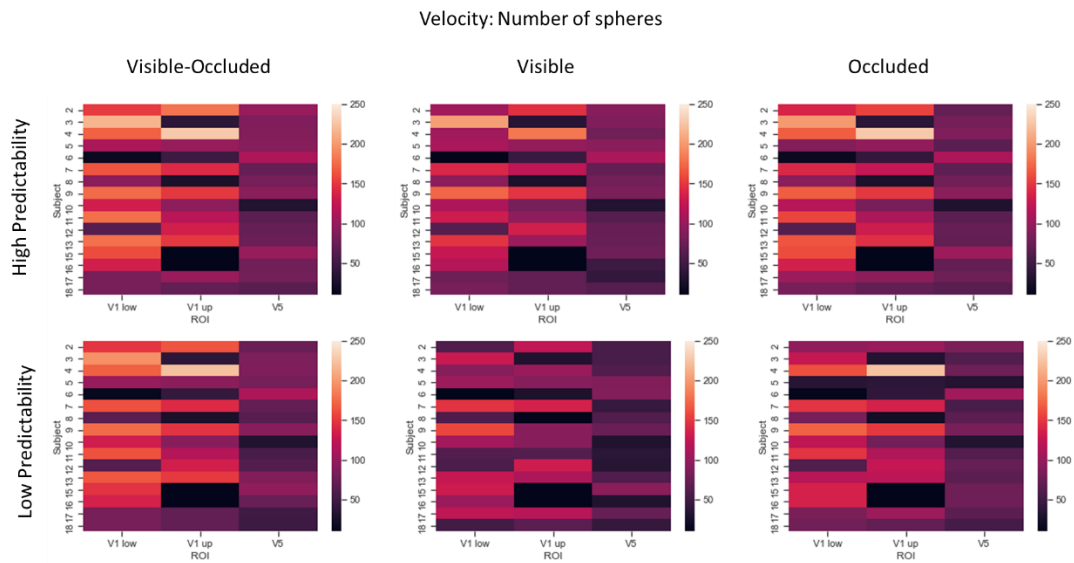
Appendix B. Figure 3 - Single-subject classification analysis of Velocity. The upper row depicts the number of spheres included in the calculation of the 5% highest accuracy values, for each subject in each ROI, for classifications which used data from high predictable context and lower row, for classifications which used data from low predictable context. The left row represents number of spheres from classification analysis in which the classifier was trained in visible phase data and tested in occluded phase data; the middle row show results of analysis in which the classifier was trained and tested in visible phase data; and right row, train and test was carried out in occluded phase data.

140

Appendix C – Chapter 4

Example of questionnaires that participants were required to fill in order to participant in the TMS experiment.

Willkommen!

Diese Broschüre beinhaltet einige Informationen über die sog. Transkranielle Magnetstimulation sowie über die Forschung, welche in diesem Center durchgeführt wird.

Was ist Transkranielle Magnetstimulation (TMS)?

Es ist eine Technik, die es uns erlaubt kortikale Hirnregionen und deren Funktionen zu untersuchen. Das Verfahren kann insbesondere dabei helfen herauszufinden, ob eine ganz bestimmte Hirnregion eine entscheidende Rolle in der Ausführung einer bestimmten kognitiven Aufgabe spielt.

Als nicht invasives Verfahren wird mithilfe der TMS die übliche elektrische Aktivität von Neuronen einer klar umschriebenen Region des Gehirns temporär und genau gezielt unterbrochen. Dabei wird mittels eines TMS-Impulses ein elektrisches Feld an der interessierenden Region angelegt. Weil sich das Gehirn mit einem Leiter verbinden lässt, entwickelt sich so ein induzierter Strom in dem stimulierten Areal des Gehirns, der die gewöhnliche, lokale Aktivität der Neuronen stört. Dieser Effekt ist nur von kurzer Dauer und beläuft sich bei einmaliger Stimulation auf wenige Millisekunden.

Wie trägt TMS zu der Erforschung des Gehirns bei?

Unter Anwendung von TMS lassen sich grundlegenden Prinzipien der Funktionsweisen des menschlichen Gehirns untersuchen. Im Rahmen der von uns durchgeführten Forschung werden die Effekte des TMS in gesunden Probanden untersucht. Somit

gewinnen wir neue und wichtige Informationen über die normale Funktion des visuellen Systems im Gehirn.

Wer wird von TMS-basierten Untersuchungen ausgeschlossen?

Vor der Durchführung eines TMS-Experiments, wird die medizinische Geschichte jedes Probanden von dem Versuchsleiter gründlich erfragt. Dabei werden unter anderem erfasst:

- Gesichte von Krampanfällen/ Auftreten von Epilepsie
- Nahe Verwandte mit Epilepsie
- Metallische Prothesen
- Elektronische Implantate (Schrittmacher, Rückenmarkstimulatoren etc.)
- Cochlea-Implantate
- Hörprobleme (z.B. Tinnitus)
- Alkoholkonsum am selben Tag
- Aktuelle Medikation (Ausschluss bei Antihistaminikum; kein Ausschluss bei Kontrazeptivum)
- Schwangerschaft

Was sind die potentiellen Risiken von TMS?

Derzeit gibt es keine Berichte über bedeutsame Nebenwirkungen beim Einsetzten von TMS bei gesunden Probanden abgesehen von sporadisch auftretenden Kopf- und Nackenschmerzen bedingt durch das Stillhalten während des Experiments (die Durchführung von TMS verlangt, dass die Kopfhaltung während der Testung nicht verändert wird), sowie möglicherweise Unbehagen auf der Kopfseite auf der das TMS appliziert wird aufgrund Muskelzucken während der Stimulation. Sollten Sie eine dieser Nebenwirkungen bemerken, melden Sie dies umgehend dem Testleiter und dieser wird bemüht sein die Situation für Sie so angenehm wie möglich zu gestalten. Sollte Ihr Unbehagen jedoch andauern, so können Sie das Experiment jeder Zeit abbrechen. TMS ist dennoch eine sehr sichere Methode solange die Sicherheitsvorschriften streng eingehalten werden.

Was sind die Vorteile von TMS für die Probanden?

Der Hauptvorteil besteht darin, dass der Proband die Möglichkeit hat, direkt die Durchführung einer neurowissenschaftlichen Untersuchung im Labor zu beobachten. Nicht zuletzt Dieser Umstand soll die Verbreitung des Wissens über die Funktionsweise des menschlichen Gehirns voran bringen. Ferner können Sie jeder Zeit nach einer Kopie

Und dann?

Nachdem Sie sich also mit den Instrumenten und der Laborumgebung vertaut gemacht haben, wird Ihnen der Versuchsleiter die Informationen dieser Broschüre detaillierter ausführen. Zusätzlich werden Sie aufgefordert eine schriftliche Zustimmung zu unterzeichnen und einen Sicherheitsfragebogen auszufüllen, in dem sämtliche medizinische Ausschlusskriterien für die Teilnahme an einem TMS-Experiment aufgelistet sind.

Im Anschluss

1. Zunächst werden Sie aufgefordert sein, sämtliche äußerliche Metallteile am Körper zu entfernen (Münzen, Schlüssel, Geldkarten, Taschenmesser, Schmuck, Piercings, etc.)
2. Sie werden eine detaillierte, schriftliche Beschreibung des folgenden Experiments und der Stimulation erhalten
3. Schließlich können Sie ohne weitere Erklärung das Experiment verweigern oder abbrechen

Was nach dem Experiment passiert

1) Da keine Kontraindikation vorliegt, können Sie im Anschluss Auto fahren
2) Sollten Sie Interesse an weiteren Informationen bezüglich der Studienergebnisse haben, können Sie die Studienleiter kontaktieren. Dabei ist jedoch zu beachten, dass es einiger Zeit bedarf, ehe diese Informationen zur Verfügung stehen.

Hiermit bestätige ich, dass ich diese Informationen gelesen und verstanden habe. Ich hatte die Möglichkeit, darüber zu reflektieren, aufgekommene Fragen zu stellen und diese zu meiner Zufriedenheit beantwortet zu bekommen.

_____   _____   _____
Name   Datum   Unterschrift

TMS Teilnahmekriterienfragebogen

Sehr geehrte/r Teilnahmeinteressierte/r,

Mit diesem Fragebogen soll ermittelt werden, ob Ihre Teilnahme am transkraniellen Magnetstimulationsexperiment (TMS-Experiment) des biopsychologischen Instituts der Otto-von-Guericke Universität (OvGU) möglich ist.

Eine ehrliche Beantwortung der folgenden Fragen ist notwendig, um Ihre Sicherheit bei einer Teilnahme gewährleisten zu können.

Rechtsgrundlage für die Erhebung dieser Daten ist Art. 6 Abs. 1 d) der Datenschutzgrundverordnung (DSGVO).

	Ja	Nein
1. Leiden Sie unter diagnostizierten psychischen Störungen oder befinden sich in psychologischer oder psychiatrischer Behandlung?		
2. Leiden Sie unter Epilepsie oder hatten Sie jemals Krampf- beziehungsweise epileptische Anfälle?		
3. Litten Sie jemals unter Synkopen oder fielen in Ohnmacht? Falls ja, nennen Sie bitte die Umstände der Ohnmacht.		
4. Hatten Sie je ein Schädel-Hirn-Trauma, das als Gehirnerschütterung diagnostiziert wurde oder mit Bewusstseinsverlust einherging?		
5. Haben Sie Hörbeeinträchtigungen (zum Beispiel Tinnitus oder Schwerhörigkeit)?		
6. Besitzen Sie ein Cochlea-Implantat?		
7. Haben Sie eine Sehbeeinträchtigung? Falls ja, welcher Art und bestünde die Möglichkeit, diese bei den Messungen durch Kontaktlinsen auszugleichen?		

8. Sind Sie schwanger oder besteht die Möglichkeit einer Schwangerschaft?		
9. Haben Sie metallene Implantate (zum Beispiel Splitter oder OP-Klammern)? Falls ja, bitten geben Sie an, wo und aus welchem Metall diese bestehen.		
10. Besitzen Sie einen implantierten Neurostimulator (zum Beispiel Hirnschrittmacher)?		
11. Besitzen Sie einen Herzschrittmacher?		
12. Besitzen Sie eine implantierte Infusionspumpe?		
13. Nehmen Sie irgendwelche regelmäßigen Medikamente ein (ausgenommen Antibabypille)? Falls ja, nennen Sie diese bitte.		
14. Haben Sie je an einem TMS-Experiment teilgenommen? Falls ja, traten bei Ihnen irgendwelche Komplikationen ein?		
15. Haben Sie je an einem MRT-Experiment teilgenommen? Falls ja, traten bei Ihnen irgendwelche Komplikationen ein?		

Hiermit versichere Ich die Richtigkeit meiner Angaben:

_____   _____   _____
Name, Vorname   Ort, Datum   Unterschrift

_____   _____
Geschlecht   Geburtsdatum

Informationen zum Experiment

Experimenteller Ablauf:

Aufgabe: Dieses Experiment untersucht die Auswirkungen der transkraniellen Magnetstimulation (TMS) auf die Fähigkeit, Bewegung wahrzunehmen und schließlich zwischen zwei sich bewegenden Reizen zu unterscheiden. Das Paradigma besteht aus zwei visuellen Stimuli, die sich von der linken Seite des Monitors in schneller Folge und in unterschiedlichen Geschwindigkeiten in Richtung eines Fixationskreuzes bewegen. Der Teilnehmer wird angewiesen, auf das Fixationskreuz zu fixieren, während die Augenbewegung von einer Eye-Tracking-Kamera überwacht wird. Die Aufgabe besteht darin, die Bewegung von zwei Stimuli mit dem peripheren Sehen zu beobachten. Wenn der zweite Stimulus verschwindet, wird der Teilnehmer aufgefordert, mit der Pfeiltaste nach links bzw. nach rechts anzugeben, ob die zweite Bewegung langsamer oder schneller als die erste war. Nach jeder Bewegungssequenz wird der Teilnehmer außerdem gebeten, sein Vertrauen in die Entscheidung und Wahrnehmung der Stimulusbewegung auf einer Skala von 1 bis 5 (s. unten) zu bewerten. Während der Proband die Aufgabe ausführt, wird eine Doppelpuls-TMS über verschiedenen Regionen des Kopfes angewendet. Die Daten werden in Übereinstimmung mit der   DSGVO   gespeichert.

Bewertungsskala:

1 = "Ich habe kein Bewegung nach dem ersten Stimulus wahrgenommen."

2 = "Ich habe eine Bewegung wahrgenommen, jedoch keinen Unterschied zum ersten Stimulus."

3 = "Ich habe den Unterschied wahrgenommen, kann jedoch nicht sagen, ob die Bewegung schneller oder langsamer war."

4 = "Ich habe die Bewegung und den Unterschied wahrgenommen und bin mir fast sicher bezüglich meiner Antwort."

5 = "Ich habe die Bewegung und den Unterschied wahrgenommen und bin mir absolut sicher bezüglich meiner Antwort."

TMS: Zeitgleich zur Aufgabe werden die Teilnehmer durch transkranielle Magnetstimulation (TMS) stimuliert. TMS ist eine Technik zur reversiblen und nicht-invasiven Beeinflussung von Gehirnfunktionen. Durch das Anlegen von kurzen magnetischen Impulsen an die Kopfhaut wird die elektrische Übertragung zwischen den Neuronen aufgrund des Magnetfeldes, das jede elektrische Leitung automatisch erzeugt, beeinflusst. Die Doppelimpuls-TMS wird in

verschiedenen Regionen über der Kopfhaut durch eine Achterspule (70mm Durchmesser) appliziert, die an einen Mag & More Stimulator angeschlossen ist. Vor dem Hauptexperiment wird die subjektspezifische Pulsstärke durch Messung der motorischen Schwelle jedes Teilnehmers bestimmt. Die Zielregionen für die TMS-Pulse werden mit Visor2 Neuronavigation von ANT Neuro identifiziert und basieren auf den strukturellen T1-Scans der Teilnehmer, die während vorheriger fMRT-Sitzungen erstellt wurden.

<u>Aufgabeninstruktionen</u>

In diesem Experiment werden Sie etwa eine Stunde lang eine Aufgabe am Computer durchführen, während eine Doppelpuls-TMS über verschiedenen Regionen Ihres Gehirns angewendet wird. Bei der Aufgabe werden Sie zwei visuelle Stimuli beobachten, die sich nacheinander von der linken Seite zur Mitte des Bildschirms bewegen. Bitte achten Sie auf die Bewegungen, während Sie jedoch Ihre Augen auf dem Fixationskreuz halten. Schauen Sie nicht direkt auf die sich bewegenden Reize. Wenn der zweite Stimulus verschwindet, antworten Sie bitte so schnell wie möglich, ob der zweite sich bewegende Stimulus schneller oder langsamer war als der erste. Danach werden Sie gebeten, eine Aussage auszuwählen, die Ihre Erfahrung mit dem vorherigen Reiz am besten beschreibt, wobei Sie eine Bewertung von 1-5 (s. oben) abgeben sollen. Diese Aufgabe besteht aus zwölf Blöcken und jeder Block enthält 36 Versuche. Zwischen den Blöcken dürfen Sie kurze Pausen einlegen. Bitte versuchen Sie, sich während des gesamten Experiments so gut wie möglich auf die Aufgabe zu konzentrieren. Der Versuchsleiter steht Ihnen während des gesamten Experiments für weitere Fragen gerne zur Verfügung. Wenn Sie sich zu irgendeinem Zeitpunkt während der Stimulation unwohl fühlen, können Sie das Experiment sofort abbrechen. Nach dem Ende des Experiments werden Sie für Ihre Zeit durch Versuchspersonenstunden oder Bezahlung entschädigt. Die Daten werden in Übereinstimmung mit der DSGVO gespeichert.

Bitte lesen Sie die folgenden Aussagen und markieren Sie diese mit Ihren Initialen, wenn Sie mit der Aussage einverstanden sind:

Ich bestätige, dass ich das Informationsblatt gelesen und verstanden habe. Ich hatte die Möglichkeit, über die Informationen nachzudenken, Fragen zu stellen und zufriedenstellende Antworten zu erhalten.

Mir ist bewusst, dass ich freiwillig teilnehme und die Messung jederzeit ohne Angabe von Gründen abbrechen kann.

☐

Mir ist bekannt, dass meine Daten vertraulich behandelt werden und in späteren Publikationen nur Daten veröffentlicht werden, die nicht auf mich zurückzuführen sind (Pseudonymisierung).

☐

Ich nehme freiwillig an der Studie teil.

☐

_____	_____	_____
Name des Teilnehmers	Ort/Datum	Unterschrift
_____	_____	_____
Name des Versuchsleiters	Ort/Datum	Unterschrift

Declaration of Honour

"I hereby declare that I prepared this thesis without the impermissible help of third parties and that none other that the aids indicated have been used; all sources of information are clearly marked, including my own publications.

In particular I have not consciously:
• fabricated data or rejected undesirable results,
• misused statistical methods with the aim of drawing other conclusions than those warranted by the available data,
• plagiarized external data or publications,
• presented the results of other researchers in a distorted way.

I am aware that violations of copyright may lead to injunction and damage claims by the author and also to prosecution by law enforcement authorities.
I hereby agree that the thesis may be electronically reviewed with the aim of identifying plagiarism.

This work has not been submitted as a doctoral thesis in the same or a similar form in Germany, nor in any other country. It has not yet been published as a whole."